



The interaction of Notch signalling, haemodynamic flow and angiogenesis in Von Hippel-Lindau mutant zebrafish

Oliver John Watson

**Thesis submitted for the degree of Doctor of
Philosophy**

University of Sheffield

Department of Cardiovascular Science

May 2013

Acknowledgements

I would like to thank my supervisors, Dr Tim Chico and Dr Freek van Eeden who have supported, encouraged and inspired my research. I am indebted to them and their labs for tolerating my continuous questions and for their patience and instruction in developing my scientific skills. I would also like to thank the MRC for funding my research and providing the facilities and environment to allow me to complete my research.

D38 is a wonderful lab in which to work and learn and I am grateful to have been a part of it over the last three years. I have made some incredible friends, shared wonderful experiences and possibly learnt a little about science along the way, thank you all.

Everyone who has helped me over the last three years deserves a mention, but I would particularly like to thank Caroline, who is an inspiration for so many reasons, thanks for all your help and for teaching me almost everything useful I know about zebrafish.

I would also like to thank my girls, Gina, Sophie and Milly for your continuous support, encouragement and love.

Abstract

Introduction: There is increasing evidence that the endothelium is able to transduce circulatory force into signals which influence angiogenic behaviour. The Von Hippel-Lindau homozygous mutant zebrafish (*vhl*^{-/-}) has increased HIF-1 α signalling and aberrant angiogenesis. In this study I therefore set out to characterise the angiogenic phenotype of the *vhl*^{-/-} mutant and examine the effect of manipulating blood flow. Both nitric oxide (NO) and Notch regulated intracellular signalling have been shown to influence endothelial angiogenic behaviour in development and disease, so I studied the role of these on development of the angiogenic phenotype in the *vhl*^{-/-} mutant.

Hypothesis: Does angiogenesis stimulated by up-regulated hypoxic signalling require blood flow?

Methods: *vhl* mutant zebrafish were crossed with endothelial reporter transgenics to assess and quantify the angiogenic phenotype. Blood flow was manipulated using genetic and pharmacological manipulation in developing zebrafish embryos. To study the effect of flow on endothelial notch signalling I utilised a novel transgenic line *Tg(CSL:venus)*, which expresses a fluorescent reporter upon activation of a Notch regulated transcription factor. The role of individual notch signalling components was investigated using reverse transcription quantitative polymerase chain reaction (RT-qPCR) for various ligands in developing zebrafish tissue during development in the absence of flow and in control embryos

Results: The *vhl*^{-/-} mutant showed early vessel changes including enlargement and sprouting. These angiogenic vessel changes were dependent on the presence of circulatory flow and are lost in mutant embryos treated with *troponin t₂* morpholino or 2,3-Butanedione monoxime (BDM). Imaging of aortic endothelium showed a significant up regulation of notch signalling in the *Tg(CSL:venus)* line in the absence of flow, induced by *troponin t₂* knockdown or BDM treatment. This increase in endothelial notch signalling in the absence of flow was mediated by increased expression of the notch ligand *dll4* in RT-qPCR and whole mount *in-situ* hybridisation experiments.

Conclusion: The aberrant angiogenesis stimulated by increased HIF-1 α signalling in the *vhl*^{-/-} mutant is dependent on blood flow. My data suggests a novel flow dependent regulation of notch signalling in the developing vasculature mediated by the suppression of *dll4* by blood flow.

Table of Contents

Acknowledgements	i
Abstract	ii
Table of Contents	iv
Table of Figures	x
Abbreviations	xiii
Chapter 1 General Introduction	1
1.1 Hypoxic signalling	2
1.1.1 Hypoxia inducible factor (HIF)	2
1.1.2 Regulation of HIF signalling.....	3
1.1.2.1 Prolyl hydroxylase enzymes (PHD)	3
1.1.2.2 Factor inhibiting HIF (FIH)	3
1.1.2.3 Von Hippel-Lindau protein (pVHL) and ubiquitin ligase degradation of HIF-1 α	
1.1.3 HIF signalling and angiogenic growth factors.....	9
1.2 Vascular development	11
1.2.1 Angiogenesis	11
1.2.2 Vascular endothelial growth factor	11
1.2.2.1 Ligands and receptors in the zebrafish.....	12
1.2.3 Tip and stalk cell formation.....	12
1.2.4 Haemodynamic flow and the regulation of angiogenesis	15
1.3 Notch signalling	17
1.3.1 Canonical notch signalling	17
1.3.2 Non-canonical Notch signalling	18
1.4 Effects of Notch signalling on endothelium and vascular development ..	18
1.4.1 Vasculogenesis	18
1.4.2 Angiogenesis	19
1.4.2.1 Tip and stalk cell selection and notch signalling	20
1.5 Nitric Oxide (NO) signalling	23
1.5.1 NO and vessel biology.....	23
1.6 Zebrafish as a model of vessel development and vascular disease	24
1.6.1 Advantages of the zebrafish for vascular research	25
1.6.1.1 Optical clarity and imaging.....	25
1.6.1.2 Genetic tractability and manipulation.....	25
1.7 The <i>vhl</i> homozygous (<i>vhl</i>^{-/-}) mutant zebrafish	27
1.7.1 Vascular phenotype of the <i>vhl</i> ^{-/-} mutant zebrafish	28
1.8 Aim of my research	30

1.9	Hypotheses	30
1.10	Objectives	30
Chapter 2	Materials and Methods	32
2.1	Zebrafish husbandry	33
2.1.1	Adult zebrafish maintenance	33
2.1.2	Zebrafish strains	33
2.1.2.1	Mutant zebrafish lines.....	33
2.1.2.2	Transgenic vascular reporter lines.....	33
2.1.2.3	Transgenic endothelial hypoxia and vascular reporter lines.....	34
2.1.2.4	Transgenic Notch reporter line	35
2.1.2.5	Maintenance of adult reporter lines	35
2.1.3	Zebrafish anaesthesia	36
2.1.4	Embryo collection & storage.....	36
2.1.4.1	E3 media.....	37
2.2	Identification of a zebrafish <i>vhl</i>^{hu2117} mutant allele	37
2.2.1	Phenotypic identification of <i>vhl</i> homozygous mutants	37
2.2.2	Genetic identification of <i>vhl</i> ^{hu2117} mutation	40
2.2.2.1	Gel electrophoresis.....	40
2.2.2.2	Genomic DNA extraction	40
2.3	In vivo imaging of embryonic zebrafish.....	44
2.3.1	Preparation of Embryos.....	44
2.3.1.1	Dechoriation.....	44
2.3.1.2	Inhibiting embryo pigment development with phenylthiourea	44
2.3.1.3	Mounting of live embryos.....	44
2.3.1.4	Microscopy.....	44
2.4	Vascular quantification and measurements	45
2.4.1	Calibration of images.....	45
2.4.2	Endothelial morphology	45
2.4.3	Endothelial nuclei quantification	46
2.5	In vivo intravascular fluorescence angiograms	46
2.6	Morpholino antisense oligonucleotides.....	47
2.6.1	Morpholino synthesis, reconstitution and storage	47
2.6.2	Morpholino sequences	47
2.6.3	Morpholino oligonucleotide injection into single cell embryos	48
2.7	Whole mount in situ hybridization.....	48
2.7.1	Embryo fixation in paraformaldehyde	48
2.7.2	Reagents & Buffers	48

2.7.3	Outline of method for whole mount in situ hybridisation	49
2.7.3.1	Embryo permeabilisation	49
2.7.3.2	Method for WISH	50
2.7.3.3	Methanol clearing	50
2.7.3.4	Imaging and mounting of WISH stained embryos	50
2.7.4	RNA antisense probe synthesis for in situ hybridisation.....	50
2.7.4.1	Outline of RNA antisense probe synthesis for whole mount in situ	50
2.7.4.2	RNA antisense probes for WISH	51
2.7.4.3	Extraction of plasmid from blotting paper	52
2.7.4.4	Transformation of Competent cells for plasmid synthesis	52
2.8	Synthesis of a novel RNA antisense DIG labelled probe	54
2.8.1	Synthesis of a <i>kaede</i> PCR product for TOPO TA cloning	55
2.8.1.1	Total RNA extraction from <i>kaede</i> positive transgenic embryos.....	55
2.8.1.2	Reverse transcription to produce cDNA of <i>kaede</i>	55
2.8.1.3	PCR to amplify <i>kaede</i> sequence from cDNA library	55
2.8.2	TOPO TA cloning vector for insertion of a Taq polymerase amplified PCR product.....	56
2.8.2.1	Incorporation of the PCR product into the TOPO TA cloning vector	56
2.8.2.2	Transformation of chemically competent cells for cloning of PCR product and construct	57
2.8.2.3	Selecting colonies for insert confirmation and glycerol storage.....	57
2.8.2.4	Large scale Plasmid DNA purification	57
2.8.2.5	Plasmid linearisation for <i>kaede</i> probe synthesis.....	58
2.8.2.6	RNA probe transcription	58
2.8.2.7	RNA probe purification.....	60
2.9	Immunohistochemistry	60
2.9.1	Phosphorylated Histone H3 antibody immunohistochemistry	60
2.9.1.1	Method for PH3 immunohistochemistry	60
2.10	Pharmacological manipulation of the zebrafish embryo.....	61
2.10.1	Pharmacological manipulation of the nitric oxide pathway	61
2.10.1.1	Inhibition of nitric oxide synthase.....	61
2.10.1.2	Pharmacological addition of nitric oxide	61
2.10.1.3	Detection of NO signalling in the developing zebrafish embryo	62
2.10.2	Pharmacological manipulation of the Notch signalling pathway.....	62
2.10.2.1	Inhibition of notch signalling with DAPT.....	62
2.11	Real time reverse transcription quantitative polymerase chain reaction	63
2.11.1	Isolation of zebrafish embryonic total RNA.....	63

2.11.1.1	Tissue preparation for RNA extraction.....	63
2.11.1.2	RNA extraction.....	64
2.11.2	Reverse transcription of extracted total RNA	64
2.11.3	Identification and optimisation of primers for real time RT-qPCR.....	65
2.11.3.1	Genes analysed and primers for RT-qPCR analysis.....	65
2.11.3.2	Primer optimisation for RT-qPCR.....	66
2.11.4	Analysis of real time RT-qPCR data.....	66
2.11.4.1	Melt curve	69
2.12	Statistics.....	69
2.12.1	Statistical analysis and significance	69
2.12.2	Graphical annotation of significance.....	69
2.12.3	Power calculations.....	69
Chapter 3	Characterisation of the angiogenic phenotype of the Von Hippel-Lindau homozygous mutant zebrafish.....	70
3.1	Introduction.....	71
3.2	Results	71
3.2.1	Characterisation of the vascular phenotype of the <i>vhl</i> ^{-/-} mutant	71
3.2.1.1	Formation of the intersegmental artery in the <i>vhl</i> ^{-/-} mutant	71
3.2.1.2	Is the vessel phenotype of the <i>vhl</i> ^{-/-} mutant due to accelerated development of the normal phenotype?	74
3.2.1.3	Lymphangiogenesis in the <i>vhl</i> mutant is also abnormal	77
3.2.1.4	Does the cerebral circulation of the <i>vhl</i> ^{-/-} mutant show the same phenotype as the trunk vessels?	79
3.2.2	Do the increases in endothelium in the <i>vhl</i> ^{-/-} mutant result in lumenised vessels?.....	81
3.2.3	Increases in endothelial cell number in the <i>vhl</i> ^{-/-} mutant.....	83
3.2.3.1	Increased endothelial cell number in the aorta of the <i>vhl</i> ^{-/-} mutant	83
3.2.3.2	Increased aortic diameter in the <i>vhl</i> ^{-/-} mutant.....	86
3.2.3.3	Increased endothelial cell number in trunk vessels of the <i>vhl</i> ^{-/-} mutant	86
3.2.4	Endothelial tip cell differentiation in the <i>vhl</i> ^{-/-} mutant	88
3.2.4.1	Increased number of endothelial cells producing filopodia in the <i>vhl</i> ^{-/-} mutant	88
3.2.5	Is the increase in number of endothelial cells in the <i>vhl</i> ^{-/-} mutant due to proliferation?.....	91
3.3	Discussion	93
3.3.1	Is the abnormal vascular phenotype endothelial cell autonomous? (Appendix 1).....	96

3.3.2	Summary	97
Chapter 4	The role of flow in the regulation of <i>vhl</i>^{-/-} mutant angiogenesis	98
4.1	Introduction.....	99
4.2	Results	99
4.2.1	The effect of absent blood flow on vascular development in <i>vhl</i> mutants .	99
4.2.1.1	Genetic manipulation of circulation in the developing <i>vhl</i> ^{-/-} zebrafish	99
4.2.2	Pharmacological circulatory arrest in the <i>vhl</i> ^{-/-} mutant.....	108
4.2.3	Are the increases in the number of erythrocytes in the <i>vhl</i> mutant required for development of the angiogenic phenotype?	113
4.2.3.1	Does early venesection reduce red cell density in the <i>vhl</i> ^{-/-} mutant?.....	113
4.2.3.2	Does venesection alter red cell velocity in the vessels of the <i>vhl</i> ^{-/-} mutant? .	114
4.2.3.3	Does venesection in the <i>vhl</i> ^{-/-} mutant block the angiogenic phenotype?	114
4.3	Discussion	118
4.3.1	Summary	121
Chapter 5	Examination of the interactions between blood flow, Notch and nitric oxide signalling in wildtype and <i>vhl</i> mutant zebrafish	122
5.1	Introduction.....	123
5.2	Results	123
5.2.1	Identification of changes in endothelial Notch signalling in response to flow using a novel Notch reporter transgenic.....	123
5.2.1.1	Morpholino knockdown of <i>troponin t₂</i> increases endothelial Notch signalling in the developing aorta	124
5.2.1.2	Pharmacological induced circulatory arrest leads to increases in endothelial notch expression.....	127
5.2.1.3	Confirmation that increased endothelial Notch signalling is mediated by a classical Notch ligand-receptor interaction	129
5.2.2	Identification of Notch signalling components differentially expressed in endothelial cells in the absence of circulatory flow.....	133
5.2.2.1	Confirmation that differential expression of <i>dll4</i> in response to flow is an endothelial specific change in expression.....	138
5.2.2.2	Knockdown of <i>dll4</i> blocks the endothelial increase in notch expression seen in response to absent flow	138
5.2.3	Effect of manipulating NO signalling on the development of the <i>vhl</i> ^{-/-} mutant vessel phenotype	141
5.2.3.1	The effect of NOS inhibition on angiogenesis in the <i>vhl</i> ^{-/-} mutant.....	141
5.2.3.2	Effect of manipulation of NO on the aortic size in the <i>vhl</i> ^{-/-} and wild type embryo	144

5.2.3.3 Total embryo NO signalling using the fluorophore DAFF-FM.....	146
5.3 Discussion	149
5.3.1 Summary	153
Chapter 6 General discussion.....	155
Chapter 7 Appendix 1	163
7.1 Endothelial cell constitutive hypoxic signalling and the initiation of an angiogenic phenotype	164
Chapter 8 References	168

Table of Figures

Figure 1.1. HIF signalling in the presence of normal cellular oxygen tension showing the hydroxylation of intracellular HIF-1 α and the proteosomal degradation via the ubiquitin ligase system in the cytoplasm.	6
Figure 1.2. HIF signalling in the presence of cellular hypoxia and the effect on downstream response genes.	7
Figure 1.3. Sequential regulation of HIF-1 α by the PHD and FIH hydroxylation enzymes at reducing oxygen tensions.	8
Figure 1.4. Schematic of differences between developmental vascular development (vasculogenesis) and the formation of new vessels from endothelial cell of an established vessels.	10
Figure 1.5 Endothelial differentiation into tip and stalk cells during angiogenesis and its molecular regulation.	14
Figure 1.6 Endothelial notch signalling determines tip and stalk cell fate.	21
Figure 2.1 Phenotypic differences between a 5 dpf <i>vhl</i> ^{-/-} mutant embryo and a wildtype sibling.	39
Figure 2.2 PCR amplification and restriction enzyme digest of the mutated region of the <i>vhl</i> allele in the <i>vhl</i> ^{hu2117} mutant zebrafish.	43
Figure 2.3 PCR of cDNA from embryos expressing <i>kaede</i> and wild types for cloning into TOPO TA cloning system.	59
Figure 2.4 Fluorescence amplification data and melt curve analysis from RT-qPCR for multiple gene targets and biological replicates.	68
Figure 3.1. Comparison of trunk vessel morphology in the <i>vhl</i> ^{-/-} mutant and wildtype at 3dpf.	73
Figure 3.2 Quantification of the differences in the vascular phenotype of the wt and <i>vhl</i> ^{-/-} mutant.	75
Figure 3.3. Progression of the angiogenic phenotype of the <i>vhl</i> ^{-/-} mutant from 3dpf to 7dpf.	78
Figure 3.4 Differences in the cerebral vasculature of the <i>vhl</i> ^{-/-} mutant using the <i>Tg(vhl</i> ^{hu2117} ^{-/-} <i>;</i> <i>fli1:eGFP)</i> line.	80
Figure 3.5 Angiograms of <i>vhl</i> ^{-/-} mutant and wt embryos at 4 dpf.	82
Figure 3.6 Aortic endothelial cell number and aortic diameter in the wt and <i>vhl</i> ^{-/-} mutant of the mid trunk aorta.	84
Figure 3.7 Quantification of aortic endothelial cell number and aortic diameter in the wt and <i>vhl</i> ^{-/-} mutant of the mid trunk aorta.	85

Figure 3.8 Assessment of the endothelial cell number in the vasculature of the wt and <i>vhl</i> ^{-/-} mutant at 3dpf.	87
Figure 3.9 Increased filopodia of the endothelial membrane of the ISV in the <i>vhl</i> ^{-/-} mutant at 3 dpf.	89
Figure 3.10 Immunohistochemistry of the proliferation marker phosphorylated histone H3 and fluorescent endothelial nuclei in 4dpf <i>vhl</i> ^{-/-} mutant and wt embryos.	92
Figure 4.1 The effect of removing circulatory flow from the endothelium of the wild type and <i>vhl</i> ^{-/-} mutant at 3 dpf.	102
Figure 4.2 Quantification of absent circulatory flow on the hypoxia driven angiogenesis in the <i>vhl</i> ^{-/-} mutant.	103
Figure 4.3 Time course of the <i>vhl</i> ^{-/-} mutant angiogenic phenotype compared with aged matched <i>vhl</i> ^{-/-} mutants injected with trop t ₂ MO.	104
Figure 4.4 Reduction in the endothelial cell number seen in the <i>vhl</i> ^{-/-} mutant in the absence of circulatory flow.	106
Figure 4.5 Endothelial nuclei counts <i>vhl</i> ^{-/-} and wild type embryos in the presence of circulatory flow or absence of flow.	107
Figure 4.6 Pharmacological inhibition of circulatory flow results in the attenuation of the <i>vhl</i> ^{-/-} angiogenic phenotype.	109
Figure 4.7 Effect of BDM, an inhibitor of cardiac contraction on the quantification of the <i>vhl</i> ^{-/-} angiogenic phenotype.	110
Figure 4.8 Effect of pharmacological inhibition of cardiac contraction on endothelial number in the <i>vhl</i> ^{-/-} aorta (A) and trunk vessels (B).	112
Figure 4.9 Polycythaemia of <i>vhl</i> ^{-/-} mutants and the resulting increased erythrocyte flow in the developing and constitutive hypoxia driven angiogenic vessels.	115
Figure 4.10 Effect of venesection on the erythrocyte density and its effect on the aortic erythrocyte velocity in the <i>vhl</i> ^{-/-} mutant.	116
Figure 4.11 Venesection at 2 dpf to reduce aortic velocity in the <i>vhl</i> ^{-/-} mutant does not change the angiogenic phenotype at 5dpf.	117
Figure 5.1 Flow dependent changes in aortic endothelial Notch signalling as a result of troponin t ₂ MO knockdown at 48 hpf and 72 hpf.	125
Figure 5.2 Quantification of endothelial notch signal at 48hpf (A) and 72hpf (B) in the presence of flow or absence (Trop T ₂), due to injection with <i>troponin t₂</i> MO.	126
Figure 5.3 Effect of pharmacological induced circulatory arrest with BDM (15mM) at 36hpf on endothelial Notch signalling imaged at 72 hpf.	128
Figure 5.4 Effect of a pharmacological Notch signalling inhibitor on the flow dependent increase in CSL-venus fluorescent signal.	131

Figure 5.5 Quantification of the mean aortic CSL-venus fluorescence in embryos injected with <i>troponin t₂</i> MO and the effect of DAPT.	132
Figure 5.6 RT-qPCR of trunk tissue from 48 hpf embryos comparing the relative expression of known angiogenic genes, Notch ligands, receptors and notch signalling targets in <i>troponin t₂</i> MO injected embryos.	134
Figure 5.7 RT-qPCR of trunk tissue from 72 hpf embryos comparing the relative expression of known angiogenic genes, notch ligands, receptors and notch signalling targets in <i>troponin t₂</i> MO injected embryos.	136
Figure 5.8 Whole mount in situ hybridisation of <i>dll4</i> mRNA expression in embryos exposed to circulatory flow and without (<i>troponin t₂</i> MO injection)	139
Figure 5.9 Effect of <i>dll4</i> MO knockdown on the flow dependent increase in notch signalling in the CSL:venus transgenic reporter.	140
Figure 5.10 Effect of NO inhibition by L-NAME on the <i>vh1^{-/-}</i> mutant angiogenic phenotype.	142
Figure 5.11 Quantification of vessel diameter, endothelial area and vessel length in wt and the <i>vh1^{-/-}</i> mutant treated with L-NAME NO synthase inhibitor.	143
Figure 5.12 Effect of L-NAME and SNP on the aortic diameter in the <i>vh1^{-/-}</i> mutant and wt embryo at 4dpf.	145
Figure 5.13 DAFF-FM fluorescence in 4 dpf wildtype and <i>vh1^{-/-}</i> mutant embryos incubated with L-NAME or SNP.	147
Figure 5.14 Quantification of whole mount DAFF-FM fluorescence at 4 dpf in wt and <i>vh1^{-/-}</i> mutant embryos treated with SNP or L-NAME.	148
Figure 6.1. Summary of the role of Notch signalling and <i>dll4</i> on the angiogenic phenotype in the presence of endothelial activation.	161
Figure 7.1. Effect of up regulated HIF-1 α signalling in the endothelium of 3 dpf embryo labelled with <i>Tg(fli:GFF;UAS:kaede)</i>	165
Figure 7.2. WISH expression of <i>kaede</i> and <i>phd3</i> genes in double transgenics and controls to confirm expression of the <i>fli1:GFF</i> promoter and the downstream UAS: <i>kaede</i> and UAS: <i>da-hif-1ab-IRES-GFP</i> constructs	166

Abbreviations

-/-	Homozygous
+/-	Heterozygous
+/+	Wildtype
ANG	Angiopoietin
Ao	Aorta
BDM	2,3-Butanedione monoxime
cDNA	complementary DNA
CSL	(CBF1, Suppressor of Hairless, Lag-1) Notch transcription factor
CtA	Central arteries (Brain)
DAPT	N-[N-(3,5-Difluorophenacetyl)-L-alanyl]-S-phenylglycine t-butyl ester, γ -secretase inhibitor
DLAV	Dorsal longitudinal vessels
Dll4 (<i>dll4</i>)	delta like ligand 4
DNA	Deoxyribonucleic acid
dpf	days post fertilisation
EC	Endothelial cell
ECM	Extracellular matrix
eGFP	enhanced green fluorescent protein
ENU	<i>N</i> -ethyl- <i>N</i> -nitrosourea
EPO	Erythropoietin
FIH (<i>fiH</i>)	Factor inhibiting HIF
FLI1 (<i>fli1</i>)	friend leukaemia integration 1
FLK (<i>flk</i>)	Foetal liver kinase
FLT (<i>flt1</i>)	fms related tyrosine kinase
gDNA	genomic DNA
GFP	Green fluorescent protein
HIF	Hypoxia inducible factor
hpf	hours post fertilisation
HRE	Hypoxia response element
ISV	Intersegmental vessels
JAG (<i>jag1</i>)	Jagged notch ligand
KDR (<i>kdr</i>)	kinase insert domain receptor
KDR-L (<i>kdr-l</i>)	kinase insert domain like receptor
LDH	Lactate dehydrogenase
M	Molar
mM	Millimolar
μ M	Micromolar
MABTw	Maleic acid buffer with tween 20 (0.1%)
MMP	Matrix metalloproteinases
MO	Morpholino
mRNA	messenger RNA
NICD	Notch intra-cellular domain
NO	Nitric Oxide
NOS	Nitric oxide synthase
NRARP (<i>nrarp</i>)	Notch regulated ankyrin repeat
NRP	Neuropilin

PBS	Phosphate buffered saline
PBT	Phosphate buffered saline with Tween
PCR	Polymerase chain reaction
PCV	Primary cardinal Vein
PFA	Paraformaldehyde
PHD3	Prolyl-hydroxylase 3
RNA	Ribonucleic acid
ROI	Region of interest
RT-PCR	Reverse transcription PCR
RT-qPCR	Reverse transcription – Quantitative PCR
SD	Standard deviation
SEM	Standard error of the Mean
TIE2	Tyrosine kinase with immunoglobulin-like and EGF-like domains
UAS	Upstream activating sequence
VEGF	vascular endothelial growth factor
VHL (<i>vhl</i>)	Von Hippel-Lindau
WISH	Whole mount in situ hybridisation
wt	wildtype

Parentheses show the the zebrafish genetic nomenclature in lower case italics (Mullins 1995) where mamallian or other genes are referenced the correct genetic nomenclature is used as per the convention for that organism.

Chapter 1 General Introduction

1.1 Hypoxic signalling

The molecular apparatus of cellular hypoxia regulation was first identified using an immortalised hepatic cell line. In this study it was demonstrated that reduction of oxygen tension resulted in increased synthesis of erythropoietin (EPO) mRNA (Goldberg et al. 1991). A novel nuclear factor was isolated which increased the expression of the *EPO* gene, this being the signalling molecule HIF-1, which was up regulated by hypoxia (Semenza & Wang 1992). Upstream binding of HIF-1 to the *EPO* promoter resulted in a fifty-fold increase in EPO transcription (Semenza & Wang 1992). Many other genes were subsequently identified which are regulated by HIF-1 including vascular endothelial growth factor (*VEGFA*) (Goldberg & Schneider 1994) and a number of glycolytic enzymes (Firth et al. 1994; Semenza et al. 1994). These transcriptional adaptations in the cell act as a response to changes in environmental oxygen and permit multiple types of cellular survival modifications, which enable the cell to survive periods of hypoxia.

1.1.1 Hypoxia inducible factor (HIF)

The HIF transcription factor is composed of two complementary subunits of the basic helix loop helix protein family (Semenza & Wang 1992; Wang et al. 1995). The HIF-1 β subunit is constitutively expressed and binds with the oxygen sensitive HIF-1 α subunit within the nucleus to form a functional transcription factor (see Figure 1.1). The HIF-1 α molecule is ubiquitously expressed and has a very short half-life of around five minutes in a normoxic environment. This rapid turnover and regulation is due to oxygen dependent enzymatic degradation by prolyl hydroxylase (PHD) and factor inhibiting HIF (FIH) enzymes and enables tight regulation of this signalling pathway (Figure 1.1 and 1.2) (Huang et al. 1996) and its downstream transcriptional effects (Lando, Peet, Gorman, et al. 2002a).

The binding domain for the HIF transcriptional complex is known as the HIF response element (HRE) and this region contains the five nucleotide binding sequence 5'-(A/G)CGTG-3'. Over seventy genes are under direct transcriptional control of this promoter (Wenger et al. 2005). In addition microarray data

suggests over 200 transcripts may be differentially regulated by HIF signalling via direct and indirect mechanisms (Elvidge et al. 2006; Lisy & Peet 2008). It has also been suggested that as much as 20% of the genome may show a transcriptional response to HIF binding (Mole et al. 2009) indicating the importance of this pathway in both cellular homeostasis and numerous disease states.

1.1.2 Regulation of HIF signalling

1.1.2.1 Prolyl hydroxylase enzymes (PHD)

HIF prolyl hydroxylases or prolyl hydroxylase domain proteins (PHD) are highly conserved dioxygenases, of which there are four isoforms in human tissues with the PHD1-3 enzyme isoforms regulating hydroxylation of the HIF molecule (Fong 2008). These enzymes are the main mechanism of oxygen sensing and subsequent HIF-1 α modification (Bruick & McKnight 2001). PHDs utilize oxygen and 2-oxoglutarate as substrates, with iron and ascorbic acid as co-factors to hydroxylate proline residues 402 and 564 of the HIF-1 α molecule (Ivan et al. 2001). The PHD enzyme has a very high affinity for oxygen but in the presence of all other co-factors, oxygen is the rate-limiting factor in its hydroxylation of the HIF-1 α residue (Fong 2008). The hydroxylation step facilitates the binding of HIF-1 α with the Von Hippel-Lindau protein (pVHL) thus targeting HIF for proteosomal degradation via the Ubiquitin E3 ligase system (Jaakkola et al. 2001) (see Figures 1.1 & 1.2 and section 1.1.2.3).

The PHD2 and PHD3 genes have been shown to contain HRE sequences so that stabilization of HIF-1 α due to hypoxia and the inactivation of the PHD3 enzymes results in up-regulation of these regulatory enzymes. This may act to facilitate rapid removal of excess HIF-1 α after re-oxygenation to avoid prolonged expression of target genes after hypoxia has resolved (Fong 2008).

1.1.2.2 Factor inhibiting HIF (FIH)

FIH functions in a similar manner to the PHD enzymes by hydroxylation of the HIF-1 α molecule although the amino acid residue is different it is found in the oxygen sensitive c-terminus activation domain (CAD) of the HIF-1 α protein

(Lando, Peet, Whelan, et al. 2002b). In normoxia FIH hydroxylates a highly conserved asparagine (851) residue in the HIF- α protein (Lando, Peet, Gorman, et al. 2002a; Fong 2009). Thus at normal oxygen tension transcription of HRE promoters is blocked due to failure of the HIF transcription factor to bind essential cofactors at the asparagine residue (Lisy & Peet 2008). Whereas the PHD3 enzymes regulate the availability of the HIF-1 α residue to bind to the HIF-1 β residue and activate transcription, the FIH hydroxylation blocks the binding of key transcriptional co-factors CBP/p300 (CREB binding protein) increasing target gene transcription. (Figure 1.3)

Some in vitro experiments have shown that FIH has a higher affinity for oxygen than the PHD family of enzymes suggesting that they (PHD) would lose catalytic function at a higher oxygen tension. FIH therefore retains some regulation over HIF mediated transcription at very low oxygen tensions (Figure 1.3) (Lisy & Peet 2008). As available molecular oxygen falls in the cell the PHD enzymes initially stabilise the HIF-1 α molecule enabling formation of the transcription factor, then further reduction of the oxygen tension activated FIH to enable full transcriptional activation via the binding of CBP/p300 co-factors (Lisy & Peet 2008; Lando, Peet, Gorman, et al. 2002a). The different targets of these oxygen sensitive hydroxylation enzymes targeting the HIF signalling molecule enable subtle regulation over this process and it's transcriptional output (Figure 1.3).

1.1.2.3 Von Hippel-Lindau protein (pVHL) and ubiquitin ligase degradation of HIF-1 α

The Von Hippel-Lindau tumour suppressor gene (VHL) binds hydroxylated HIF1- α and acts as a recognition component of a complex, which upon binding enables enzymatic ubiquitination and subsequent proteosomal degradation removing HIF-1 α rapidly from the cytosol. The proline residue hydroxylation by the PHD family of enzymes has been shown to block the binding of the pVHL which acts as an F-box like recognition element (Jaakkola et al. 2001). The ubiquitin ligase system involves several enzymatic steps which result in polyubiquitination of the substrate protein, in this case HIF-1 α , enabling

degradation by the 26S proteasome (Iwai et al. 1999). Essential to the effective ubiquitination are the co-factors which bind to pVHL includes elongin B and elongin C, Rbx1 and Cul2 which enables ubiquitination of HIF- α (Pause et al. 1997; Stebbins et al. 1999). Elongin B has been shown to be homologous to the ubiquitin molecule with in this complex, with elongin C, which has been shown to regulate some of the pVHL tumour suppressor activity (Stebbins et al. 1999). The complex formed by these co-factors and the VHL protein has homology to the SCF (Skp1-Cul1-F-box protein) which is known to target proteins for degradation (Stebbins et al. 1999).

The ubiquitination process is catalysed by the by a series of enzyme steps, the first of these involves activation of the ubiquitin by formation of a high energy bond with the E1 ubiquitin activating enzyme, utilising ATP. This is then transferred to a E2 ubiquitin conjugating enzyme, when this step occurs in the presence of an E3 substrate recognition complex the substrate protien is successfully ubiquitinated. The VHL protein has been shown to act as the critical recognition complex enabling specific ubiquitination of HIF-1 α . Repeated activation of this process leads to polyubiquitination of HIF- α which is targeted to the 26S ribosome for proteosomal degradation, rapidly removing intracellular HIF in normoxic conditions (Maxwell et al. 1999) (Figure 1.1 & 1.2).

Mutations in VHL lead to a number of tissue specific, highly vascularised tumours. These are as a result of HIF independent activity, including microtubule stability, cilia interaction, p53 transcription and cell survival signaling (Van Rooijen et al. 2009).

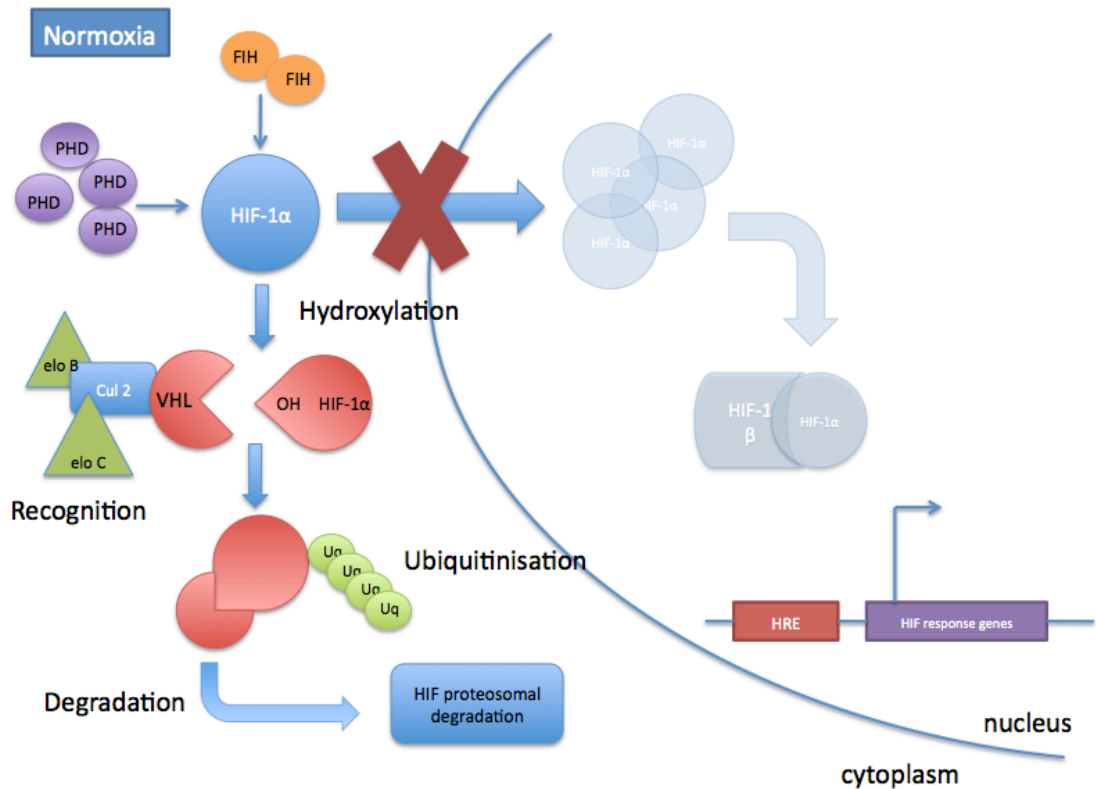


Figure 1.1. HIF signalling in the presence of normal cellular oxygen tension showing the hydroxylation of intracellular HIF-1 α and the proteosomal degradation via the ubiquitin ligase system in the cytoplasm.

Adapted from (Fong & Takeda 2010). In a normoxic environment the prolyl hydroxylase (PHD) and factor inhibiting HIF (FIH) enzymes hydroxylate specific prolyl and asparagine residues within the oxygen sensitive c-terminus of the HIF-1 α residue. This hydroxylation results in binding of the HIF-1 α to the Von Hippel-Lindau (pVHL) tumour suppressor protein, which acts as a recognition component of the Ubiquitin ligase proteasome degradation complex. This complex contains elongin B (elo B) and C (elo C) and the co-factor cullin 2 Cul 2) and enables rapid degradation of HIF-1 α in the presence of adequate cellular oxygen due to the oxygen dependent hydroxylation of HIF-1 α by the PHD and FIH enzymes.

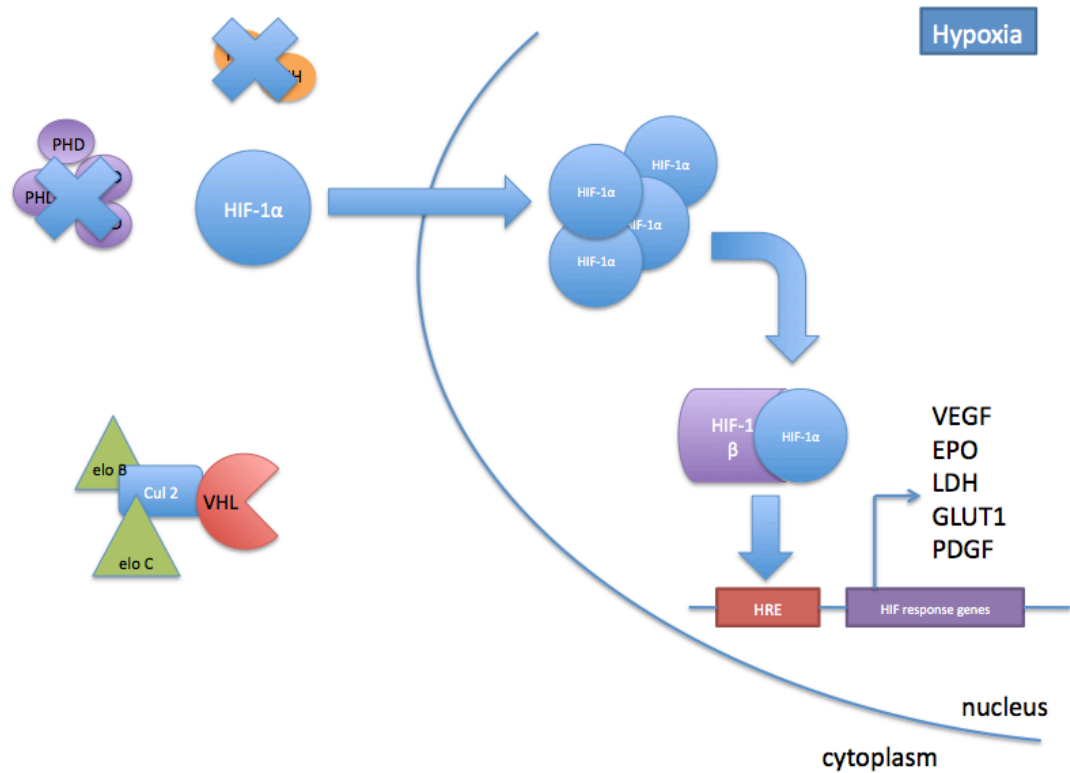


Figure 1.2. HIF signalling in the presence of cellular hypoxia and the effect on downstream response genes.

Adapted from (Fong & Takeda 2010) In a hypoxic environment the prolyl hydroxylase (PHD) and factor inhibiting HIF (FIH) enzymes are inactivated which results in accumulation of HIF-1 α in the nucleus. The absence of specific hydroxylated residues on the HIF-1 α protein blocks interaction with the VHL/ Cul 2/Elo B/Elo C complex. Stabilised HIF-1 α then translocates to the nucleus where it can associate with the constitutively active HIF-1 β subunit to form an active transcription factor, which binds to the HIF response element of target genes including those annotated to increase expression.

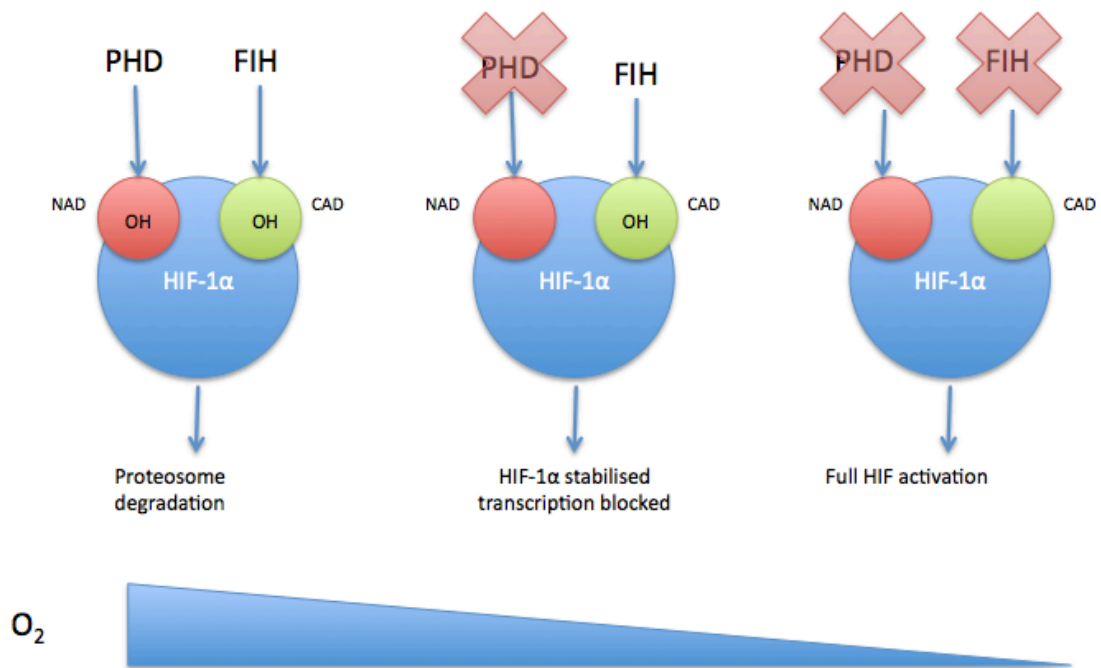


Figure 1.3. Sequential regulation of HIF-1 α by the PHD and FIH hydroxylation enzymes at reducing oxygen tensions.

This hypothesised sequential regulation of hydroxylation sites of the HIF-1 α residue enables a progressive activation and control over the activation of the HIF signalling system at different oxygen tensions. The N-terminal activation domain (NAD) is the specific site of PHD hydroxylation; the C-terminal activation domain (CAD) is the site for FIH hydroxylation essential for binding of the transcriptional co-factors CRB/p300 for full transcriptional activation. The differential regulation is based on the different affinities of the PHD and FIH enzymes for oxygen, only at the lowest oxygen tension is FIH blocked leading to full HIF transcriptional activation on binding to HIF-1 β . Adapted from (Lisy & Peet 2008).

1.1.3 HIF signalling and angiogenic growth factors

Hypoxia leads to the accumulation of the heterodimeric HIF1 transcription factor. This results in the expression of numerous genes, many implicated in angiogenesis (Rey & Semenza 2010). A number of angiogenic genes have been shown to contain a HIF response element (HRE), a DNA sequence motif that directly links the gene to the binding and activation by HIF 1 α . This includes: *VEGFA* (Liu et al. 1995), *VE-cadherin*, *ANG2* (Rey & Semenza 2010) and *VEGFR1 (flt1)*, all key elements in the angiogenic process. There are also genes which have been shown to be up regulated by hypoxia or HIF 1 α but lack a HRE motif, including *VEGFR2 (flk1)*, *PGDF-B*, *ANG1*, *MMP-9* and *TIE2* (Fong 2008). These genes may either be activated by transcription factors which are HIF dependent or may contain an unidentified HRE (Fong 2009). The activation of *VEGFA* and its receptor *VEGFR1 (flt1)* by HIF signalling is one of the earliest steps in activation of an endothelial adaptation to hypoxia in the form of angiogenesis (Gerhardt 2003).

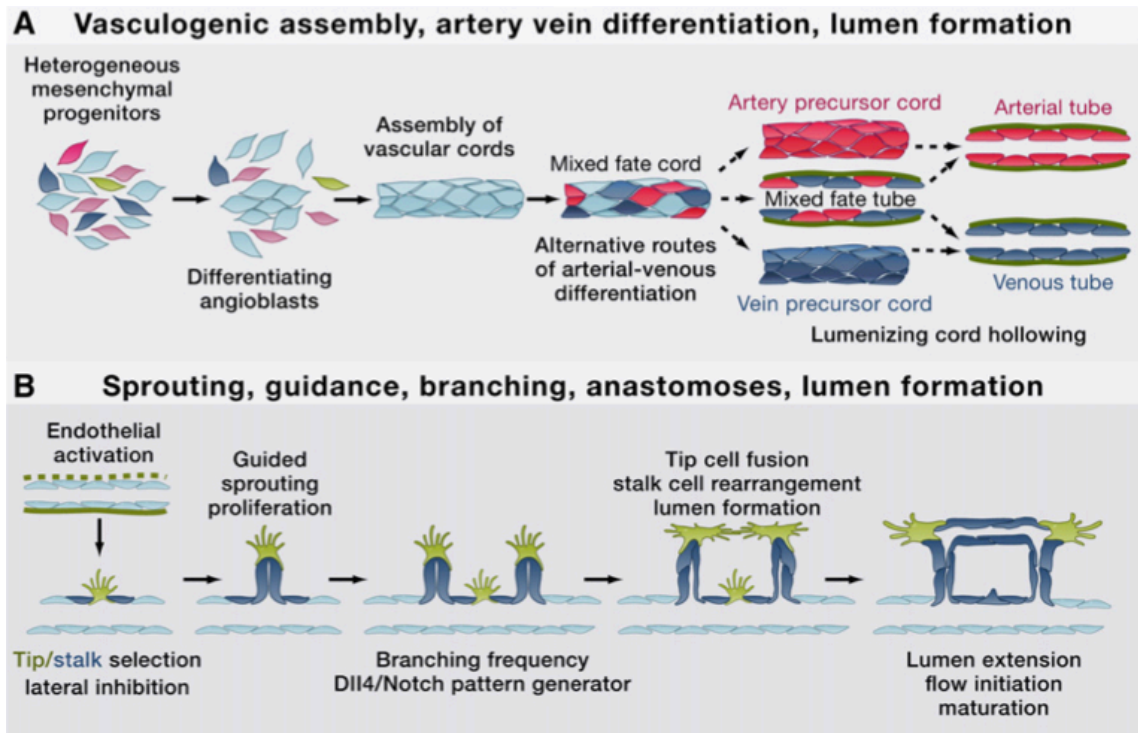


Figure 1.4. Schematic of differences between developmental vascular development (vasculogenesis) and the formation of new vessels from endothelial cell of an established vessels.

A. Mechanism for vasculogenic vessel formation from migrating angioblasts to form new vessels during embryonic development. **B.** New vessel formation by angiogenesis from established endothelial cells (Potente et al. 2011).

Reproduced with kind permission from Elsevier publishing.

1.2 Vascular development

Vasculogenesis is the formation of the primitive vascular system by the recruitment and differentiation of pluripotent mesenchymal cells into angioblasts. The angioblasts migrate under the control of VEGF-A and VEGFR2 to form the undifferentiated primitive vessels before differentiation into arteries or veins *in situ* (see Figure 1.4) (Carmeliet 2000).

1.2.1 Angiogenesis

Angiogenesis is the formation of a new vessel from the endothelium of a pre-existing vessel (Carmeliet & Jain 2011). This enlarges and builds upon the initial vascular network formed by vasculogenesis during embryonic development of the organism (Swift & Weinstein 2009) and aids formation of new organs and tissue by neovascularisation (Adams & Alitalo 2007). It is the plasticity of the endothelial cell which permits this effective reorganisation (Potente et al. 2011).

Given the critical role of blood vessels in maintaining oxygenation and nutrient supply, perturbation of vessel structure or function can lead to a number of diseases. Vessel overgrowth by angiogenesis is a key step in tumour development and retinal diseases, whereas vessel degeneration and occlusion can lead to strokes and heart disease (Carmeliet & Jain 2011).

1.2.2 Vascular endothelial growth factor

VEGF was identified as vascular permeability factor as early as 1983 (Senger et al. 1983) but subsequently renamed VEGF. There are now five isoforms characterised (VEGF-A, B, C and D and Placental growth factor) The ligands binds with the tyrosine kinase receptors (VEGFR1 / 2 and 3). In the mature vessel endothelial cells are maintained in a quiescent phase by the autochrine production of VEGF-A and other ligands including notch ligands, fibroblast growth factors (FGF) and angiopoietin-1 (ANG1) (Carmeliet & Jain 2011) The absence of this local VEGF-A production has been shown to lead to increased levels of endothelial apoptosis and dysregulation (Warren & Iruela-Arispe 2010).

Paracrine secretion of VEGF due to increased HIF production leads to activation of endothelial cells. This activation results initially in increased permeability of the endothelium and enlargement of the vessel. At the same time there is digestion of the basement membrane to enable endothelial cell migration by matrix metalloproteinases (MMP). This digestion of the basement membrane and removal of mural cells liberates angiogenic factors, which facilitate the differentiation of a tip cell (Arroyo & Iruela-Arispe 2010). This tip cell acts as the central focus of the angiogenic process, stimulated by local gradients of VEGF and co-ordinated at a cellular level by notch signalling (Potente et al. 2011).

1.2.2.1 Ligands and receptors in the zebrafish

In the zebrafish there are the same three VEGF ligands as described in the mammalian systems VEGF-A, B and C. However the tyrosine kinase receptor population contains an additional gene. The three receptors with orthologous mammalian genes are *flt1* (VEGFR1), *kdr* (FLK1 or VEGFR2) and *flt4* (VEGFR3), the *kdr-l* gene is thought to have existed prior to the teleost gene duplication. However it is thought that this fourth receptor was lost in mammalian (human and mouse) lineages (Bussmann et al. 2008).

1.2.3 Tip and stalk cell formation

VEGF-A gradients lead to the stimulation of a differentiated endothelial cell, known as the tip cell, by activation of the VEGFR2 receptor. The tip cell shows a number of behaviours which facilitate the modification of vascular networks. Tip cells are polarised and produce filopodia which respond to local guidance signals such as semaphorins, which act via the plexin receptors and the family of ephrin signalling molecules (Carmeliet & Jain 2011), to facilitate migration. These signals act to direct the mobile tip cell by repulsion or attraction to produce a vascular network (Childs et al. 2002; Torres-Vázquez et al. 2004) (Figure 1.5).

Stalk cells, also modified endothelial cells, form behind the tip cell by a process of lateral inhibition stimulated by Notch signalling (Jakobsson et al. 2010). Stalk cells proliferate to maintain contact with the motile tip cell and produce less

filopodia. The differentiation into a tip or stalk cell in the angiogenic sprout is not a fixed cell fate and alters continuously depending on levels of notch signalling and other local factors. It has been suggested that Notch signalling is the mechanism by which continuous branching and sprout elongation is regulated via the expression of Notch-regulated ankyrin repeat protein (Nrarp) and induction of local Wnt signalling (Phng & Gerhardt 2009). The stalk cell must also form the vascular lumen to enable blood flow and undergo complex reorganisation to form an effective vessel (Herwig et al. 2011; Blum et al. 2008). In addition these cells must form tight junctions with surrounding cells and produce a basement membrane to form a stable and effective vessel (Jain 2003) (Figure 1.5).

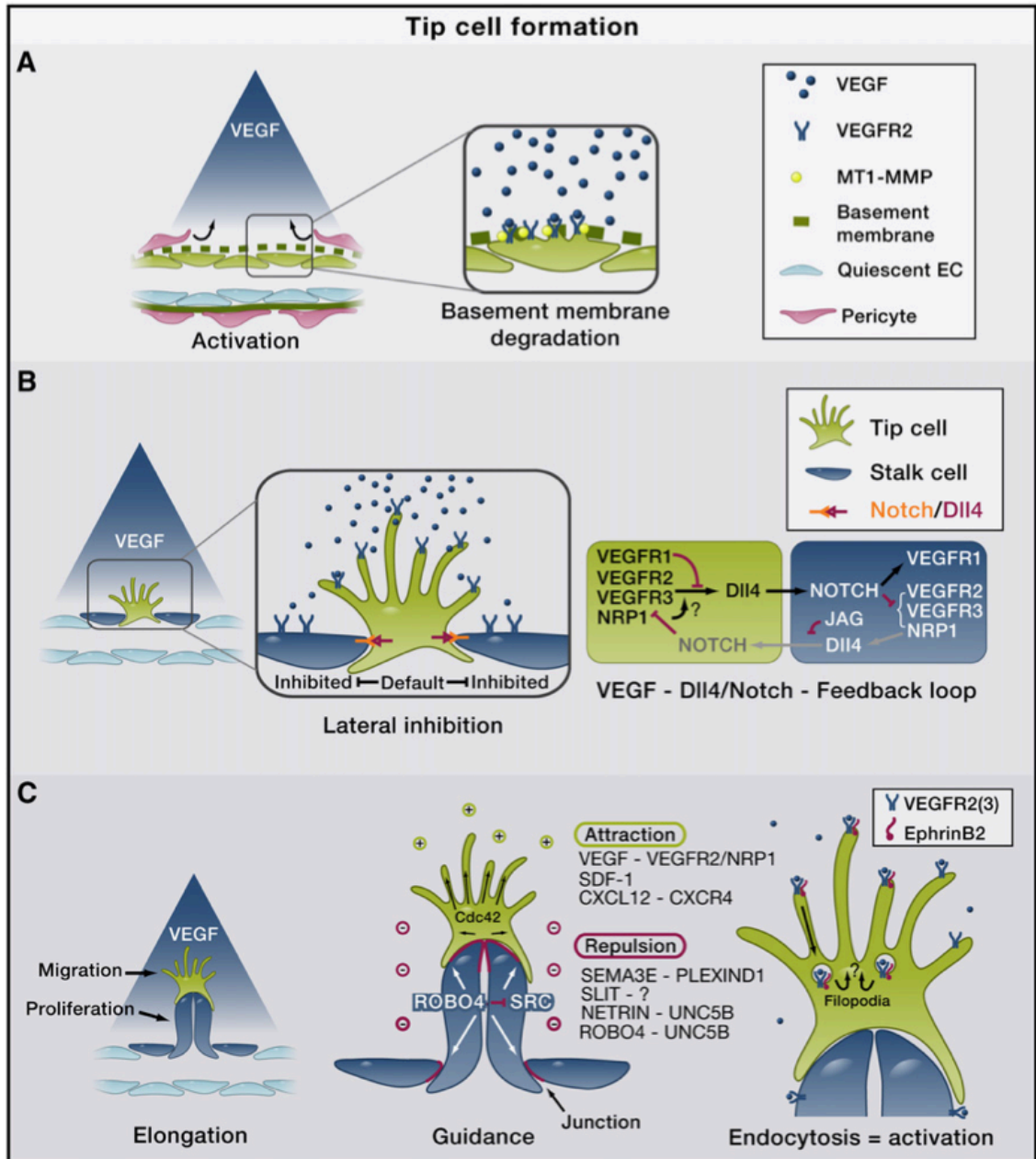


Figure 1.5 Endothelial differentiation into tip and stalk cells during angiogenesis and its molecular regulation.

A. Initial endothelial activation from mature quiescent vessel in the presence of VEGFA. B. Selection of a tip cell and the lateral inhibition of adjacent cells to stalk cell fate by notch signalling. C. Maintenance and guidance signals for elongation and activation of the angiogenic sprout. (Potente et al. 2011)

Reproduced with kind permission from Elsevier publishing.

1.2.4 Haemodynamic flow and the regulation of angiogenesis

There is a large body of literature on the importance of haemodynamic flow signals and particularly shear stress in endothelial maintenance and pathology (Reneman et al. 2006; Davies 2008). The majority of this data is derived from endothelial cell culture experiments using flow chambers to look at migration, polarity, growth and endothelial gene expression in different, “flow” environments. Although this data provides numerous insights into the effect of shear stress on the endothelial cell it doesn’t address the role of associated vessel cell types like pericytes and smooth muscle on endothelial behaviour in the more complex *in vivo* environment (Egginton 2011). In addition it is only possible to study the effects of shear stress in isolation on the endothelium where clearly in the *in vivo* situation other physical forces and physiological signals are constantly modifying the endothelial response (Hoefer et al. 2013). In the field of arteriogenesis research there is data demonstrating the increases in endothelial cell numbers in response to increased axial force or radial distension as an initiating factor for sudden recruitment of primitive arterial channels (Hoefer et al. 2013).

There remains very little data on the role of haemodynamic flow on angiogenesis despite the increasing amounts of data on its effects on endothelial expression, behaviour and phenotype. Research using the chick embryo as a developmental model has shown the role of flow on arterial and venous specification during developmental angiogenesis (le Noble et al. 2008). In these experiments the authors were able to show that circulatory flow in an *in vivo* model is able to regulate various aspects of angiogenic remodelling including fusion of primitive vessels and shear stress directed guidance of developmental angiogenesis (le Noble et al. 2008).

Using the zebrafish model it has also been shown that flow in the developing intersegmental vessels regulates the arterial of venous specification after vasculogenesis and onset of cardiac contraction with subsequent flow (Isogai 2003). Their data indicates that flow is important in the production of a balanced complement of arterial and venous intersegmental vessels. More recent data has shown that haemodynamic flow and intact VEGF signalling is required for

effective formation of the dorsal longitudinal plexus which forms by a process of angiogenic sprouting and endothelial regression to form effective circulatory loops from the intersegmental vessels (Zygmunt et al. 2012).

Additional data utilising the zebrafish to study *in vivo* angiogenesis have shown that flow has a role in the angiogenic behaviour of developing vessels in the hindbrain of the developing zebrafish. This particular vascular territory utilises the chemokine receptor CXCR4a as an endothelial signal to switch off the angiogenic programme in these vessels (Bussmann et al. 2011). This study showed that this flow dependent signalling pathway is not present in the trunk vessels of the same embryos indicating different regulatory pathways in the development of different vascular beds.

Despite these studies and those describing the effects of flow on endothelial cells to date only one paper has described a regulatory signalling pathway by which developmental angiogenesis is regulated in the zebrafish embryo. There is no available data on the role of flow on pathological or hypoxic driven angiogenesis in the *in vivo* environment. The paper by (Nicoli et al. 2010) using the zebrafish identifies a flow dependent aortic arch vessel which requires flow to form by a process of angiogenesis after the onset of circulation. They identified a microRNA (miRNA-126), which regulates the response of the endothelium to localised VEGF-A gradients in the presence of flow. Their experiments showed that the endothelium of this specific developmental vessel in the presence of flow increase the zinc finger transcription factor *kruppel like factor 2a* (*klf2a*). This transcription factor has been shown to regulate endothelial expression in response to flow in other *in vivo* and *in vitro* models (Lee et al. 2006). The upregulation of *klf2a* in response to flow increases levels of miRNA-126 suppresses expression of *spred1* which inhibits angiogenesis (Nicoli et al. 2010).

The available data on flow dependent angiogenesis in the *in vivo* environment indicates that there is likely to be different regulatory pathways at work in endothelial cells in response to the physiological stimuli to regulate physiological angiogenesis (Bussmann et al. 2011). It therefore doesn't seem

unreasonable to suspect that different processes of spatial and temporal regulation of angiogenesis might be further altered by transduction of physical forces by the endothelial cell in pathological angiogenesis.

1.3 Notch signalling

The Notch signalling system is a pathway by which cells interact with external signals and integrate them into a coordinated developmental response by regulation of differentiation, proliferation and apoptosis. Components of this pathway have been conserved from nematodes to humans indicating its importance in development. This signalling pathway was originally identified in *Drosophila* over eighty years ago when it was noted that haploinsufficiency of the Notch gene leads to a notched appearance of the developing wing (Artavanis-Tsakonas et al. 1999).

1.3.1 Canonical notch signalling

On the surface of “signalling” cells a transmembrane Notch ligand is expressed. In mammals there are five ligands (Delta-like 1,3 & 4, Jagged 1 & 2) of the delta/serrate/LAG-2 family. These ligands binds to a Notch receptor expressed on the membrane of an adjacent or “receiving” cell (Bray 2006). Activation of the notch receptor leads to sequential cleavage by the ADAM and γ -secretase enzymes at the cell membrane. This yields an extracellular domain fragment (NECD), which is targeted by the ligand-expressing cell for internalisation and lysosomal degradation. The Notch intracellular domain (NICD) translocates to the nucleus of the receiving cell where it associates with the CBF1/Suppressor of Hairless/LAG-1 (CSL) protein in the presence of the Mastermind-like (MAML) protein to form a transcription factor complex which drives expression of the Notch immediate target genes (Andersson et al. 2011). In the absence of NICD the CSL complex inhibits transcription due to binding of a repressor, which is displaced by NICD (Pursglove & Mackay 2005; Phng & Gerhardt 2009).

This relatively simple Notch core-signalling pathway has no amplification step or phosphorylation in its signalling pathway, which means that the level of ligand signal determines the output in the receiving cell. This is unusual in the highly

conserved intracellular signalling pathways like Wnt, JAK/STAT, PI3K/AKT, and Hedgehog, all of which contain amplification steps (Andersson et al. 2011). Despite the relatively simple components of the core-signalling pathway extensive research has identified numerous auxiliary proteins, which modulate this signalling pathway but are dependent on the timing and cell type in which the pathway is active. This complex modulation system enables the diverse effects and spatial responses of Notch signalling (Andersson et al. 2011; Artavanis-Tsakonas et al. 1999).

1.3.2 Non-canonical Notch signalling

In addition to the modification of the canonical Notch signalling pathway by accessory proteins there is also additional evidence that non-canonical pathways exist which are capable of activating notch target genes but not by the traditional activation of the Notch receptor and cleavage of the NICD (Martinez Arias et al. 2002). These non-canonical pathways may facilitate cross-talk of other developmental intracellular signalling pathways, like hedgehog and Wnt to integrate environmental cues into organised cellular responses (D'Souza et al. 2010).

1.4 Effects of Notch signalling on endothelium and vascular development

Endothelial cells express the Notch ligands Dll1, Dll4, Jagged-1 and Jagged-2 along with the Notch receptors Notch-1 and Notch-4. Notch signalling has been shown to influence a variety of endothelial behaviours and cell fate decisions (Iso 2003).

1.4.1 Vasculogenesis

One of the earliest developmental effects of Notch signalling, in concert with VEGF-A during early development is the migration and maturation of angioblasts (Flamme et al. 1995) to form the primitive vascular system, a process known as vasculogenesis (Roca & Adams 2007). After migration of pluripotent angioblasts there is early differentiation into arterial and venous

fates even before onset of circulation. During zebrafish development, changes in *notch* (Lawson et al. 2001) or the ligand *dll4* (Leslie et al. 2007; Siekmann & Lawson 2007a) result in abnormal arterial and venous cell fate (Phng & Gerhardt 2009). Further evidence for the role of notch signalling in arterio-venous fate are found in two zebrafish mutant lines: In the *mindbomb* mutant there is a mutation in the delta ubiquitin ligase which inhibits Notch signalling leading to arterio-venous abnormalities (Lawson et al. 2001). This is replicated in the *gridlock* mutant which has a mutation in the downstream Notch transcription factor ortholog of HEY2 which results in a loss of arterial cell fate of the developing aorta with characteristic arterio-venous malformations (Zhong et al. 2001).

1.4.2 Angiogenesis

Suppression of Notch signalling by treatment of zebrafish embryos with N-[N-(3,5-Difluorophenacetyl)-L-alanyl]-S-phenylglycine t-butyl ester (DAPT), a γ -secretase inhibitor, results in inhibition of Notch signalling and increased number of filopodia due to blockade of *dll4* (Leslie et al. 2007). Whereas binding of the alternative Notch ligand Jagged1 in the mouse retinal endothelial model blocks filopodia production due to competition with the Dll4-Notch1 ligand-receptor complex (Benedito et al. 2009). The Notch pathway also influences proliferation of endothelium to facilitate angiogenesis, vessel migration and lumenisation. Activation of the Notch signalling pathway leads to inhibition of endothelial cell division in mouse, zebrafish and cell culture (Phng & Gerhardt 2009).

Studies by (Siekmann & Lawson 2007b) in the developing zebrafish showed that knockdown of both *dll4* and the recombining binding protein suppressor of hairless (*Rbpsuh*, ortholog of CSL) resulted in an increased tip cell phenotype in the developing intersegmental vessels of the embryos. Endothelial cells with over-expression of notch show reduced migration of cells into a tip cell position. An excess angiogenesis was also seen in the zebrafish embryo after knockdown of the Notch receptor *notch1b* (Leslie et al. 2007). Transplant experiments in the zebrafish vasculature demonstrated cells with induced over

expression of the NICD are less likely to migrate to a tip cell position (Siekman & Lawson 2007b).

Increased notch signalling acts on endothelial cells to suppress the angiogenic phenotype by reducing motility, and the production of filopodia characteristics of a tip cell, specified by reduced levels of notch signalling (Phng & Gerhardt 2009).

1.4.2.1 Tip and stalk cell selection and notch signalling

An increase in *dll4* expression is seen in tip cells, with increases in Notch expression a feature of stalk cells in the ISV and DLAV of the developing zebrafish vasculature (Leslie et al. 2007). Genetic knockdown of Dll4 has been shown to increase number of tip cells, filopodia and genes expressed in tip cells; FLT4, VEGFR2 and PDGF in endothelial cell culture and mouse retinal studies (Hellström et al. 2007). The key regulator of tip cell behaviour has been shown to be the ligand Dll4 (figure 1.5 and 1.6); this ligand drives many of the adaptations and expression patterns which define a tip cell. Dll4 also induces lateral inhibition which determines the behaviour and fate of the trailing stalk cells (Phng et al. 2009). In the developing zebrafish vasculature defective *dll4* signalling results in aberrant angiogenesis in the presence of a functional *vegfaa* gene. Although initial sprouting angiogenesis is preserved there appears to be no off switch when the stereotyped vascular circuits are completed (Childs et al. 2002; Leslie et al. 2007).

1.4.2.1.1 MicroRNA regulation of the DLL4 notch ligand

Although the role of DLL4 has been extensively studied in relation to angiogenesis and its regulation of tip cell selection little was known until recently about how the levels of DLL4 are regulated in endothelium. Studies by (Bridge et al. 2012) using cultured lymphatic endothelial cells and transgenic zebrafish embryos have shown a role for the microRNA-30 family in the regulation of DLL4. Increased levels of mirRNA-30b and c in the developing zebrafish embryo phenocopied the effect of *dll4* MO knockdown on the ISV and DLAV, resulting in increased sprouting and migratory activity. This mirRNA-30 effect was partially rescued by co-injection of a target protector blocking the

mirRNA site of the upstream transcriptional region (UTR) of *dll4* (Bridge et al. 2012).

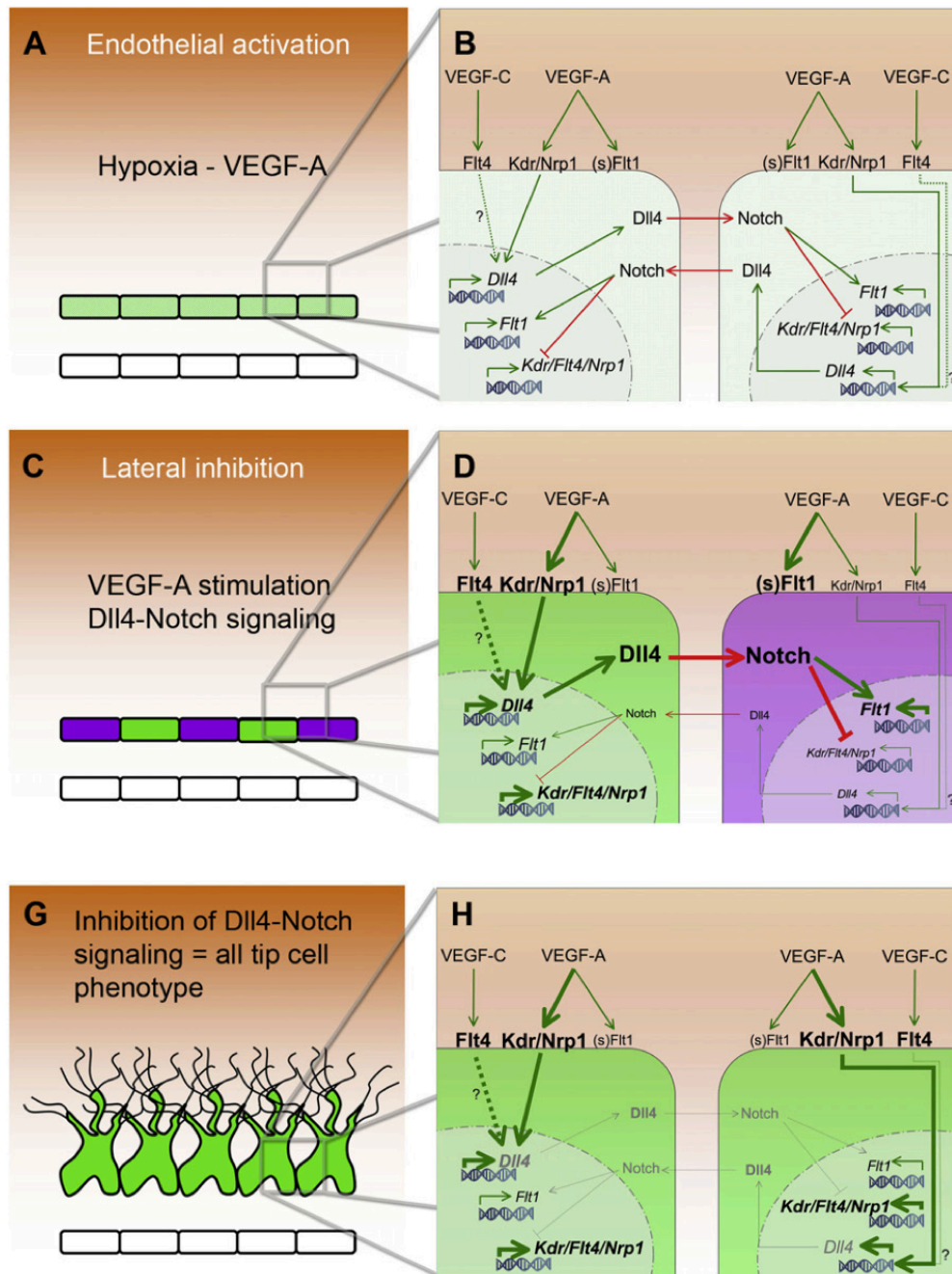


Figure 1.6 Endothelial notch signalling determines tip and stalk cell fate.

The figure shows an current scheme for the mechanism by which endothelial tip and stalk cell fate is determined based on data from cell culture, zebrafish and murine retinal angiogenic models. **A.** Simplified 2D diagram of endothelium

forming a quiescent vessel, with stimulating factors for angiogenesis in terms of hypoxia and the production of local gradients of VEGF-A. **B.** The cell – cell Notch signalling in the quiescent vessel isn't activated, the key signalling factors are indicated in this schematic but with no activation. (Activation of a signal is shown in bold text and arrows inhibition is shown with red termination lines) **C & D.** The increase in local VEGF-A activates the KDR receptor on the endothelial cell which in turn leads to the transcription and expression of the notch ligand on the membrane of the activated tip cell (green endothelial cell). This ligand binds to the notch receptor on adjacent endothelial cells activating the expression of soluble FLT1 on the stalk cells (purple endothelial cells), this results in binding of the VEGF-A ligand without activation of downstream transcriptional targets reducing the sensitivity of these stalk cells to the VEGF-A gradient. This process allows for the selection of tip cells and the subsequent suppression of additional tip cells with the activation of a stalk cell fate. **D.** The levels of expression of Dll4, Notch1, VEGF ligands and receptors determine tip cell fate. **G & H.** In experiments where notch signalling is inhibited either by chemical treatment or my genetic knockdown of the notch ligand DLL4 this leads to all endothelial cells becoming tip cells, in the presence of a VEGF-A gradient. Adapted from (Phng & Gerhardt 2009) reproduced with kind permission from Elsevier.

1.5 Nitric Oxide (NO) signalling

Nitric oxide is a key signalling molecule in vascular biology. Since its identification there has been extensive study of this molecule and its role in all aspects of vessel biology and disease (Sessa 2009). NO was initially identified as endothelial derived relaxation factor, released by endothelial cells in response to acetylcholine and shear stress in preparations of rabbit aorta (Furchgott & Zawadzki 1980; Palmer et al. 1987).

1.5.1 NO and vessel biology

NO is synthesised from L-arginine by the highly conserved nitric oxide synthase family of enzymes. The NO produced by endothelial NOS (eNOS) diffuses into the adjacent smooth muscle in the artery where it activates guanylate cyclase to synthesise cGMP resulting in arterial dilatation via modification of calcium flux and potassium channels (Yu et al. 2002). In addition to the regulation of arterial tone eNOS and NO have been shown to be critical to the correct embryonic development of cardiac valves, structures and arteries (Liu & Feng 2012). In addition to a role in correct developmental cardiac patterning NO has been shown to be a critical factor in vasculogenesis and angiogenesis.

Recent data has shown that VEGF-A signalling in the developing mouse embryo modifies NO signalling which alters proliferation of angioblasts, influencing vasculogenesis (Gentile et al. 2013). It is suggested that VEGF receptor activation in the developing mouse embryo results in the phosphorylation of a serine residue in expressed eNOS. This occurs in populations of primitive angioblasts and embryonic endothelial cells altering levels of proliferation in cells which produce primitive vessels (Gentile et al. 2013).

There is also a role of NO on vascular permeability, which has been studied as a co-factor to early VEGF-A induced permeabilisation of endothelial cells during the initiation of angiogenesis. It has been suggested that endothelial NOS may be a key early regulator of the VEGF-A induced vascular permeability which is a hallmark of early angiogenesis (Sessa 2009). In addition to modulation of flow

NO maintains stability and health of the endothelium of the vessel wall (Sluimer & Daemen 2009).

The role of NO as a signalling molecule in vascular development is a huge area of research but it is becoming increasingly apparent that the regulation of flow has indirect effects on other embryonic developing systems. Recent studies in the zebrafish showed that blood flow and vessel regulation by NO and other signalling factors is key to the migration of haemopoietic stem cells (North et al. 2009). These cells are also involved in the correct patterning of the angiogenic blood vessels of the somites and arterial and venous fate decisions in concert with VEGF, Hedgehog and Notch signalling (Wilkinson et al. 2012).

1.6 Zebrafish as a model of vessel development and vascular disease

The zebrafish (*Danio rerio*) is a small freshwater fish that originates from Southern Asia and the Indian sub-continent. The adult can grow to 4cm in length and lives between three and five years. The zebrafish was initially used in the 1930's as a classical embryonic and developmental model. However this model has become a powerful tool with which to study vessel development and behaviour (Chico et al. 2008).

In terms of cardiovascular development, the zebrafish forms a rudimentary circulation by twenty-four hours (Isogai 2003); aorta, cardinal vein and erythrocytes can be easily visualised using microscopy at this stage and then the continuing vascular development (Isogai et al. 2001). Another unique advantage of the embryonic vasculature of this model is that the embryo does not require circulation for oxygen delivery (Pelster & Burggren 1996) (maintained by oxygen diffusion), which means lethal cardiovascular abnormalities in other organisms can be tolerated and the effects assessed using zebrafish.

A number of non-invasive techniques have developed, which take advantage of the optical clarity of the embryo to obtain detailed information about the

developing circulation (Chico et al. 2008). The vascular system demonstrates similar molecular signals and functional conservation with the human circulatory system (Lieschke & Currie 2007) despite differences such as a lack of pulmonary circulation.

1.6.1 Advantages of the zebrafish for vascular research

Female zebrafish produce eggs from three months of age and lay up to three hundred eggs a week. The combination of this fecundity and the low costs of maintenance compared to other animal models makes it an attractive organism for biomedical research (Chico et al. 2008; Lieschke & Currie 2007).

1.6.1.1 Optical clarity and imaging

The large lays of eggs develop externally after fertilisation, enable non-invasive study of embryonic development. The developing embryo is transparent which enables visualisation of numerous developmental processes including: Organogenesis, vasculogenesis, cardiac contraction, angiogenesis and inflammation by microscopy (Lieschke & Currie 2007). When combined with transgenic zebrafish lines this enables the study of these processes *in vivo* and over time in the same individual. This repetitive observation is a particular advantage in the study of vascular development and adaptation. A particularly striking example of these unique advantages is the real time *in vivo* interactions and behaviours of individual endothelial cells during angiogenesis (Jakobsson et al. 2010).

1.6.1.2 Genetic tractability and manipulation

Over the last twenty years there has been massive development in genetic manipulation techniques and sequencing of the zebrafish genome making the organism highly genetically tractable (Sprague et al. 2006).

1.6.1.2.1 Transgenesis

Non-homologous modification allows generation of transgenic zebrafish. Recent techniques using the Tol2 transposon, a genetic sequences which can relocate within an organisms genetic code, have enhanced the generation of transgenic lines. Using this specific transposons and the transposase enzyme techniques

have been developed to insert multiple copies of the flanked genes and reporter constructs into the host genome (Kawakami 2004). These modifications have made it simpler and quicker to produce transgenic lines and as a result, enormous numbers of different reporter lines now exist.

With relevance to the study of vessel biology, transgenic lines exist which specifically label endothelial cells (Lawson & Weinstein 2002) with green fluorescent protein (GFP). The Friend leukaemia integration 1 transcription factor (*Fli1*) a proto-oncogene has been shown in the embryonic zebrafish and mouse to be expressed in predominately endothelial cells resulting in its use as an endothelial promoter to produce a vascular reporter transgenic (Mélet et al. 1996; Lawson & Weinstein 2002). More recently lines which label only a specific endothelial cell region (such as membrane or nucleus) or subset of endothelium such as arterial or venous cells can be generated and combined in the same organism to provide useful insights into the dynamic process of vessel formation within the model organism (Herwig et al. 2011; Zygmunt et al. 2012).

1.6.1.2.2 Forward genetic manipulation of the zebrafish

Forward genetic techniques have provided large numbers of mutant lines with identified genetic mutations and developmental phenotypes which have been used for the study of many human genetic conditions (Wienholds et al. 2003). These screens produce groups of phenotypically similar mutants and the ease of observation of the developing embryo using simple optical microscopy and identification of mutations by targeting induced local lesions in genomes (TILLING) has increased the number of stable mutants with characterised gene defects (Lieschke & Currie 2007).

1.6.1.2.3 Reverse genetic techniques in the zebrafish

Several techniques for production of stable mutant lines now exist using a reverse genetic approach including zinc finger (Sander et al. 2010) or TALEN targeted mutagenesis (Bedell et al. 2012). These techniques enable the relatively rapid mutation of a gene of interest.

1.6.1.2.3.1 Morpholino antisense oligonucleotide

Transient genetic knockdown in the developing zebrafish embryo can be achieved using injection of these modified RNA sequences (Bill et al. 2009). The modification of the MO nucleotide backbone stabilises the construct protecting it from degradation. The MO is injected into the 1-4 cell fertilised embryo and results in a transient translational block of an mRNA target. There are no endogenous enzymes to degrade MO residues and it is thought that the effect is diluted by cellular division, by 3 dpf in the zebrafish embryo, although some reports have shown effects as late as 5 dpf (Bill et al. 2009). The MO can be designed against either an ATG start site or various splicing sites. Despite the low cost and relatively easy targeting of morpholinos for gene knockdown the technique is not without its limitations: Certain morpholinos have been shown to induce cell death by a process of p53 activation, which can lead to off target effects in the embryo. Due to difficulties with the zebrafish and the production of antibodies for Western blotting this makes it difficult to demonstrate that genetic knockdown results in protein loss. It is possible in some situations incomplete knockdown by MO may still result in biologically relevant amounts of protein, which are then impossible to quantify. Accepting these limitation this technique still provides an effective screening tool of targeted reverse genetics in a short time period and at relatively low cost (Eisen & Smith 2008; Lieschke & Currie 2007).

1.7 The *vhl* homozygous (*vhl*^{-/-}) mutant zebrafish

The *vhl*^{-/-} mutant zebrafish was identified from an ethyl-N-nitrosourea (ENU) mutation library which was screened *in silico* for targeted mutations using the Hubrecht TILLING protocol (Wienholds et al. 2003). This mutant has nonsense mutation within the HIF-1 α binding domain; the *vhl*^{hu2117} line has an inactivating germline mutation as a result of a C/T substitution on chromosome 6 at position Q23X within the zebrafish *vhl* orthologue. Given that the mouse knockout of *vhl* results in embryonic lethality and limited homology to the human disease (Haase 2005; van Royen et al. 2009), this mutant line has provided a useful tool with which to study function of this gene.

Two lines were identified from this screen carrying mutations in the zebrafish ortholog *vhl*, both being nonsense mutations in the HIF binding domain. These alleles are loss of function mutations as no VHL protein can be detected on western blots of homozygous mutants (*vhl*^{-/-}) (Van Rooijen et al. 2009). The zebrafish ortholog *vhl* encodes a single transcript for a 175 amino acid protein, which is 52% identical and 70% similar to human VHL. The key binding domains of this protein are highly conserved compared to human including the Elongin C and HIF-1 α domains essential for hypoxic signalling (Van Rooijen et al. 2009).

The *vhl*^{-/-} zebrafish mutants demonstrate numerous features of up regulated hypoxic signaling induced by HIF. Whole mount *in situ* hybridization experiments indicate up-regulation of *phd3*, lactate dehydrogenase (*ldh*), *epo* and *vegf* mRNA; all classical HIF target genes (Weidemann & Johnson 2008; Van Rooijen et al. 2009). The mutants also demonstrate changes in behaviour consistent with increased hypoxia signaling including hyperventilation.

In addition to behavioural and molecular adaptations the mutant embryo has developmental adaptations of the cardiovascular system. They have similar heart rates to wild type siblings (wt sib) at 4 dpf although after 7 dpf the mutant heart rate is higher until 10dpf (Van Rooijen et al. 2009). Zebrafish cardiac output would be expected to fall during early development in a wild type embryo (Schwerte et al. 2003); in the mutant there is a 3.2-fold increase in cardiac output at 4 dpf and 15-fold increase at 10 dpf. This results in cardiomegaly, oedema and high output cardiac failure leading to death of the homozygous embryo at between 8 and 11 dpf (Van Rooijen et al. 2009).

1.7.1 Vascular phenotype of the *vhl*^{-/-} mutant zebrafish

Vascular endothelial growth factor is a key initiator and regulator of all forms of angiogenesis (Yancopoulos et al. 2000), however many other signaling molecules are able to influence the developing vessel. The *vhl*^{-/-} mutant shows increased expression of *vegfaa* (ortholog of mammalian *VEGFA*), due to the up regulation of HIF signaling. The mutant also demonstrates up regulation of receptors for *vegfaa* (Van Rooijen et al. 2010) including *kdr* and *kdrl* in the liver,

kidney, glomerulus and *kdr* in developing blood vessels, indicating potentially higher sensitivity to *vegfa* (Van Rooijen et al. 2009).

Initial patterning of the vasculature in the *vhl^{-/-}* mutant is normal, but an increase in cranial vessels is present as early as 58 hpf. By 4 dpf there are clear differences in numerous vascular territories. Increased angiogenic sprouting from Intersegmental vessels (ISV) is detectible at 3.5 dpf and 5.75 dpf but although a qualitative description of these differences has been described only a detailed description of the retinal vessels has been published (Van Rooijen et al. 2010).

This vascular phenotype seen after 58 hours in the *vhl^{-/-}* mutant has been shown to be *vegfa* (*aa/ab*) dependent and the areas of greatest angiogenesis correlate with the highest levels of *vegfa*. By administering a *kdr* tyrosine kinase inhibitor from 58 hpf for 3 days formation of new vessels was blocked in the mutant. This demonstrates that up-regulation of the *vegfa* pathway is likely to be the dominant signal in activating the pro-angiogenic phenotype in this mutant (Van Rooijen et al. 2010). This model of pathological angiogenesis is consistent with the established literature which shows that VEGF-A is essential for paracrine activation of endothelial tissue and also stimulation of the endothelium to divide and form new vessels (Carmeliet & Jain 2011) as previously described.

1.8 Aim of my research

My aim is to characterise the aberrant angiogenesis and mechanisms underlying the initiation and maintenance of these vessels in the *vhl* homozygous mutant zebrafish.

1.9 Hypotheses

The aberrant vasculature seen in the *vhl*^{-/-} mutant zebrafish is initiated by tip and stalk cell differentiation with classical features of angiogenesis.

The aberrant vessels of the mutant *vhl*^{-/-} zebrafish are dependent on haemodynamic force for initiation.

The aberrant vessels of the mutant *vhl*^{-/-} zebrafish are a result of reduced notch signalling which produces increased levels of angiogenesis in the presence of *vegfaa/ab*.

The aberrant vessels of the mutant *vhl*^{-/-} zebrafish are dependent on haemodynamic force for initiation.

The aberrant vessels of the mutant *vhl*^{-/-} zebrafish are dependent on the presence of nitric oxide for initiation and maintenance and that this molecule mediates endothelial flow detection in the mutant.

1.10 Objectives

I am to test these hypotheses by completing the following experimental objectives:

- Characterise and quantify differences in the vessels and the angiogenic phenotype of the *vhl*^{-/-} mutant.
- Identify differences in endothelial cell number in the *vhl*^{-/-} mutant and wild type siblings.
- Identify if the differences in endothelial number is due to increases in proliferation or apoptosis.

- Assess the effect of changes in circulating volume and red cell density in the *vhl*^{-/-} mutant on the angiogenic phenotype.
- Manipulate haemodynamic flow in the angiogenic vessels of the *vhl*^{-/-} mutant to assess its effect on angiogenic sprouting and endothelial number.
- Identify if the aberrant angiogenesis of the *vhl*^{-/-} mutant is lumenised early in development.
- Assess the role of NO signalling in the transduction of flow in the endothelium of the developing zebrafish.
- Identify differential regulation of notch signalling components in endothelial cells in response to changes in circulatory flow.
- Manipulate notch signalling in an attempt to regulate flow sensitive angiogenesis in the *vhl*^{-/-} mutant.

Chapter 2 Materials and Methods

2.1 Zebrafish husbandry

2.1.1 Adult zebrafish maintenance

Adult zebrafish were maintained in accordance with UK Home office regulations, under project licences 40/3434 and 40/3082 issued to Dr T. J. Chico and Dr F. van Eeden. All experiments were performed under these project licences and my personal licence 40/9855. The adult fish were maintained as per standard protocols (Nüsslein-Volhard & Dahm 2002). Adult fish were housed in a recirculating aquarium system with a water temperature of $28\pm 1^\circ\text{C}$, and a 14:10 hour light/dark cycle. Adults were fed *Artemia nauplia* larvae and maintained at a maximum density of five fish per litre of aquarium water.

2.1.2 Zebrafish strains

Experiments utilising wild type zebrafish were performed with AB or London wild type (LWT) strains.

2.1.2.1 Mutant zebrafish lines

The *vhl* mutant zebrafish line was obtained from the Hubrecht institute (Netherlands) and all experiments were performed with the *vhl*^{hu2117} (C/T Q23X) mutant allele (Van Rooijen et al. 2009).

2.1.2.2 Transgenic vascular reporter lines

The *vhl*^{hu2117} line was crossed to the following vascular reporter lines to study the vascular phenotype in detail: *Tg(fli1:eGFP)* (Lawson & Weinstein 2002) which labels endothelial cytoplasm, *Tg(flkl1:EGFP-NLS)* (Blum et al. 2008) which labels endothelial nuclei, *Tg(kdrl:HRAS-mCherry)*^{s916} (Hogan, Bos, et al. 2009a) which labels the endothelial cellular membrane with red fluorescence. A dual reporter line was also raised with both *Tg(kdrl:HRAS-mCherry)*^{s916} and *Tg(flkl1:EGFP-NLS)* in the *vhl*^{hu2117} mutant background, enabling endothelial behaviour and quantification to be assessed in the same line. The *Tg(fli1:eGFP)* line was crossed with a fluorescent erythrocyte reporter *Tg(gata1a:dsRed)*^{sd2} (Traver et al. 2003) to give dual fluorescence of vessels and circulating blood

cells to study vascular lumenisation and effects of increased erythrocyte number in the *vhl* mutant.

To maintain adult populations carriers of the fluorescent reporters were identified at embryonic stage (3dpf) with fluorescence microscopy, and embryos expressing fluorescence were raised as adults. To identify *vhl*^{r/+} (heterozygous) carriers in the adult population, fin clipping was performed to provide genetic material to identify carriers of the mutated *vhl* allele from their wild type siblings by PCR and enzyme digest.

The zebrafish cytoplasmic endothelial reporter line *Tg(fli1;eGFP)* was obtained from the Zebrafish International Resource Centre (University of Oregon, USA). The endothelial nuclear transgenic reporter line *Tg(flkl1:eGFP-NLS)* and the photo-convertible endothelial reporter *Tg(fli1:Gal4(GFF);UAS:kaede)* were a kind gift from Marcus Affolter (University of Basel, Switzerland). The erythrocyte fluorescence transgenic *Tg(gata1a:dsRed)^{sd2}* was a kind gift from Leonard Zon (Harvard University, USA).

2.1.2.3 Transgenic endothelial hypoxia and vascular reporter lines

To investigate the role of endothelial cell hypoxia, in contrast to the global up regulation of hypoxic signalling induced by the *vhl*^{r/-} mutation, I used a transgenic line utilising the *Tg(fli1:GFF)* promoter (Asakawa et al. 2008). This reporter uses a modified Gal4 promoter (GFF), and a yeast transcriptional activator that binds a recognition sequence, the upstream activating sequence (UAS) (Scheer & Campos-Ortega 1999) this in turn drives expression of the *KAEDE* gene as a fluorescent reporter. This line enables endothelial specific expression of the photo-convertible stony coral protein *KAEDE*. This line was used as it was already established in our department with the appropriate molecular machinery to utilise the GAL4:UAS system. The *KAEDE* protein can be used as a traditional green fluorescence reporter without photo conversion and as it had already been crossed into the *Tg(fli1:GFF)* line. I was able to use this as a specific endothelial fluorescent reporter without the requirement to produce a new construct and establish a stable zebrafish line. Colleagues in our department have developed a dominant active form of the zebrafish *hif-1α* gene

by site-directed mutagenesis, this has generated *hif-1α* which lacks a PHD3 recognition site, thus rendering the HIF-1α protein stable to bind *hif-1β* and generate a transcriptional response, despite normal cellular PHD3 and oxygen-dependent hydroxylation (Elks et al. 2011). Their group subsequently generated a stable line expressing the dominant active *hif-1α* downstream of the UAS sequence: *Tg(UAS:da-hif-1ab-IRES-GFP)ⁱ²¹⁸* (Elks et al. 2011). This was crossed into a *Tg(fli1:Gal4(GFF);UAS:kaede)* line with the aim to produce an endothelial specific up-regulation of the hypoxic response and enable imaging of *in vivo*, endothelial and vessel development with the fluorescent reporter KAEDE to identify any phenotypic changes in the vasculature.

The UAS dominant active *hif-1α* line was a kind gift from Stephen Renshaw (Centre for Developmental Biology and Genetics, University of Sheffield, UK).

2.1.2.4 Transgenic Notch reporter line

The notch reporter line *Tg(CSL-venus)^{qmc61}* was a kind gift from M. Gering (Nottingham, UK), this line acts as an intracellular notch-signaling reporter. The line is produced using the Tol2 transposase system (Kawakami 2004). A 12x repeat of the CBF1/suppressor of hairless/Lag-1 (CSL) binding site sequence with a downstream sequence for venus (a modified yellow fluorescent protein) flanked by the Tol2 repeats is co-injected into single cell zebrafish embryos with transposase mRNA. The resulting embryos expressing the fluorophore are raised and their progeny identified for carriage of the construct.

The carriers of this construct express the fluorescence reporter on binding of the CSL transcription factor activated by NICD signalling which can be observed *in vivo* by fluorescence microscopy.

2.1.2.5 Maintenance of adult reporter lines

All fluorescent reporter stocks were maintained by outcrossing to wildtype stocks to maintain a normal genetic background and fluorescence carriers raised for adult breeding stocks.

2.1.3 Zebrafish anaesthesia

MS222 or Tricaine (PharmaQ, Hampshire, UK) was obtained via the University of Sheffield veterinary services department. Stock solution contains 400 mg of powder in 97.9 ml milliQH₂O, distilled deionized and ultra-filtered water (mQH₂O) (Millipore MA, USA) to give a final concentration of 4mg/ml, this pH adjusted to 7.0 with 1M Tris. This stock solution is diluted in a ratio of 4.2 ml to 100 ml of aquarium water (final concentration 0.168 mg/ml) for adult fish anaesthesia, (fin clipping or other procedures). For embryo manipulation and sedation 420 µl of stock solution is added to 10 ml of E3 media. This final concentration can be adjusted depending on the duration and depth of sedation required, lower concentrations have been used for embryo manipulation and mounting for imaging. In cases where an alternative doses of anaesthesia was used the reason is specified, dosing is consistent across both treatment and control groups.

2.1.4 Embryo collection & storage

Embryos were obtained from pair mating an individual male and female adult fish over an embryo trap, enabling control over the genetic pedigree of a lay of embryos. Alternatively to obtain large numbers of embryos from a tank of identified mutants or wild type fish, marble tanks can be placed into the adult stock tank of up to forty fish, facilitating multiple egg lays from different females and fertilisation by different males (Nüsslein-Volhard & Dahm 2002). Collected embryos are maintained in E3 media (see section 2.1.4.1) at 28±1°C supplemented with methylene blue as a fungicide and antibacterial agent.

Embryos stored in 90 mm petri dishes (Sterilin, Newport, UK) in E3 media at a density of 40-60 embryos to maintain adequate aeration. Unfertilised, dead or empty chorions were removed every 24 hr after fertilisation and the E3 refreshed to minimise any detrimental effect on embryo growth and development. In all experiments embryos were maintained for up to 5.2 dpf prior to protected status unless being raised as adults, all embryos not raised for adult stocks were destroyed in bleach solution prior to 5.2 dpf.

2.1.4.1 E3 media

Used as incubation media for all zebrafish embryo until 5.2 dpf. Made as a 10x stock and diluted with distilled H₂O (dH₂O), contains the following at final concentrations and stored at 28°C:

NaCl	5 mM
KCl	0.17 mM
CaCl	0.33 mM
MgSO ₄	190.33 mM
Methylene Blue	0.00005% (w/v)

2.2 Identification of a zebrafish *vhl*^{hu2117} mutant allele

2.2.1 Phenotypic identification of *vhl* homozygous mutants

To obtain homozygous *vhl*^{-/-} mutants requires an incross of identified heterozygous adult carriers by fin clipping and PCR, as *vhl*^{+/-} heterozygous carriers lack a vascular phenotype. Homozygous *vhl*^{-/-} mutants can be sorted from their wild type siblings (a mixture of wild type and heterozygous carriers) from 3 dpf based primarily on a number of phenotypic features.

From 3 dpf angiogenic changes can be used to identify homozygous *vhl*^{-/-} mutants. Homozygous *vhl*^{-/-} mutants showed loops of blood vessels emerging from the DLAV above the pigment line when embryos are imaged in a lateral position using a dissection microscope, enabling them to be sorted from wild type embryos (Figure 2.1 C & D). At 2 dpf there was some looping of the primitive DLAV as it begins to remodel to form the mature plexus (Zygmunt et al. 2012) in the wild type however these loops rarely extend above the pigment line. By 3 dpf in the *vhl*^{-/-} mutant there are numerous loops running the length of the DLAV, again this phenotype can be identified with dissection microscopy (Figure 2.1 D arrow). In addition the *vhl*^{-/-} mutant shows expansion of the primitive blood island, expanding the potential space between the caudal artery and primary caudal vein, leading to increased tortuosity of the venous system (Fig 2.1 D arrowhead). The final defining phenotypic feature, which identifies homozygous *vhl* mutants at this development stage, is extensive pericardial

oedema, shown in the homozygous mutants (Figure 2.1B arrow) and is not seen in the wild type siblings (Figure 2.1A arrow).

Live imaging of these vessels and of the movement of red cells within vessels during cardiac contraction highlights some of these features, which may not be easily appreciated in the static images represented in (Figure 2.1) static images.

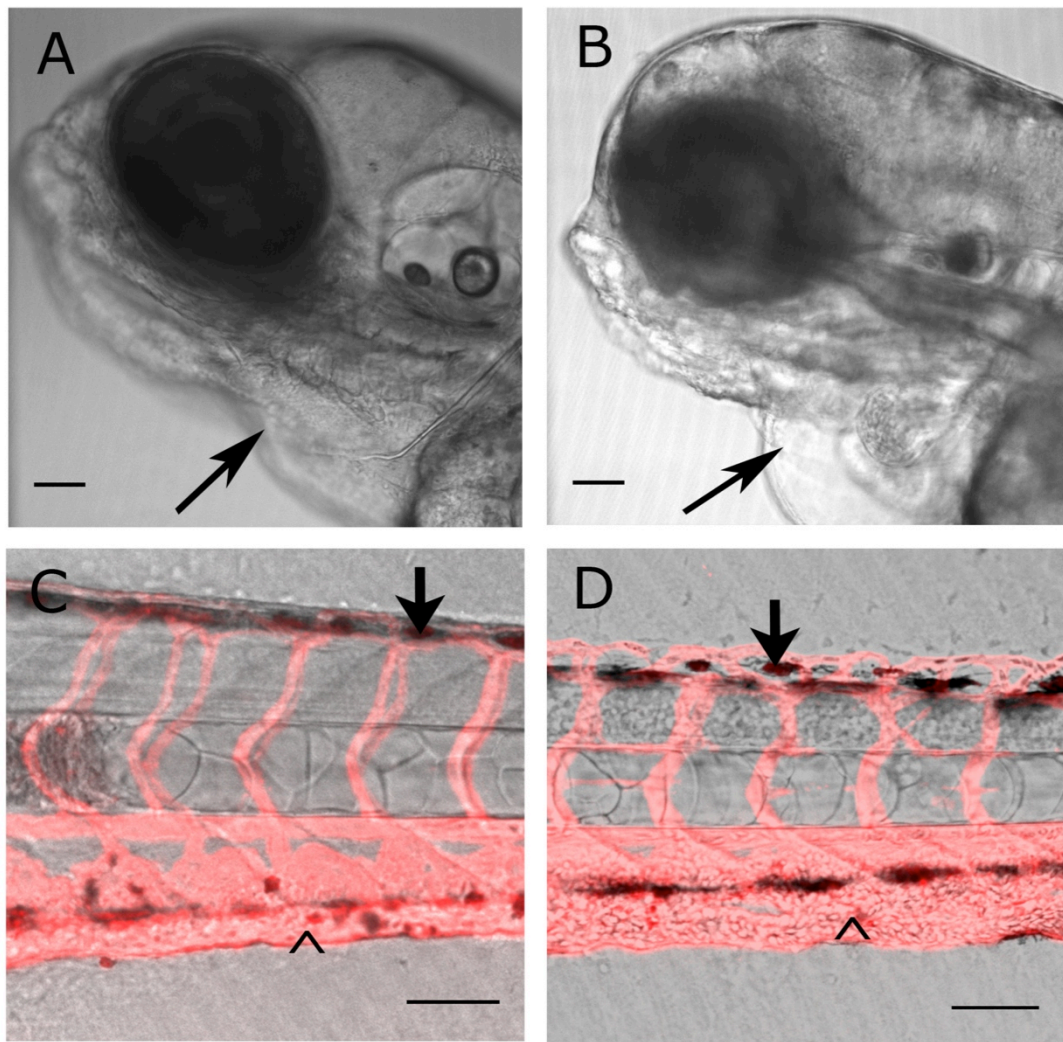


Figure 2.1 Phenotypic differences between a 5 dpf $vhl^{-/-}$ mutant embryo and a wildtype sibling. **A.** Bright field microscopy of the head of a 5dpf wt embryo arrow indicates normal pericardial sac. **B.** Bright field microscopy of the head of the $vhl^{-/-}$ mutant at 5 dpf, arrow indicates pericardial oedema (scale bar 100 μ m). **C.** Mid trunk of 5 dpf wt embryo, overlay of bright field and *Tg(kdrl;HRAS-mCherry)*, arrow shows normal DLAV plexus formation, arrowhead shows normal venous plexus size. **D.** Mid trunk of 5 dpf $vhl^{-/-}$ embryo with bright field and *Tg(kdrl;HRAS-mCherry)* overlaid, arrow shows looping of DLAV above the pigment line arrowhead shows expansion of venous plexus in the mutant embryo (scale bar 100 μ m).

2.2.2 Genetic identification of *vh*^{hu2117} mutation

2.2.2.1 Gel electrophoresis

PCR product was loaded onto a 1.5% molecular grade agarose gel (Bioline, London, UK) and run at 100V for 30 minutes dependent on product size. Hyperladder IV (Bioline, London, UK) DNA ladder was loaded (5 µl) for size comparison of products of 100-1000bp. Larger PCR products and visualisation of plasmids were run against Hyperladder I 200- 10,000 bp (Bioline, London, UK). Gels and PCR product were imaged using UVdoc imager (UVItec Cambridge, UK).

2.2.2.2 Genomic DNA extraction

2.2.2.2.1 Genomic DNA extraction from Fin clip

All genomic DNA (gDNA) isolation from zebrafish fin clip samples were performed using a REExtract-N-Amp Tissue PCR kit (Sigma-Aldrich, Gillingham, UK). To extract genomic DNA from the resected fin tissue residual methanol was evaporated off the sample at 80°C for 10 min. Tissue was then resuspended in 25 µl Extraction solution and 6.25 µl of Tissue solution and vortexed. This mixture was subsequently incubated at room temp for 15 min to complete the digestion. This mixture was then heated at 95°C for 3 min to denature the digestion enzyme and 25 µl of neutralisation solution added. This neutralised and digested tissue sample can be stored at 4°C for up to 6 months without degradation of genomic DNA and this buffered mixture can be added directly to a standard PCR mixture containing Taqman and nucleotides (Biomix Red).

2.2.2.2.2 Genomic DNA extraction from individual embryos

Isolation of gDNA from embryos less than 5.2 dpf was performed using a Proteinase K digest. Embryos were anaesthetised with tricaine as per protocols or placed on ice for fifteen minutes E3 media was removed and 25 µl of Phosphate Buffered Saline (PBS) (Sigma-Aldrich, Gillingham, UK) was added, 5 µl of 10 mg/ml Proteinase K was added to the embryo and PBS then incubated over night at 55°C. The enzyme was denatured at 95°C for 15 min

then vortexed to mix the digested embryonic tissue and a further 25 µl of PBS was added. This was used directly into the PCR mixture to amplify the *vhl*^{hu2117} allele.

2.2.2.2.3 PCR amplification of the *vhl*^{hu2117} mutant allele

A polymerase chain reaction is performed on the isolated gDNA extract using specific primers to amplify the mutated region of the *vhl* ortholog gene in the zebrafish. All PCR primers (Invitrogen, Paisley, UK) used from a 10 mM stock and at a final master mix concentration 0.5mM

2.2.2.2.4 Primers for *vhl*^{hu2117} mutation amplification

Forward 5' TAAGGGCTTAGCGCATGTTC 3'

Reverse 5' CGAGTTAAACGCGTAGATAG 3'

2.2.2.2.5 PCR mastermix for *vhl*^{hu2117} amplification

Table 2.1 PCR mastermix components for *vhl*^{hu2117} amplification from genomic DNA

Biomix Red (Bioline UK)	10 µl
F primer	0.5 µl
R primer	0.5 µl
mQ H ₂ O	5 µl
gDNA	4 µl
total	20 µl

2.2.2.2.6 PCR protocol for amplification of the *vhl*^{hu2117} allele

Table 2.2 Thermal cycler parameters for PCR amplification of a 414 bp segment of the mutated *vhl*^{hu2117} region (Figure 2.2 A).

Step		Temp	Time
1	Initial denaturing	94°C	4 min
2	Denaturing	92°C	1 min
3	Annealing	56°C	30 sec
4	Extension	72°C	40 sec
5	Cycle to step 2	x39	
6	Final elongation	72°C	10 min
7	Hold	4°C	∞

2.2.2.2.7 Restriction enzyme digest of the *vhl*^{hu2117} PCR product to identify mutated alleles

The amplified *vhl* PCR product is incubated with the restriction enzyme BciVI (New England Biolabs, Ipswich, USA) to identify wildtype, heterozygous and homozygous *vhl*^{hu2117} mutants. The enzyme recognition site is located in the wild type PCR product. Figure 2.2 C shows the restriction site, the red highlighted cytosine is mutated in the *vhl*^{hu2117} (C/T) and thus the mutant lacks the recognition site for BciVI. In the heterozygous carriers there is a partial DNA digestion and no digestion in the homozygous mutant. (Figure 2.2 B)

Table 2.3 Restriction enzyme mixture for digest of the wildtype *vhl* gene.

<i>vhl</i> PCR product	5 µl
NEB buffer 4	1.8 µl
BciVI enzyme	0.2 µl
mQH ₂ O	13 µl
Total	20 µl

Incubated overnight at 37°C, the complete digestion mixture is run, 20 µl on a 1.5% gel 100V for 30 min (Figure 2.2 B).

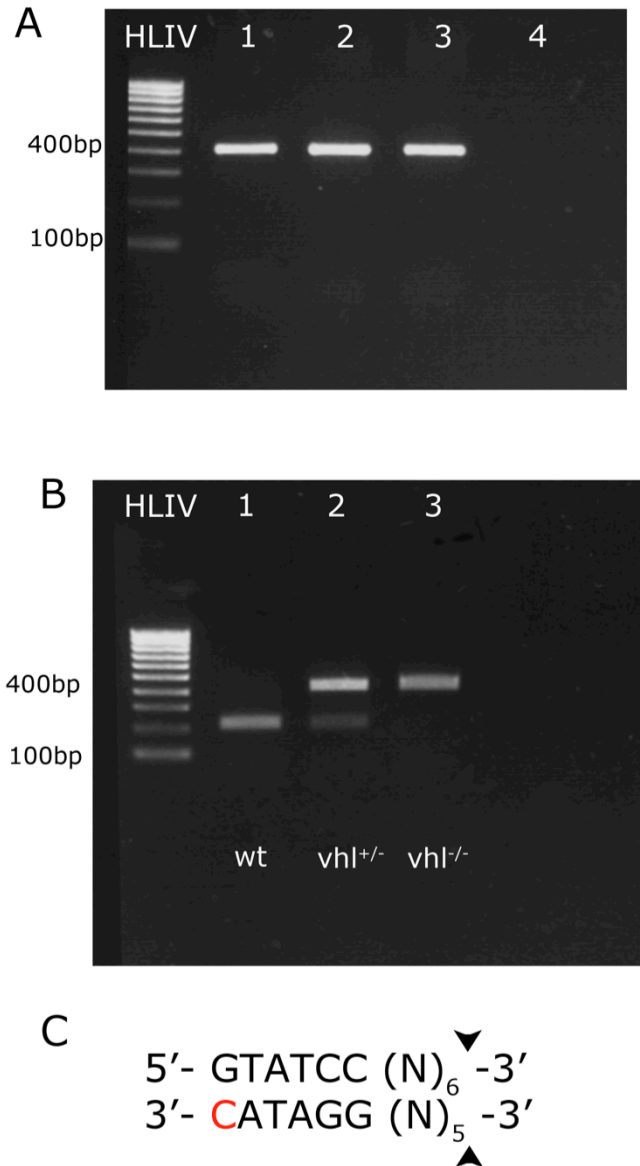


Figure 2.2 PCR amplification and restriction enzyme digest of the mutated region of the *vhl* allele in the *vhl*^{hu2117} mutant zebrafish.

A. PCR amplification product 414bp of 3 adult fin clips (lanes 1-3) and a genomic DNA extraction blank (lane 4) 1.5% agarose gel run at 100 V for 30 min.

B. Restriction enzyme digest of the *vhl* PCR product with BciVI restriction enzyme. Restriction site is preserved in the wt but not the *vhl*^{hu2117} mutant. 1.5% agarose gel products run for 30 min at 100 V. **C.** Restriction enzyme site for BciVI enzyme, which contains the *vhl*^{hu2117} mutation (C/T) highlighted in red.

2.3 In vivo imaging of embryonic zebrafish

2.3.1 Preparation of Embryos

2.3.1.1 Dechoriation

Wild type embryos spontaneously dechorionate at 2.5 dpf at 28°C, however in mutants and transgenics this may be delayed (Nüsslein-Volhard & Dahm 2002). Embryos were manually dechorionated under a dissecting microscope using a pair of Dumont #5 tweezers (WPI, Florida, USA) to mechanically remove the chorions to aid normal development.

2.3.1.2 Inhibiting embryo pigment development with phenylthiourea

To enhance transparency for vascular imaging, the addition of 1-phenyl 2-thiourea (PTU) (Sigma-Aldrich, Gillingham, UK) after shield stage (6-8 hpf) inhibits development of melanin in the melanophores in the skin of the embryo. PTU 80mg was dissolved in 25 mls of Phosphate Buffered Saline (3.2 mg/ml), 400µl is added to 10ml E3 0.00128% (w/v). In mutant or injected embryos to reduce toxicity a 1:2 dilution of the PTU every 24 hr reduced pigment without developmental toxicity.

2.3.1.3 Mounting of live embryos

Embryos were mounted on glass cover slips (22x50 mm, Thermo scientific, New Hampshire, USA). After Tricaine anaesthesia to manipulate and sort embryos, they were mounted in 1% (w/v) low melting point agarose (Sigma-Aldrich, Gillingham, UK) with 0.0168 mg/ml Tricaine. The embryos were positioned in the agarose during cooling in a lateral position for optimal visualisation of the trunk vasculature.

2.3.1.4 Microscopy

Fluorescence microscopy was performed using an IX81 inverted motorised microscope (Olympus, Southend-on-sea, UK), Ultraview VOX confocal spinning disc imaging system (Perkin Elmer, Massachusetts, USA). Images were acquired using Volocity software v5.3.2 (Perkin Elmer, Massachusetts, USA).

This microscope and software package was used as it enabled multiple embryos to be imaged with using motorised stage control, which enabled me to image large numbers of embryos in a single experiment. This was an important experimental consideration as from an incross of $vhl^{+/+}$ carriers only 1:4 embryos will be $vhl^{-/-}$ so significant numbers of embryos need to be imaged in order to ensure the numbers of mutants in an experiment required for statistical significance.

Z stack images were acquired in 2 μm slices using sequential laser scanning of the region of interest (ROI). All analysis and quantification of vessel parameters was performed using ImageJ software (v1.44 public domain software <http://rsbweb.nih.gov/ij/>). Image analysis performed on extended focus images of the Z-stack unless specified.

Whole mount in situ hybridisation images were taken using a Leica M165 FC dissection scope and Leica DFC310 FX camera (Leica microsystems, Milton Keynes, UK) with sample immobilized in 100% Glycerol and illuminated with a Zeiss KL1500 LCD light source (Zeiss microscopy, Cambridge, UK).

2.4 Vascular quantification and measurements

2.4.1 Calibration of images

All measurements were calibrated to an image of a graticule (10 mm/ 0.1 mm division graticule, (Pyser SGI, Edenbridge, UK) taken on the same microscope at the same magnification. This image is then used to calibrate images taken using imageJ and quantify measurements.

2.4.2 Endothelial morphology

All measurements were taken from the mid vessel, unless specified. Aortic diameter was measured at a point corresponding to the adjacent mid somite point and calliper markings for measurement taken as the outer leading edge to outer leading edge of fluorescence. ISV measurements were taken above and below the parachordal vessel (Isogai et al. 2001) and averaged. If difficulty arose over overlying vessels in an extended focus image the Z stack was

analysed to isolate the measurement in a single vessel. Total vessel length was taken over two somites at the level of the cloacae for consistency, all vessels including sprouts were measured using the segmented line function in Image J software and the total obtained.

2.4.3 Endothelial nuclei quantification

Quantification of the number of endothelial cells using the *Tg(flk1;GFP-NLS)* reporter line were manually counted using an extended focus image of the vasculature of two somites at the level of the cloacae. Individual Z stack images were used to identify overlying endothelial nuclei and counts made of all nuclei of the ISV and DLAV above the level of the dorsal aorta (Isogai et al. 2001) but not including aortic nuclei.

2.5 In vivo intravascular fluorescence angiograms

Embryos were mounted as per previous method (section 2.3.2) and Quantum nanoparticles were injected into the circulation (Qdots) (Sigma-Aldrich, Gillingham, UK) to produce intravascular angiograms. Qdot 205nm non-targeted quantum dots were injected into 4 dpf embryos at 2 μ M and 200 nM concentration. Non-capillary 1.0mm diameter boroscillate needles (WPI Florida, USA) were pulled using a micropipette puller (Sutter instruments California, USA) and loaded with 1 μ l of the Qdot solution. Using a PV820 pneumatic picopump (WPI) and micromanipulator (WPI) the Qdots were injected into the Duct of Cuvier, the venous confluence overlying the yolk, at 2 and 3 dpf. This structure is a flat venous confluence of about 50-100 μ m at the widest point. In older 4 dpf embryos these venous structures are less accessible for injection so the distal common cardinal vein or directly into the region just proximal to the atrium of the heart is used as the site of injection (Isogai et al. 2001). For all injections the embryo was immobilised in 1% agarose in a lateral position and the micropipette is introduced from the dorsum of the embryo over the yolk and into the venous circulation of the embryo.

Using a gated injection which delivers a fixed volume using a time gated pressure release of compressed gas (PV820 pneumatic picopump, WPI), small

volumes of the working Qdot solution, were injected into the circulation. The delivery of the injection was observed entering the circulation by light microscopy due to distortion of adjacent tissues and subsequent fluorescent microscopy using a 488 nm laser and GFP filter to image the vascular opacification. The volume injected varied depending on the needle position as loss of the Qdot solution back along the needle track and into the subcutaneous tissues occurs to varying degrees, but adequate intravascular contrast can be assessed with fluorescent microscopy. Repeated small volume injections are required to avoid compromising the circulation leading to cessation of cardiac contraction, small volume injection also allows for intermittent visual assessment of the intravascular opacification.

2.6 Morpholino antisense oligonucleotides

2.6.1 Morpholino synthesis, reconstitution and storage

All Morpholino (MO) were designed and synthesised by Gene Tools (Oregon, USA). All morpholino are made up to 1 mM stock in mQH₂O and frozen -20°C. Prior to use aliquots of the stock solution were defrosted and heated to 70°C for 5min to reduce secondary structure and dissolve any precipitated morpholino (Bill et al. 2009). The working solution is then vortexed then placed directly onto ice. Equal volume of Phenol red (Sigma-Aldrich, Gillingham, UK) was added to give a final injection concentration of 0.5 mM. To manipulate the final concentration of morpholino alternative dilution ratios of morpholino stock to Phenol red are used (specified if not 0.5 mM).

2.6.2 Morpholino sequences

Troponin t₂ (ATG/start) blocking morpholino (Sehnert et al. 2002):

5' CATGTTTGCTCTGACTTGACACGCA 3'

Control morpholino: 5' CCTCTTACCTCAGTTACAATTTATA 3'

dll4 ATG morpholino (Geudens et al. 2010):

5' GAGAAAGGTGAGCCAAGCTGCCATG 3'

2.6.3 Morpholino oligonucleotide injection into single cell embryos

Single cell stage embryos were injected as per standard published methods (H William Detrich et al. 2011). 1.0 mm diameter borosilicate glass capillary needles (WPI Florida, USA) were pulled using micropipette puller (Sutter instruments California, USA), after filling with MO, these are mounted on a PV820 pneumatic picopump (World Precision Instruments Florida, USA). Using a dissection microscope S6E (Leica) the tip of the capillary needle is removed and the volume of MO injection quantified using a 10 mm/0.1 mm division graticule (Pyser SGI, Edenbridge, UK) and immersion oil. A sphere of MO is injected into the oil the diameter of the sphere can be manipulated by alterations in delivery pressure and duration through the Picopump. Thus a sphere of 100 μm has a volume of 0.52 nl ($\frac{4}{3}\pi r^3$) after calibration a total volume of 1.04 nl is injected into each single celled embryo, at a stock concentration of 0.5mM this delivers 4.205ng of *troponin t₂* morpholino. Further alterations in MO dose were achieved through manipulation of the 1 mM stock by dilution with Phenol red as specified.

2.7 Whole mount in situ hybridization

2.7.1 Embryo fixation in paraformaldehyde

4% (w/v) Paraformaldehyde (PFA) made in Phosphate buffered saline (PBS) stored at -20°C in 10ml aliquots. Embryos fixed in defrosted solution for 2 hr at room temperature or at 4°C overnight. Fixed embryos are dehydrated in stages into 25%, 50%, 75% and finally 100% Methanol (v/v) (Fisher, Paisley, UK) and then stored at -20°C

2.7.2 Reagents & Buffers

All reagents obtained from Sigma-Aldrich, Gillingham, UK unless otherwise specified.

- Phosphate buffered saline: 1 (PBS) tablet dissolved in 200 ml of mQH₂O.
- PBS-tween (PBT): 1x PBS + 0.1% (w/v) Tween 20.

- Proteinase K 10 µg/ml in PBT
- 20x SSC buffer: 3 M NaCL, Citric acid trisodium salt 300 mM
- Hybridisation solution: 50% (v/v) formamide, 5xSSC, 0.1% (v/v) Tween 20, 50 µg/ml of heparin, 500 mg/ml of RNase-free tRNA, 5% dextran sulphate, solution adjusted to pH 6.0 with citric acid (460 ml of 1M citric acid solution for 50 ml of hybridisation solution).
- Maleic acid buffer (MABTw): 0.1 M Maleic acid, 0.15 M NaCl, pH to 7.5 with NaOH (1 M), Tween20 0.1%
- BCL III buffer: 0.1 M Tris HCl (pH 9.5), 50 mM MgCl₂, 0.1 M NaCl, 0.1% (v/v) Tween20
- Staining solution: 1:1 of BCLIII and BM Purple (Roche diagnostics Germany).
- Blocking solution 2% (v/v) Blocking reagent (Boehringer Ingelheim, UK) in MABTw
- anti- DIG antibody (1:5000 dilution) (Roche, UK)
- Glycerol 25%-100% (v/v) for mounting

2.7.3 Outline of method for whole mount in situ hybridisation

2.7.3.1 Embryo permeabilisation

Proteinase K 10 µg/ml was used to enable RNA probe penetration for whole mount in situ hybridisation; duration of incubation was dependent on the age of the embryo.

Table 2.4 Duration of proteinase K digestion to permeabilise embryonic tissue for WISH

Embryo age	Incubation proteinase K (10µg/ml)
24 hpf	15 min
48 hpf	35 min
72 hpf	45 min

2.7.3.2 Method for WISH

We used a modification of the published method, (C. Thisse & B. Thisse 2008) embryos are rehydrated by successive washes in increasing PBT/methanol mixture. The tissues are then permeabilised with proteinase K (Sigma-Aldrich, Gillingham, UK) as per section 2.7.3. The embryos are then re-fixed in 4% PFA (w/v) solution, after a series of washes they are then pre-hybridised at 68°C for 2-5 hr before adding the probe in hybridisation mixture with dextran 5% (w/v) (Lauter et al. 2011) overnight at 68°C at a dilution of 1:200. The probe is then recovered and a series of washes in increasing concentrations of 2x SSC and then MABTw. Blocking buffer is then added for 3 hours to minimise the effect of non-specific probe binding, the embryos are then incubated overnight at 4°C with secondary anti-Digoxigenin (DIG) antibody (1:5000 dilution) (Roche, Welwyn Garden City, UK). After a series of washes to remove any residual antibody, the embryos are transferred to staining solution until adequate staining is observed, the duration of staining is specific to each probe.

2.7.3.3 Methanol clearing

A methanol clearing step can be used to remove any excess background staining after which the embryos are then fixed in 4% PFA (w/v) for 20min at room temperature, prior to imaging.

2.7.3.4 Imaging and mounting of WISH stained embryos

Embryos are incubated in successively increasing concentrations of glycerol (Sigma-Aldrich, Gillingham, UK) and mounted on coverslips. Imaging of whole mounts was with a Leica M165 FC dissection scope and DFC310 FX digital camera, using a Zeiss KL1500LCD external light source.

2.7.4 RNA antisense probe synthesis for in situ hybridisation

2.7.4.1 Outline of RNA antisense probe synthesis for whole mount in situ

Antisense RNA probes are generated against known mRNA sequences this enables complimentary binding to the mRNA and subsequent labelling to localise the expression of the target mRNA within the embryo. This means that

the spatial distribution of a specific gene and the timing of its expression can be demonstrated in the whole organism in a qualitative manner. The antisense probes are synthesised using digoxigenin labelled bases, which are synthesised from a DNA sense strand using an RNA polymerase specific to the gene fragment of interest. Once purified this enables the probe to be used to hybridise to the mRNA of interest and then using an anti-DIG antibody labelled for visualisation.

2.7.4.2 RNA antisense probes for WISH

Table 2.5 List of RNA antisense probes used for WISH with the restriction site, RNA polymerase and original reference.

A/S Probe	RNA polymerase	Restriction site	Reference
<i>fli1</i>	T3	XbaI	(Brown et al. 2000)
<i>kaede</i>	Sp6	NotI	unpublished
<i>dll4</i>	T7	SpeI	R.Patient
<i>cxcr4a</i>	T7	Not 1	(Knaut et al. 2003)
<i>kdr-l</i>	T7	EcoRI	(Fouquet et al. 1997)
<i>her12</i>	T3 (primer)	EST clone	unpublished
<i>flt4</i>	T7	EcoRI	(Thompson et al. 1998)
<i>vegfc</i>	T7	EcoR1	(Hogan, Herpers, et al. 2009b)

Many of the antisense RNA in situ probes used in this project have been synthesised from plasmids kindly provided by the original groups and linearised based on restriction enzyme sites and sequences as published. The *kaede* antisense probe was synthesised de novo, and the *her12* probe was synthesised from an EST clone by a project student our lab (Freek van Eeden Sheffield, UK). The *dll4* probe was a kind gift from Roger patients lab (Oxford,

UK) The restriction site and RNA polymerase in conjunction with the plasmid provides the DNA template for RNA antisense probe synthesis as per standard methods (C. Thisse & B. Thisse 2008).

2.7.4.3 Extraction of plasmid from blotting paper

Blotting paper containing a purified plasmid is placed in 100 µl of mQH₂O to dissolve the plasmid. This is then mixed for 5 min using a pipette tip and then incubated at 37°C for 2hrs to ensure adequate plasmid goes into solution. This solution of purified plasmid is then used to transform competent cells directly or can be stored at -20°C for later use.

2.7.4.4 Transformation of Competent cells for plasmid synthesis

2.7.4.4.1 Reagents

- LB broth (Sigma-Aldrich, Gillingham, UK) 20g / 1l mQH₂O + ampicillin (amp) 50 µg/ml
- LB agar (Sigma-Aldrich, Gillingham, UK) 17.5g/500ml mQH₂O autoclaved +amp 50 µg/ml
- SOC media (Sigma-Aldrich, Gillingham, UK)

2.7.4.4.2 Method for transformation of E.Coli

DH5α chemically competent cells (Sigma-Aldrich, Gillingham, UK) were used for transformation with plasmid-derived sequences. 100 µl of competent cells are defrosted on ice from -80°C, 2 µl of ligated plasmid was added and incubated on ice for 30 min. The cells are then transformed by heat shock, incubating at 42°C for 30 sec and then immediately transferred to ice for 2 min. 250 µl of SOC media (Sigma-Aldrich, Gillingham, UK) is added then incubated at 37°C at 225 rpm (Innova44, New Brunswick scientific, Enfield, USA). 1/10th and 9/10th of the total volume is then inoculated onto sterile petri dishes of LB agar +amp and incubated for 12 hr at 37°C. Individual colonies were picked for inoculation of 200 ml of LB broth +amp and grown overnight in conical flasks at 37°C in an orbital shaker incubator at 225 rpm.

2.7.4.4.3 Glycerol stocks of plasmids transformed into competent cells

500 µl of the inoculated LB broth is aliquoted into 1.5 ml eppendorf with 500 µl of sterile glycerol (Sigma-Aldrich, Gillingham, UK) this is stored at -80°C. This allows a stock of the transformed *E.Coli* to be reconstituted rapidly by inoculation of fresh LB broth using only a pipette tip scrape of the frozen glycerol.

2.7.4.4.4 Purification of plasmid DNA from transformed competent cells

2.7.4.4.4.1 MIDI prep purification of Plasmid DNA

The 200 ml of inoculated LB broth is centrifuged 4500 rpm for 30 min at 4°C the resulting pellet of cells is purified by plasmid MIDI DNA purification kit (QIAGEN, Manchester, UK).

2.7.4.4.4.2 Phenol Chloroform DNA purification of linearised plasmid

To improve the yield for low copy number plasmid transformation a phenol/chloroform purification of plasmid DNA can be used instead of MIDI prep purification. This purification is also used to purify probes synthesised de novo after the restriction enzyme digestion prior to RNA probe synthesis (section 2.7.4.6.):

- 400 µl of Plasmid DNA combined with 400 µl Phenol:chloroform:isoamylalcohol (25:24:1) (Sigma-Aldrich, Gillingham, UK)
- Mix then centrifuge 13,000 rpm for 5 min at room temp
- To the supernatant add 400 µl Chloroform:isoamylalcohol (24:1) (Sigma)
- Mix then centrifuge 13,000 rpm for 5 min at room temp
- To removed supernatant add 40 µl 2 M Sodium acetate and 1 µl ethanol and freeze at -80°C for 30 min
- Centrifuge at 13,000 rpm for 30 min at 4°C
- Remove supernatant and wash pellet with 70% (v/v) ethanol then air dry
- Resuspended in RNase free H₂O (Sigma-Aldrich, Gillingham, UK)

2.7.4.4.5 Linearisation of plasmid and RNA Probe transcription

Plasmids were linearised in a restriction enzyme step using specific enzyme (see table 2.5) (New England Biosciences, Ipswich, USA) and appropriate buffer based on original published method. After confirmation of linearisation of the plasmid and quantification by gel electrophoresis, purification using the phenol chloroform method (section 2.7.4.4.2) was performed to remove any residual enzymes and nucleotides. Quantification of linearised plasmid was performed by spectrophotometry (Nanodrop ND100 spectrophotometer, ThermoFisher Scientific, Paisley, UK) and 1 µg of template DNA was used for RNA transcription using a DIG labelled transcription kit (Roche, Welwyn Garden City, UK).

RNA probes were purified after RNase free DNase treatment (Roche, Welwyn Garden City, UK) by precipitation into 7.5 M Ammonium acetate and 100% ethanol at -20°C. All purified digoxigenin labelled RNA probes stored in 70% formamide (v/v) (Sigma-Aldrich, Gillingham, UK) at -80°C. The probes were used at a final dilution of 1:200 in Hybridisation mix (section 2.7.2) for embryo WISH.

2.8 Synthesis of a novel RNA antisense DIG labelled probe

For confirmation of *kaede* expression I synthesised a novel RNA DIG-labelled antisense probe, using the TOPO TA cloning and transformation kit (Sigma-Aldrich, Gillingham, UK). This kit allows the insertion of a Taq polymerase PCR product to be cloned directly into the TOPO vector for transformation of One-shot Top10 cells (Sigma-Aldrich, Gillingham, UK). This vector has a number of restriction sites and RNA polymerase sites to allow easy determination of insert direction and probe synthesis.

2.8.1 Synthesis of a *kaede* PCR product for TOPO TA cloning

2.8.1.1 Total RNA extraction from *kaede* positive transgenic embryos

An incross of the *Tg(fli1;GFF:UAS;kaede)* was used to identify embryos expressing *kaede* based on fluorescence. 20 fluorescence positive embryos were pooled and 20 wild type embryos from a LWT incross with no *kaede* expression. Total RNA was extracted into 250 µl of Trizol reagent (Sigma) and homogenised by repeat aspiration through a 25 g needle (microlance 3 BD, UK) and 1 ml syringe (Plastipak BD, UK). RNA was extracted using 50 µl of chloroform after centrifugation (13,000 rpm, 15 min at 4°C) the supernatant was precipitated into 85 µl of Isopropanol (Fisher, UK). A pellet was formed by centrifugation (13,000 rpm, 15 min at 4°C) and washed in 75% ethanol (v/v), then resuspended in 15 µl of RNAase free H₂O and quantified by spectrophotometry Nanodrop ND100 spectrophotometer, (ThermoFisher Scientific, Paisley, UK).

2.8.1.2 Reverse transcription to produce cDNA of *kaede*

Reverse transcription to synthesise a cDNA library from embryonic total RNA including the *kaede* transgene was performed using the Superscript II kit (Invitrogen, Paisley, UK). Effective synthesis was confirmed by gel electrophoresis and this cDNA was stored at -20°C.

2.8.1.3 PCR to amplify *kaede* sequence from cDNA library

The sequence for the *kaede* mRNA was obtained from the European bioinformatics database where it was identified from a BAC clone. (<http://www.ebi.ac.uk/ena/data/view/BAC20344>) Primers were designed using Primer3Plus (<http://www.bioinformatics.nl/cgi-bin/primer3plus/primer3plus.cgi/>) a primer pair was chosen which gave a 504 bp product from the 678 bp gene. A nucleotideBLAST search (<http://www.ncbi.nlm.nih.gov/BLAST/>) using this *kaede* PCR product against the zebrafish genome showed no alignment with any other endogenously expressed genes as would be expected with a transgene. Figure 2.3 A shows a single PCR product of the expected size by gel electrophoresis.

The PCR product was purified and sequenced to confirm that the band represented the desired segment of the *kaede* gene.

2.8.1.3.1 *kaede* primer sequences

Forward 5' TAAACGGGCACCCAGTTTGT 3'

Reverse 5' ACTTGACACCCTCCTGCCTA 3'

2.8.1.3.2 PCR programme for amplification of *kaede* DNA sequence

Table 2.6 PCR programme parameters for *kaede* amplification

Step		Temp	Time
1	Initial denaturing	94°C	4 min
2	Denaturing	92°C	1 min
3	Annealing	54°C	30 sec
4	Extension	72°C	40 sec
5	Cycle to step 2	x35	
6	Final elongation	72°C	10 min
7	Hold	4°C	∞

Annealing temp taken as 5°C less than the lowest melting temp of the primer pair (59.7°C). A mastermix was used as per table 2.1 substituting 1 µl of cDNA as PCR template for the gDNA.

2.8.2 TOPO TA cloning vector for insertion of a Taq polymerase amplified PCR product

A feature of the *Taq* DNA polymerase is that it produces an adenine base overhang on the PCR product, the TOPO TA cloning system utilises this features and a thymine overhang on the ends of the linearised vector to enable accurate insertion of the PCR product for cloning, by the Topoisomerase enzyme.

2.8.2.1 Incorporation of the PCR product into the TOPO TA cloning vector

1 µl of the *kaede* PCR product was added to 1 µl of the TOPO TA vector, 1 µl of salt solution (TOPO TA cloning kit Invitrogen, Paisley, UK) and 3 µl of mQH₂O. This is incubated for 5 minutes at room temperature then transferred to ice for immediate transformation of chemically competent *E. Coli*.

2.8.2.2 Transformation of chemically competent cells for cloning of PCR product and construct

2 µl of the TOPO cloning reaction is added to a vial of OneShot chemically competent *E. Coli* (Invitrogen, Paisley, UK) and incubate on ice for 30min. The cells are then heat shocked for 42°C for 30 sec in a non circulating water bath and transferred to ice where 250 µl of 37°C SOC media is added then transfer to 37°C rotating incubator at 225 rpm for 1hr. 1/10th and 9/10th of this culture is inoculated onto LB agar +amp petri dishes and incubated at 37°C overnight.

2.8.2.3 Selecting colonies for insert confirmation and glycerol storage

10 individual colonies were selected and picked and sub-cloned onto LB agar plates +amp, then each of these was re-picked to perform colony PCR and sequencing to identify correct insert and the orientation of sense and antisense to produce complimentary RNA sense and antisense probes. Each of these colonies was grown in 10 ml of LB broth from which glycerol stocks were taken 500 µl of inoculated LB was mixed with 500 µl of sterile glycerol then frozen at -80°C, until sequencing results were available.

2.8.2.4 Large scale Plasmid DNA purification

After confirmation by DNA sequencing using M13 forward and reverse priming sites confirmation of the correct insert and its orientation in each colony PCR. The glycerol stock for the selected colony can be grown in 200ml of LB broth overnight in a conical flask at 37°C in a rotary shaker 225rpm to produce large amounts of the plasmid and insert. The cell compartment is isolated from this mixture by centrifugation in 50 ml Falcon tubes at 4500rpm for 30min. Plasmid DNA is then purified from this bacterial pellet using a MIDIprep kit (Qiagen, Manchester, UK) to produce a concentrated solution plasmid DNA, which can be used to provide a template for RNA probe synthesis after linearisation.

2.8.2.5 Plasmid linearisation for *kaede* probe synthesis

Restriction enzyme site was chosen based on pre-existing restriction sites in the vector, and the colony PCR sequencing data. This allows for a restriction enzyme and RNA polymerase pair to be selected to synthesise a sense and antisense RNA probe depending on the orientation that the PCR product is inserted into the vector. For synthesis of an antisense RNA probe a NotI restriction site was selected and for a sense RNA probe a HindIII restriction site was selected. The *kaede* insert was checked to ensure that there was no restriction site within the insert for either of the selected restriction enzymes. Restriction enzymes were obtained from New England biosciences USA and purified plasmid DNA incubated as per manufacturers recommended conditions. Linearised DNA was run on an agarose gel to confirm successful linearisation along side uncut purified plasmid DNA.

2.8.2.6 RNA probe transcription

For probe synthesis 1 µg equivalent of linearised and purified plasmid is used as a DNA template. The restriction site is selected downstream of the PCR product insert so that the selected RNA polymerase site initiates synthesis of the RNA probe upstream of the PCR insert until the cut site after the insert. For the *kaede* antisense probe Sp6 was the RNA polymerase used and for the sense probe T7 RNA polymerase. RNA DIG-labelling kit (Roche, Wellyn Garden City, UK) was used to synthesise probes.

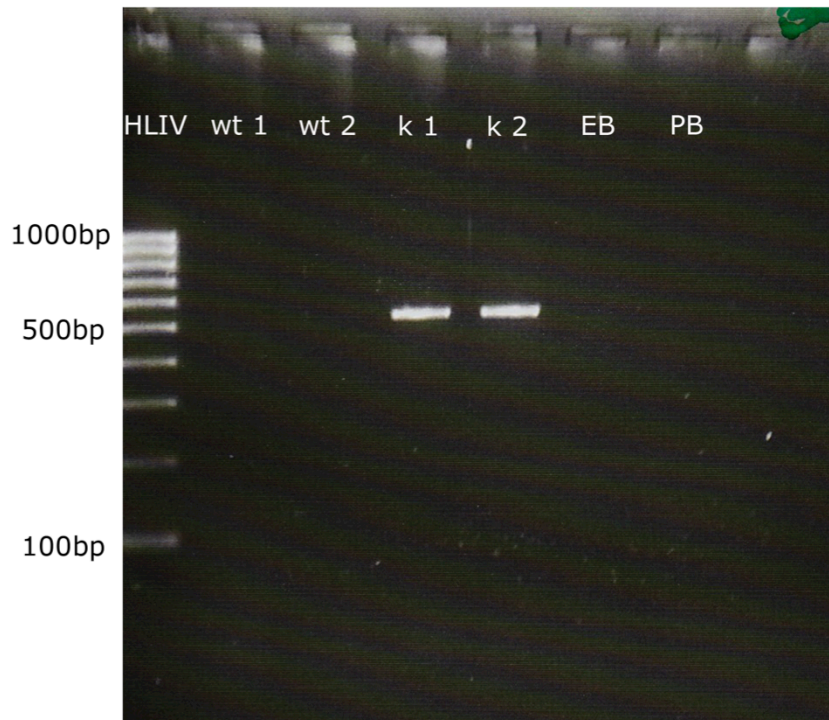


Figure 2.3 PCR of cDNA from embryos expressing *kaede* and wild types for cloning into TOPO TA cloning system.

1.5% agarose gel, run at 100V for 30 min, Hyperladder IV in lane 1, PCR product using *kaede* primers with wildtype cDNA in lanes 2 and 3 (wt1 and wt 2). Lanes 4 & 5 show a single PCR product of ~510bp from cDNA isolated from *kaede* expressing embryos (k1 & k2). EB, extraction blank no tissue in extraction and RNA purification process. PB, PCR blank no cDNA added to PCR mastermix.

2.8.2.7 RNA probe purification

After probe synthesis there is a DNase treatment for 30 min at 37°C to degrade any remaining DNA template. Then the probe is precipitated into Ethanol (Fisher, Paisley, UK) with 7.5 M Ammonium acetate and spun down (13,000 rpm 15 min at 4°C) to form a pellet which is washed in 70% Ethanol (v/v) then resuspended into 30 µl of RNase free H₂O and 70 µl of formamide (Sigma-Aldrich, Gillingham, UK) and stored at -80°C. *Kaede* sense and antisense probes were both used at a final dilution of 1:100 in hybridisation mix with 5% (w/v) dextran sulphate.

2.9 Immunohistochemistry

2.9.1 Phosphorylated Histone H3 antibody immunohistochemistry

Histone H3 is one of the protein constituents of chromatin, during mitosis this particular histone H3 is phosphorylated at a specific serine residue. Immunohistochemistry of this marker of cell division enables the identification of actively dividing cells, which can be co-localised to transgenic cells in the developing zebrafish embryo to identify differences in proliferation in specific cell groups. I attempted to co-localise PH3 Ab staining to endothelial cells to look at differences in endothelial proliferation between the *vhl*^{-/-} mutant and its wild type siblings.

2.9.1.1 Method for PH3 immunohistochemistry

Embryos were fixed as for WISH (see section 2.7.1) in groups of 20 embryos of matched developmental stage. The embryos were rehydrated back into PBS through reducing percentage of methanol (75%, 50% and 25%). They were washed in PBS to remove any residual solvent then incubated in 100% acetone (Fisher, UK) for 7 min at -20°C then washed in PBS. The embryos were then permeabilised as per WISH (table 2.4) with proteinase K (10 µg/ml) then fixed in PFA 4% (w/v) for 20 min at RT. After washing in Maleic acid buffer with tween 20 0.1% (MABTw) and blocking buffer for 2 hours the embryos were incubated with the PH3 primary antibody (1:200) overnight at 4°C. After repeated MABTw

washes to remove any unbound primary antibody the secondary antibody sheep anti-rabbit antibody conjugated to Alexa 546 fluorophore (1:500) was incubated with the embryos in 2% blocking buffer (w/v) (Roche, Welwyn Garden City, UK) overnight at 4°C. Embryos washed in PBS then gradually equilibrated in glycerol 75% (v/v) and stored at 4°C until imaging, see section 2.3.2 and 2.3.3.

2.10 Pharmacological manipulation of the zebrafish embryo

2.10.1 Pharmacological manipulation of the nitric oxide pathway

2.10.1.1 Inhibition of nitric oxide synthase

L-nitro arginine methyl ester (L-NAME) is a non-specific inhibitor of the nitric oxide (NO) synthase enzyme. L-NAME (Sigma-Aldrich, Gillingham, UK) was made up in E3 media with 1% DMSO as solvent then diluted to a final concentration of 1mM as per the method previously published (North et al. 2009). Although L-NAME has good solubility published data using small molecule drug screens and local methods for drug exposure using embryonic zebrafish use DMSO as an initial solvent with subsequent dilution into E3. This working solution was added to embryos from 24hr post fertilisation and exchanged with freshly made L-NAME every 24hr due to the short half-life of the drug. All imaging was performed in 1% (w/v) low melting point agarose made with the L-NAME dosed E3 media.

2.10.1.2 Pharmacological addition of nitric oxide

Sodium nitroprusside acts as a NO donor to increase the available NO *in vivo*. This compound has been used by a previous PhD student in our lab and has been shown to produce reproducible vascular effects in the developing zebrafish embryo at the time points I was interested in observing, with existing methods. Sodium nitroprusside (Sigma-Aldrich, Gillingham, UK) was made up in 1% DMSO (Sigma) and diluted in E3 to a final concentration of 100 µM.

Media with the active compound was made up fresh and exchanged every 24 hrs.

2.10.1.3 Detection of NO signalling in the developing zebrafish embryo

The diaminofluorophore 4-amino-5-methylamino-2,7-difluorofluorescein diacetate (DAF-FM-DA) (Molecular probes, Invitrogen, Paisley, UK) fluoresces in the presence of NO. This fluorescence, which can be detected using laser excitation at a wavelength of 488 nm and detected at 530 nm has been used to identify alterations in NO production in the developing zebrafish embryo *in vivo* (Lepiller et al. 2007). Data from this paper shows this fluorophore to be a specific reporter of NO levels in the developing zebrafish embryo, reduction in fluorescence was seen after incubation with the NOS inhibitor N-monomethyl-L-arginine monoacetate (L-NMMA) and a specific NO scavenger carboxy-2-phenyl-4,4,5,5-tetramethylimidazolinone-3-oxide-1-oxyl (c-PTIO). Levels of the reporter were also increased in the zebrafish embryo by SNP exposure a NO donor. Embryos incubated in 5 μ M final concentration of DAF-FM for 2 hours at 28°C protected from light. The embryos are then mounted as per previous methods for *in vivo* fluorescence imaging (section 2.3.2)

2.10.2 Pharmacological manipulation of the Notch signalling pathway

2.10.2.1 Inhibition of notch signalling with DAPT

N-[N-(3,5-Difluorophenacetyl)-L-alanyl]-S-phenylglycine t-butyl ester (DAPT) is a gamma secretase inhibitor which inhibits the enzymatic cleavage of the Notch ligand receptor complex at the cell membrane. This leads to reduction of Notch receptor, which activates transcription of Notch target genes in the signalled cell. DAPT stored at 50 mM stock in DMSO was used for zebrafish experiments diluted into E3 media at final concentrations of 100 μ M and 0.2% (v/v) DMSO. The DAPT was added to the embryo media at 48 hpf until imaging and quantification at 72hpf.

2.11 Real time reverse transcription quantitative polymerase chain reaction

Real time reverse transcription quantitative polymerase chain reaction (RT-qPCR) allows for the quantitative assessment of mRNA expression in differing environmental conditions. The expression of a gene of interest is normalised to expression levels of a known housekeeping or control gene, the expression level of which should remain constant between the conditions. Using a PCR reaction the amplification rates of the gene of interest in the different conditions can be compared to derive differences in gene expression or mRNA/cDNA copy number after normalisation for housekeeping gene expression differences. This technique allows us to quantify the effect of different conditions on even very lowly expressed genes by virtue of the PCR amplification phase of the RT-qPCR reaction. We used SYBR-green for quantification for our RT-qPCR reactions; this fluorophore incorporates into double stranded DNA and causes fluorescence. This fluorescence allows the detection and quantification of double stranded DNA amplification by PCR reaction after each amplification cycle.

2.11.1 Isolation of zebrafish embryonic total RNA

2.11.1.1 Tissue preparation for RNA extraction

For total RNA isolation I chose to use the trunk tissue from the embryonic zebrafish to look at expression differences in the vascular tissue and surrounding peri-vascular tissue. As we were interested in the changes in gene expression related to different flow conditions we were unable to isolate endothelial tissue from the other tissues of the trunk as the time taken to isolate it was felt would alter the expression levels.

The trunk and tail of the Tricaine anaesthetised zebrafish was isolated from the head using a scalpel blade #6 (Swann-Morton, Sheffield, UK) and forceps Dumont #5 tweezers, the trunk and tail tissue was then immediately transferred to 250 µl TRIzol (Sigma-Aldrich, Gillingham, UK) on ice. For 48 hpf embryos 30 sectioned embryo trunks were pooled together, for 72 hpf embryo 20 trunks

were pooled to ensure adequate yields of total RNA. The pooled tail sections in TRIzol were then snap frozen in liquid nitrogen and transferred directly to the -80°C freezer until total RNA extraction. The rapid processing and snap freezing is performed to minimise the possibility of RNA degradation after tissue sectioning and allows multiple groups of total RNA to be extracted together without any time delays or differences in processing time which may influence subtle expression changes in the tissue.

2.11.1.2 RNA extraction

Pooled tail sections were transferred from -80°C freezer directly on to ice and as the TRIzol reagent melted the tissue was homogenised using an eppendorf pestle (Carl Roth, Karlsruhe, Germany) and then aspirated through a 1 ml syringe (plastipak BD, New Jersey, USA) and 25 gauge needle (Microlance 3 BD, New Jersey, USA) to fully homogenise the tissue for RNA extraction. 50 µl of chloroform is added to the homogenate and TRIzol reagent, inverted and left at room Temperature (RT) for 3 min then centrifuged at 13,000 rpm for 15 min at 4°C. The aqueous supernatant containing the RNA is removed and is then precipitated into 85 µl of isopropanol and pelleted by centrifugation (13,000rpm, 15 min at 4°C). This is resuspended in 15 µl of RNase free H₂O and stored at -80°C until required for reverse transcription to form cDNA. Prior to storage RNA is quantified by spectrophotometry Nanodrop ND100 spectrophotometer, (ThermoFisher Scientific, Paisley, UK).

2.11.2 Reverse transcription of extracted total RNA

cDNA synthesis is performed using the Verso reverse transcriptase kit (Thermo scientific, Paisley, UK). 1 µg equivalent of RNA template is initially heated to 70°C for 5 min to remove any secondary structure incubated with a synthesis buffer, reverse transcriptase enhancer, verso enzyme and primer mixture. A primer mixture of 3:1 (v:v) of random hexamers:oligo-dT was used for all cDNA synthesis of zebrafish total RNA. The reaction was incubated at 42°C for 30 min, then cDNA quantified by Nanodrop spectrophotometer and stored at -20°C.

2.11.3 Identification and optimisation of primers for real time RT-qPCR

2.11.3.1 Genes analysed and primers for RT-qPCR analysis

Table 2.7 Primers for RT-qPCR analysis with amplification product size and efficiency.

Gene	GenBank Accession Number	Primer Seq 5' – 3'	Primer efficiency (%)	Fragment size (bp)
<i>vegfab</i>	NM_001044855.2	CAGTGTGAGCCTTGCTGTTCC CCATAGGCCTCCTGTCATTT	102.7	230
<i>vegfc</i>	NM_205734	CAGTGTGAATGCCGAAAAGA GAGGTTGACTCCTCGGACAC	95	178
<i>kdr/flk1</i>	NM_001024653	CGCGCAACAGGTCACTATT GTGAGGAGGATGTCGAGGAG	91	235
<i>kdr-l/flt1</i>	NM_131472	GCCAAGTTCAGATTTGA GGAAACTCCCATTGTTGCT	97.5	117
<i>flt4</i>	NM_130945	TCTCGTTAGTGCCGTATCCA GATGATGTGTGCTGGCTGTT	98.6	164
<i>ephrinB2</i>	NM_131023	ACCACGTTGTCACTCAGCAC AGATGTTTCTGGGCTCTGT	93.3	205
<i>her6</i>	NM_131079.1	CGCCATGAACTATCCAACAC CATGGGTTGACTGAAGGATG	95	70
<i>her12</i>	NM_205619	GCTGAGGAAGCCGATAGTTG GCGAGAGGAAGTGGACAGAC	94	248
<i>notch3</i>	NM_131549	CGGCCTGGTTATATTGGTTC TCTAAAGCCTCGCTGACACA	101	138
<i>nrarpa</i>	NM_181495	AGCTGCTTCGGACTCGTTAC CGAGGTAGCTGATGCAGAGA	95.3	229
<i>dll4</i>	NM_001079835	GCTTGGCTCACCTTTCTCAT CGGAAGAAAGTCTGCAGTC	92.15	155
<i>cxcr4a</i>	NM_131882	TTGTGCTCACTCTGCCATTC ACCGGTCCAACTGATGAAG	90	144
<i>β-actin2</i>	NM_181601	GCAGAAGGAGATCACATCCCTGGC CATTGCCGTACCTTCAACGGTTC	95.70	322

Primers were designed using Genscript RT-qPCR primer design software (<http://www.genscript.com/>) to produce a PCR product of between 70 and 250bp.

2.11.3.2 Primer optimisation for RT-qPCR

2.11.3.2.1 Primer specificity

Primers were then run on a gradient PCR program with wildtype cDNA as a template, the gradient provides a range of annealing temperatures in 1°C increments across the thermal cycler. This enables the optimum annealing temperature to be identified and when the product is then run on an agarose gel confirmation of a single and thus specific PCR product can be determined. If a primer pair, produce multiple bands across the annealing temperature gradient then new primers are designed for the gene of interest, as specificity is inadequate. Confirmation of the specificity of the PCR product is done by DNA sequencing (Core facility University of Sheffield Medical school, UK) of the purified PCR product then in silico analysis of sequence similarities using BLASTn (<http://blast.ncbi.nlm.nih.gov/Blast.cgi>) to search against the zebrafish genome.

2.11.3.2.2 Primer efficiency

Primer pairs were then run using the IQ SYBR-green mastermix (Bio-Rad, Hemmel-Hempstead, UK) with a standard curve of wildtype cDNA serial dilutions from 10 pg-1 µg. Accepted primer efficiency for RT-qPCR is 90-105%, the efficiency of our primers is derived by calculating the slope of the line of best fit for the cDNA standard curve, slope of 3.32 correlates to a primer efficiency of 100% (Graphpad Software, San Deigo, USA). Each standard curve was run in duplicate with non-template controls to derive primer efficiency data.

2.11.4 Analysis of real time RT-qPCR data

All RT-qPCR was performed on a MyIQ single colour real time PCR detection system (Bio-Rad, Hemel-Hempstead, UK) using IQ SYBR-green supermix (Bio-Rad, Hemel-Hempstead, UK). Each gene of interest and control gene (β -actin2) pair was run in duplicate to ensure technical reproducibility of the PCR amplification. The analysis was performed on 3 biological replicates of cDNA, which was pooled from 20-30 embryos depending on the age of embryos to ensure reproducibility of any changes in gene expression derived from this analysis.

Table 2.8 SYBR-green mastermix for RT-qPCR

SYBR-green supermix	10 μ l
F primer (conc as per optimisation)	0.5 μ l
R primer (conc as per optimisation)	0.5 μ l
mQ H ₂ O	5 μ l
cDNA (conc as per optimisation)	1 μ l
total	20 μl

Data analysis was performed on IQ5 optical system software (Bio-Rad, UK) which converts the raw Relative Fluorescence Units (RFU) into a mean threshold cycle for replicated samples based on plate templates. The cycle threshold (Ct) is then used to obtain a $\Delta\Delta$ Ct value which adjusts the change in expression of the gene of interest to any change in expression of the control gene (β -actin2) this can then be converted into a fold change for the gene of interest by the equation: $2^{-(\Delta\Delta\text{Ct})}$. Graphical representation of the amplification rates of a number of assayed genes as generated by the analysis software can be seen in figure 2.4 A, each individual coloured line represents an individual gene with the point it crosses the threshold (horizontal green line) in the linear amplification phase.

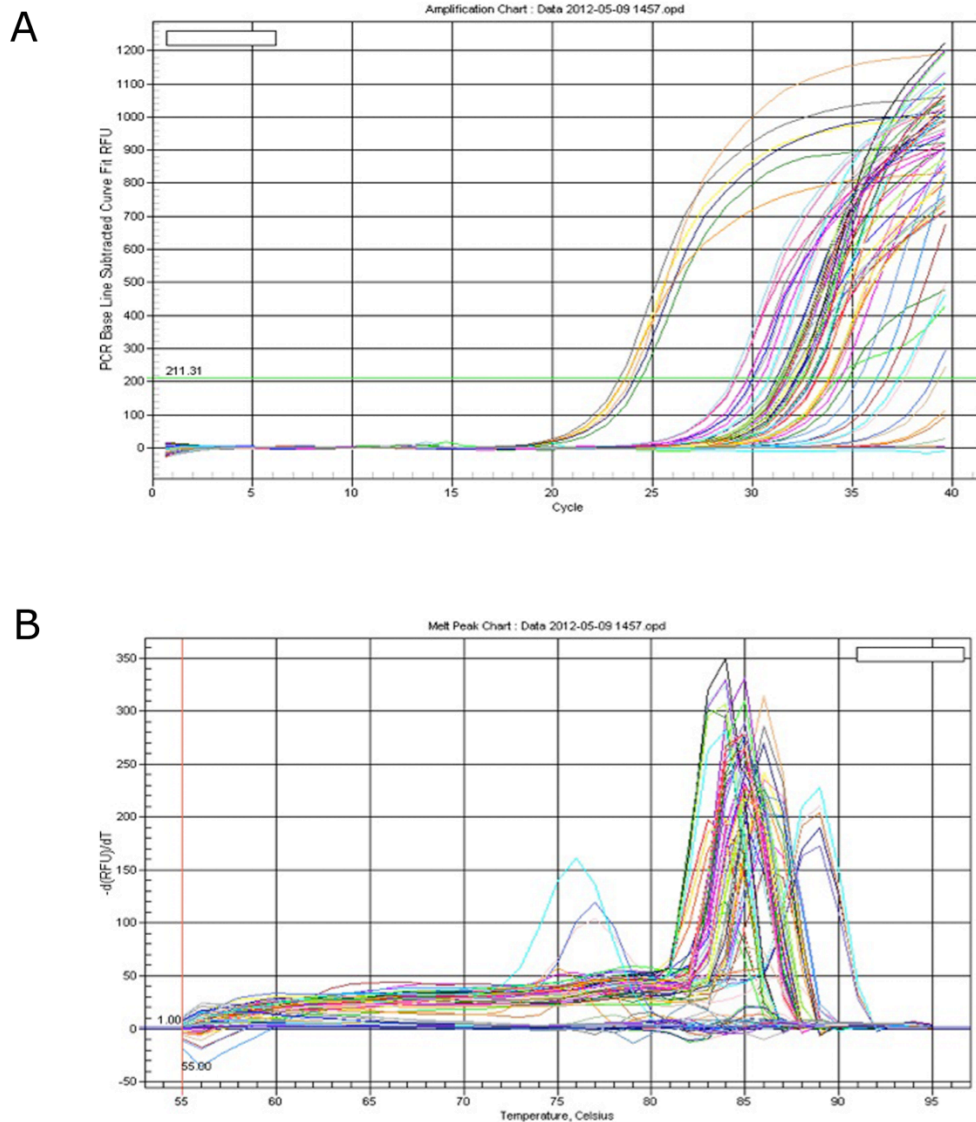


Figure 2.4 Fluorescence amplification data and melt curve analysis from RT-qPCR for multiple gene targets and biological replicates.

A. Graph showing the fluorescence amplification (RFU) of individual PCR reactions (coloured line) against PCR cycle. B. Melt curve data showing a single fluorescence peak for the majority of PCR products indicating single PCR product. Light blue line shows multiple peaks that may indicate contamination with multiple primers or excess primer dimer product.

2.11.4.1 Melt curve

On completion of the PCR amplification the PCR product is analysed for specificity by quantifying the amount of fluorescence during incremental heating of the product. In the presence of a single PCR product all the fluorescence will be lost in a tight temperature range as the single product has a specific size dependent denaturing temperature. If the multiple products are present as a result of non-specific priming then multiple melt curve peaks will be seen for a single gene product. This provides additional confirmation of specific gene amplification for each RT-qPCR analysis (Figure 2.4 B).

2.12 Statistics

2.12.1 Statistical analysis and significance

All statistical analysis and graphical representation was done with GraphPad Prism v5.0 Software (GraphPad Software, San Diego USA). Data presented as mean \pm Standard error of the mean (SEM), n notates the number of embryos in the group analysed. The statistical test used to analyse significance is annotated in the individual figure along with the post-test analysis where appropriate

2.12.2 Graphical annotation of significance

Table 2.9 Statistical significance as represented on all graphical results.

Graphical annotation	Statistical significance
*	P<0.05
**	P<0.01
***	P<0.001

2.12.3 Power calculations

Post hoc power calculation performed using G*power v3 software (<http://www.psych.uni-duesseldorf.de/abteilungen/aap/gpower3/download-and-register>) open source software.

Chapter 3 Characterisation of the angiogenic phenotype of the Von Hippel-Lindau homozygous mutant zebrafish

3.1 Introduction

Hypoxic signalling drives angiogenesis in both normal physiology and pathology. The *vhl* homozygous mutant zebrafish has been shown previously to undergo angiogenesis as a result of constitutive hypoxic signalling (Van Rooijen et al. 2009). In this chapter I have extended these initial descriptions by undertaking a detailed assessment of development of the intersegmental and dorsal longitudinal vessels of the *vhl*^{-/-} mutant compared with wildtype, as a preliminary to mechanistic studies in later chapters. This characterisation will enable me to use this model to test hypotheses regarding the role of regulatory pathways in the genesis of these angiogenic vessels.

3.2 Results

3.2.1 Characterisation of the vascular phenotype of the *vhl*^{-/-} mutant

3.2.1.1 Formation of the intersegmental artery in the *vhl*^{-/-} mutant

Tg(vhl^{hu2117}^{-/-};fli1:eGFP) embryos were imaged using spinning disc confocal fluorescence microscopy and the vascular pattern compared to that of wildtype controls (Figure 3.1). I focused on formation of the ISV, an easily imaged vessel. These have been extensively studied and provide an accessible model of embryonic vessel formation. The ISV is formed from angiogenic sprouts emerging from the aorta and primary cardinal vein. This vessel is one of the earliest vessels formed in the developing zebrafish embryo (Isogai 2003; Childs et al. 2002), beginning around 21 hpf.

My observations of vessel patterning in 2 dpf *vhl* mutants revealed little or no differences in vessel patterning, even though the ISVs have already formed by this stage. However, at 3 dpf, I found that the diameter of ISVs in *vhl* mutants was significantly increased compared with wildtype embryos (Figures 3.1 and 3.2).

3.2.1.1.1 Increased diameter of the DLAV in the *vhl*^{-/-} mutant

The DLAV forms from the angiogenic sprouts of the ISV which join with ipsilateral sprouts from adjacent somites and subsequently branch across the midline to form the DLAV plexus which progressively remodels into a single vessel from two initially adjacent vessels during development (Zygmunt et al. 2012) (Figure 3.1 arrowhead). Since this vessel is formed after the ISV is established, and by a somewhat different process of fusion and remodelling (Armer et al. 2009), I wanted to see if the enlargement in diameter seen in the ISV was also seen in the DLAV. Figure 3.2 C shows that the increase in diameter of the DLAV at 3 dpf is about 60%, even greater than the increase seen in the ISV at the same time point.

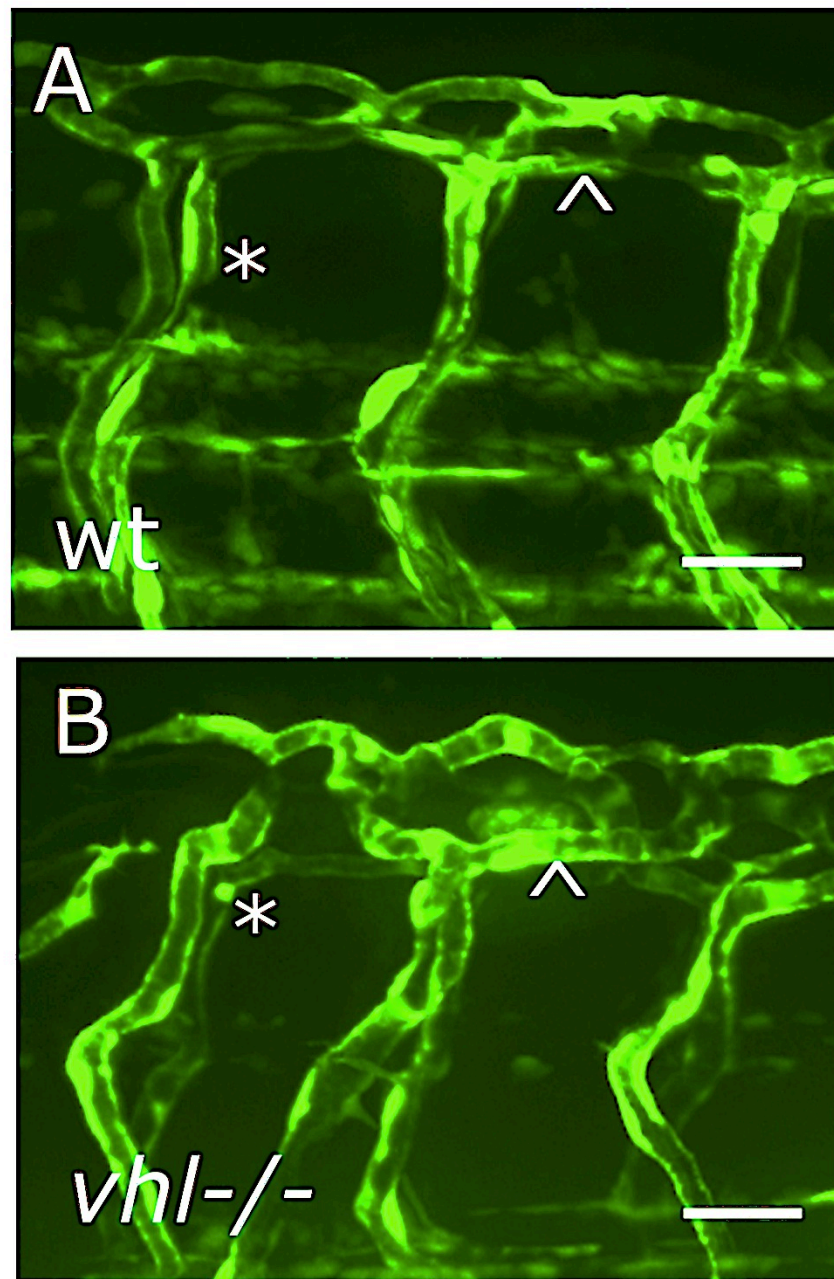


Figure 3.1. Comparison of trunk vessel morphology in the *vhl*^{-/-} mutant and wildtype at 3dpf.

A. Wild type *Tg(fli1:eGFP)* imaged at the mid trunk at 3 dpf, * indicates paired intersegmental vessel (ISV) and ^ indicates the dorsal longitudinal vessel (DLAV) Scale bar 50 μ m. **B.** *vhl*^{-/-} mutant showing enlargement of the ISV and DLAV vessels in addition to increased tortuosity of the DLAV with looping which extends above the pigment line.

3.2.1.1.2 Increased total trunk vessel length in the *vhl*^{-/-} mutant

In addition to the significant change in ISV and DLAV diameter I observed an increase in tortuosity of both the ISV and DLAV at 3 dpf in addition to an increased number of angiogenic sprouts of both vessels in the *vhl*^{-/-} mutant. I measured total vessel length in a two-somite region to quantify this. This data showed a significant 50% increase in total vessel length in *vhl*^{-/-} mutants compared to controls at 3 dpf (Figure 3.2 B). Any additional loops or vessel sprouts are included in this quantification, giving quantification of both the increased tortuosity and branching in the trunk vessels in the *vhl*^{-/-}.

3.2.1.1.3 Increases in the area of endothelial cytoplasm in the *vhl*^{-/-} mutant

Figure 3.2 D, shows the total endothelial area in the same two-somite mid trunk region in the *vhl*^{-/-} mutant and wildtype. This measurement was obtained by comparing the same two-somite region of a *vhl*^{-/-} mutant and control embryo. The *vhl*^{-/-} mutant has a significantly larger area of fluorescence ($46.54 \pm 3.1\%$ than wildtypes $28.97 \pm 1.47 \mu\text{m}^2$), (SEM n=5), indicating around 60% increase in the area of endothelium in the *vhl*^{-/-} mutant.

3.2.1.2 Is the vessel phenotype of the *vhl*^{-/-} mutant due to accelerated development of the normal phenotype?

The vascular phenotype of the *vhl*^{-/-} mutant, particularly the looping of the DLAV, can be identified as early as 3 dpf as shown in figure 3.1. The patterned trunk vessels develop normally by angiogenesis prior to appearance of this abnormal phenotype. It was possible that the phenotype I identified might have represented acceleration of normal development. I therefore imaged the same region at 4,5 and 7 dpf. The photomicrographs of the same region over this timeframe can be seen in figure 3.3.

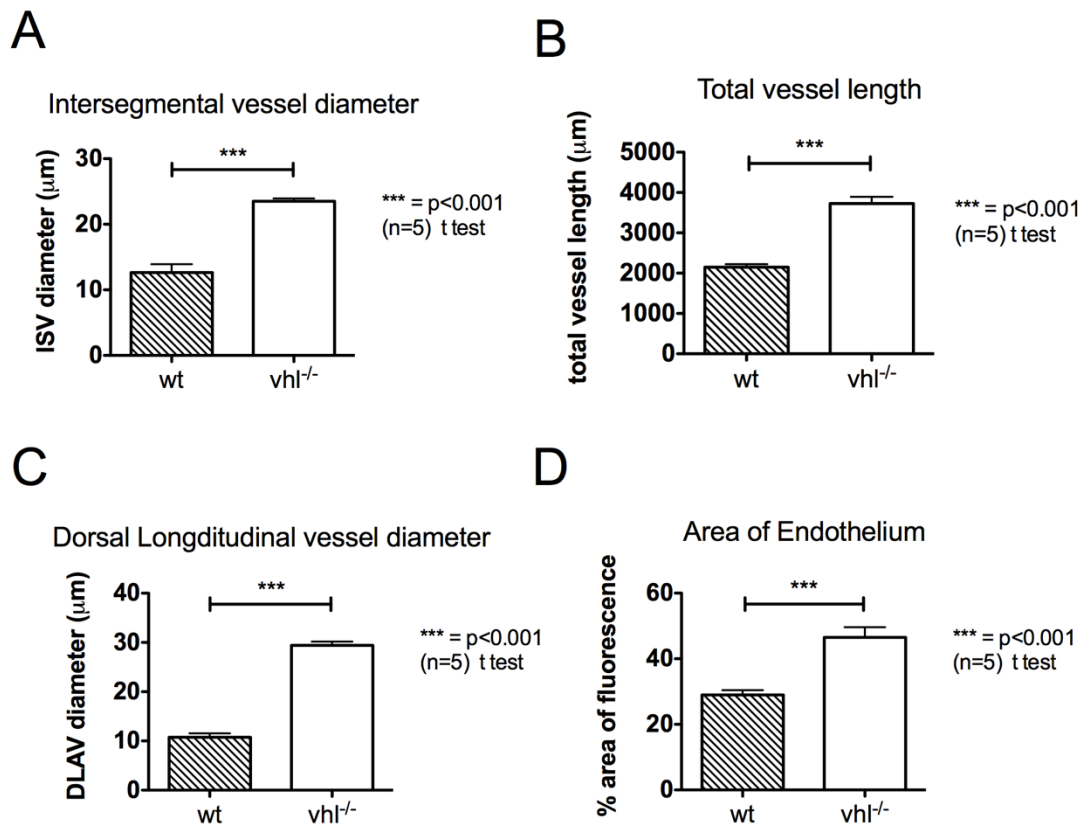


Figure 3.2 Quantification of the differences in the vascular phenotype of the wt and *vhl*^{-/-} mutant.

A. ISV diameter using 3 dpf *Tg(vhl^{hu2117-/-};fli1eGFP)* over a 2 somite mid trunk region of interest (ROI). The ROI is taken from the level of the cloacae, mid trunk and contains the 2 adjacent somites with associated vessels (for full method see section 2.4.2). The ISV was measured at 2 points in each of the three vessels and the mean of this was used for statistical comparison across the 5 embryos. **B.** Total vessel length in *vhl*^{-/-} vs wt in the same ROI.

Figure 3.2 (cont) The length of the ISV, DLAV and additional aberrant vessels was measured using the segmented line tool in imageJ to give a total vessel length within the ROI. **C.** DLAV diameter at 3dpf in the *vhl*^{-/-} compared to wt, same ROI. 2 measurements of the vessel diameter were taken from the mid somite point **D.** Total area of GFP fluorescence in *vhl*^{-/-} vs wt. Total area obtained by forming a binary image in image J software using the same threshold level. This gave a total area of GFP within the ROI, which could be used to derive the 2D area of GFP within the ROI when the image is flattened to a compressed focus image. All groups mean \pm SEM, n=5, *** p<0.001, unpaired t test.

From 4 to 7 dpf there was continued enlargement of the ISV and DLAV. The DLAV becomes increasingly tortuous, dilated and forms loops above the pigment line as the fusion of the DLAV plexus is abnormal compared to the remodelling seen in wildtypes (Zygmunt et al. 2012). However by 7 dpf there is extensive angiogenesis in the mutant, which is never seen in the wildtype even at later time points (Isogai et al. 2001). This aberrant angiogenesis progresses from the distal ISV, with sprouts forming from 3dpf and progresses proximally down the ISV towards the aorta and PCV over time. Significantly, in the wildtype, patterning of the ISV and DLAV is limited to the somite boundaries and follows a characteristic pattern (Childs et al. 2002). The aberrant angiogenesis of the mutant initially can only be seen at the distal ISV at 3 dpf, but then begins to penetrate the somite boundaries; a feature not observed in wildtypes (Childs et al. 2002). By 7 dpf these angiogenic sprouts form lumenised communications between pairs of ISV by crossing the somite and from the ISVs to the expanded DLAV plexus.

3.2.1.3 Lymphangiogenesis in the *vhl* mutant is also abnormal

Tg(fli1:eGFP) labels endothelium of the developing lymphatic system as well as the arterial and venous vessels. In Figure 3.3 this can be seen in the wildtype embryo as the emergence of fine sprouts between 3 and 4 dpf at the horizontal myoseptum consistent with previous reports (Hogan, Herpers, et al. 2009b). Between 4 dpf and 7dpf there is enlargement, increased tortuosity and angiogenic sprouting of these developing lymph channels in the *vhl*^{-/-} mutant compared with the tightly regulated patterning seen in the wildtype embryos (Figure 3.3 arrow in 7 dpf panels).

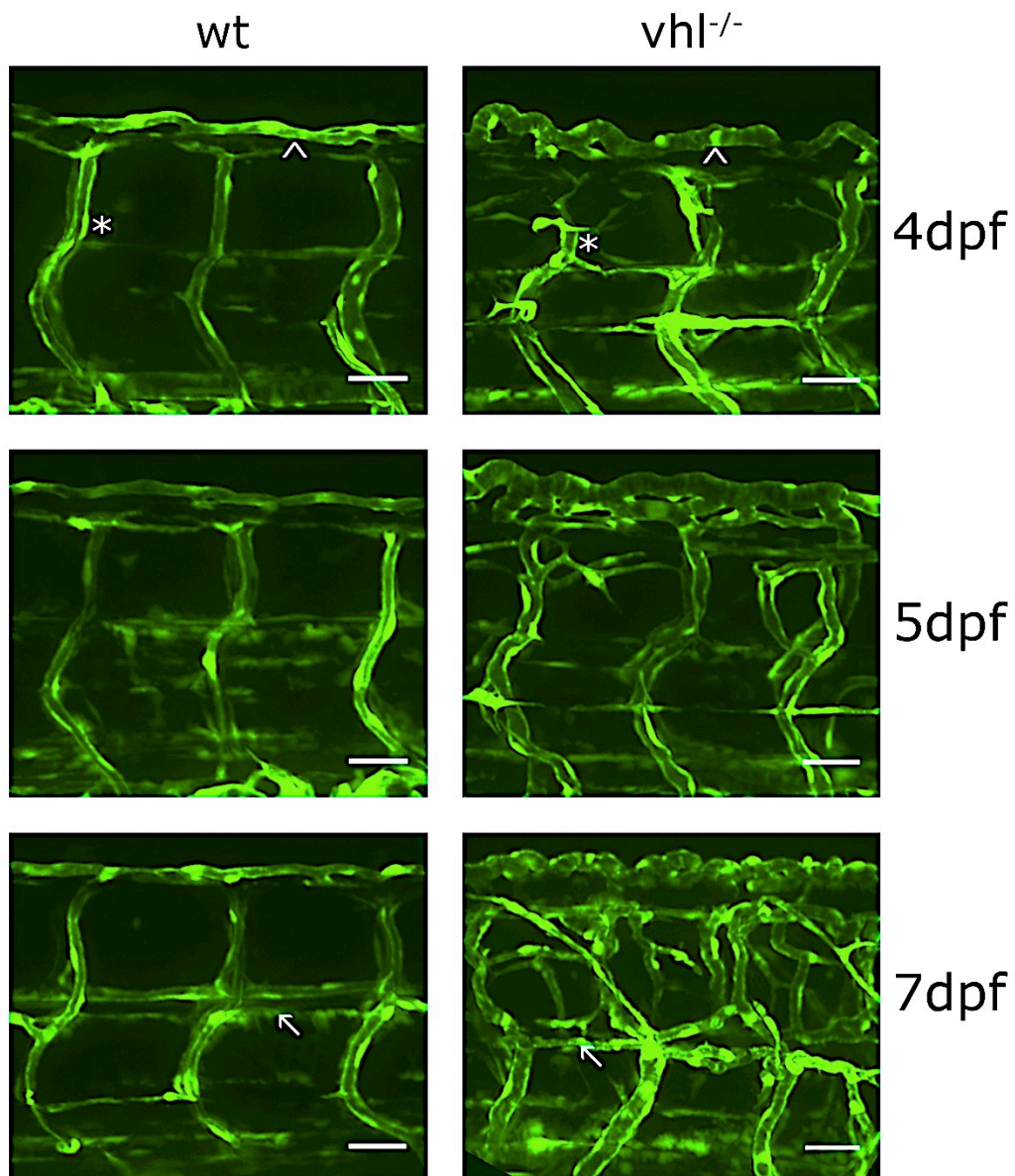


Figure 3.3. Progression of the angiogenic phenotype of the *vhl*^{-/-} mutant from 3dpf to 7dpf.

Top panel shows a comparison of the mid trunk vessel morphology photomicrographs of *Tg(fli1:eGFP)* of 2 somites showing the ISV and DLAV of the wildtype and *vhl*^{-/-} mutant at 4,5 and 7 dpf. Scale bar 50 μ m. Asterisk = ISV; arrowhead = DLAV; arrow = lymphatic vessels at the myoseptum.

3.2.1.4 Does the cerebral circulation of the *vhl*^{-/-} mutant show the same phenotype as the trunk vessels?

Since the *vhl*^{-/-} mutant has constitutive activation of hypoxic signalling the vessel changes I identified in trunk vessels would be likely to be present in other vascular beds. I next sought to confirm this.

Previously published data indicated that the central arteries (CtA) of the mid and hindbrain project up into the brain from the posterior communicating segment and the basilar artery (Isogai et al. 2001). Although these vessels are formed by angiogenesis the mechanism by which they sprout and re-model is different to that of the trunk vessels (Bussmann et al. 2011). Despite this, I found a significant enlargement in diameter of the CtA in *vhl*^{-/-} mutants, an increase of 50% compared to controls (Figure 3.4).

This difference in diameter of the CtA in the *vhl*^{-/-} mutant is similar to the increases in size seen in both the ISV and DLAV seen in Figure 3.2. This suggests that the angiogenic phenotype of the *vhl*^{-/-} mutant is seen in spatially distinct vascular beds.

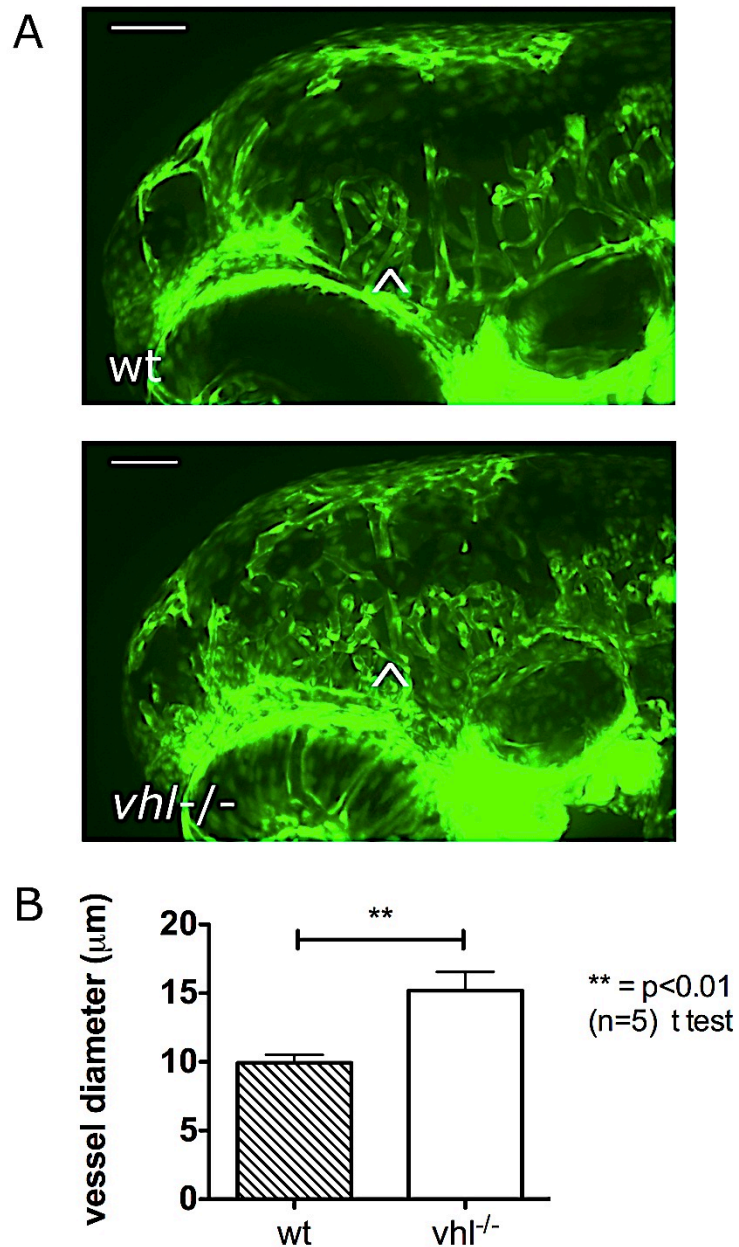


Figure 3.4 Differences in the cerebral vasculature of the *vhl*^{-/-} mutant using the *Tg(vhl^{hu2117}-/-;fli1:eGFP)* line

A. Cerebral vasculature at 60 hpf in the top panel shows the Central arteries (CtA) of the wt embryo penetrating the mid and hind-brain. In the lower panel the same vessels in the *vhl*^{-/-} mutant are dilated and form multiple sprouts and communications. Scale bar, 100 µm. **B.** Comparison of the diameter of the CtA in the wt and *vhl*^{-/-} (Mean and SEM; ** p<0.01; t test; n=5).

3.2.2 Do the increases in endothelium in the *vhl*^{-/-} mutant result in lumenised vessels?

The *Tg(fli1:eGFP)* line labels the cytoplasm of endothelial cells. Although the dynamics and morphology of this fluorescent protein have been used by some groups to indicate lumenisation of trunk vessels this has only been published in established developmental vessels of the zebrafish (Herwig et al. 2011), not in angiogenic sprouts stimulated by hypoxic signalling. I wanted to ascertain whether the increase in endothelial cytoplasm and vessel sprouting in the *vhl*^{-/-} mutant led to lumenisation and formation of patent vessels. To assess lumenisation I injected nanoparticles Qdots (Sigma UK).

The photomicrographs in the lower panel of Figure 3.4 show angiogenic sprouts emerging from the distal ISV in the *vhl*^{-/-} mutant containing intravascular Qdot nanoparticles. This is the region of the vasculature I have imaged using the endothelial GFP marker. The intravascular Qdots injected into the circulation indicate these sprouts are lumenised and thus are likely to be formed by or connected to stalk cells which form the bulk of the developing angiogenic vessel behind the tip cell (Potente et al. 2011). Although these primitive sprouts do not carry erythrocytes they clearly form a lumen in continuity with the circulation and vasculature. This suggests the endothelium of these developing angiogenic sprouts, are exposed to haemodynamic forces.

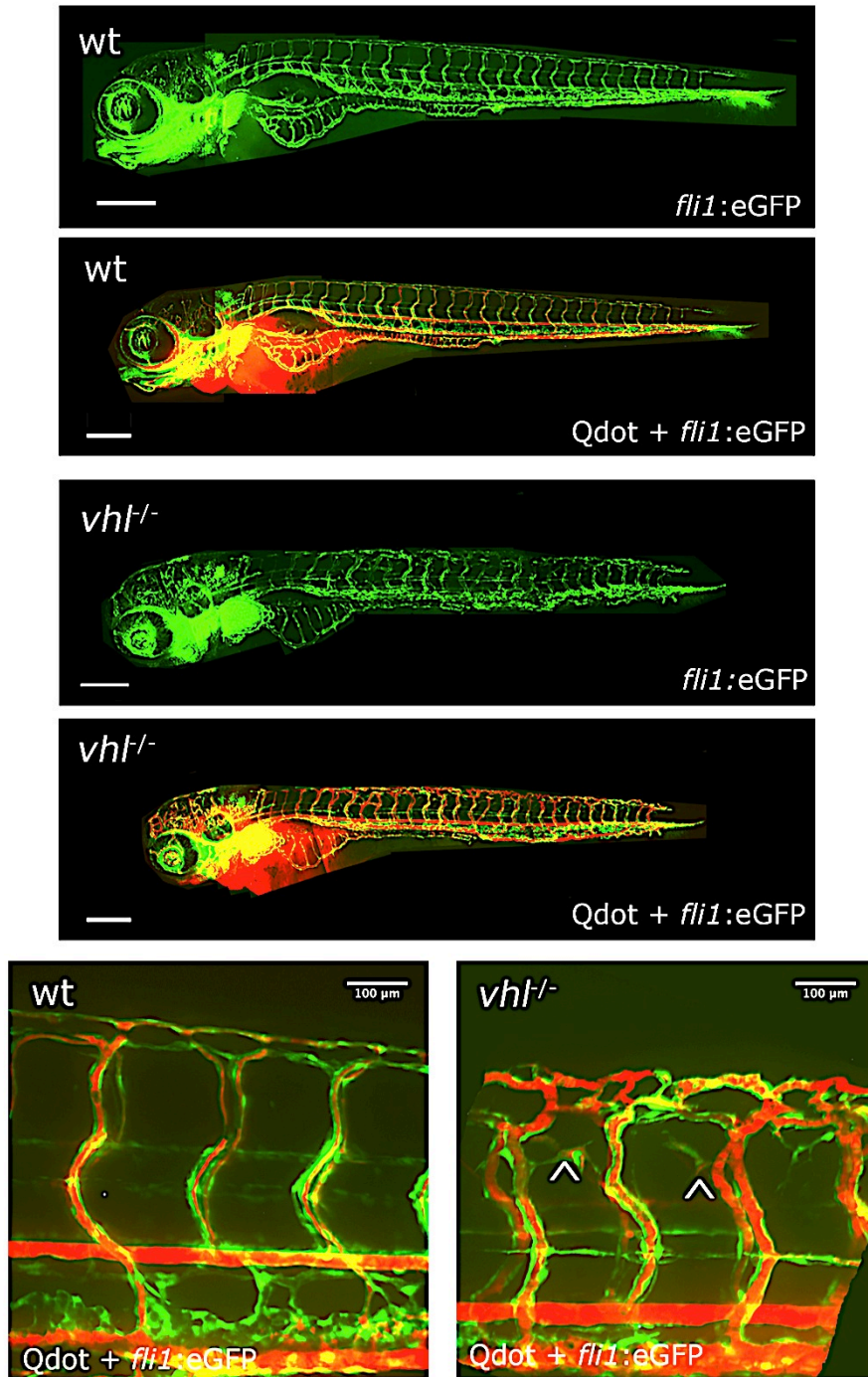


Figure 3.5 Angiograms of *vhl*^{-/-} mutant and wt embryos at 4 dpf. Qdot 205 nm non-targeted nanoparticle were injected into the circulation of 4 dpf wt and *vhl*^{-/-} embryos. Top two panels shows whole mount wt *fli1:eGFP*, lower two panel shows *vhl*^{-/-}; *fli1:eGFP* and Qdot fluorescence overlay. Scale bar, 400 μ m. Bottom panel shows expanded mid trunk region (lumenised angiogenic sprouts containing Qdots, arrowhead). Scale bar 100 μ m.

3.2.3 Increases in endothelial cell number in the *vhl*^{-/-} mutant

Since the *vhl* mutant has increased endothelial area and vessel size, I hypothesised that these changes were likely to be accompanied by increased endothelial number. I therefore crossed the *Tg(flk1:eGFP-NLS)* into the *vhl* mutant background enabling more detailed assessment. This transgenic line uses the *flk1* zebrafish promoter to drive endothelial expression of GFP tagged with a nuclear localising signal that restricts fluorescence to the nuclei. This transgenic line enabled me to quantify endothelial cell number.

To simultaneously examine both membrane behaviour and nuclear dynamics in the *vhl* mutant I then also crossed the *Tg(flk1:eGFP-NLS)* with the *Tg(kdr-l:HRAS-mCherry)* expressing endothelial membrane-tagged RFP. This dual transgenic enabled me to examine both endothelial cell number and accurately measure the aortic lumen in the wildtype and the *vhl*^{-/-} mutant, in addition to vessel morphology.

3.2.3.1 Increased endothelial cell number in the aorta of the *vhl*^{-/-} mutant

In the *vhl*^{-/-} mutant at 3 dpf I found a significant increase in endothelial cell number in the aorta. Within the same two somite mid trunk region examined in Figure 3.6 there was a highly significant 50% increase in endothelial cell number in *vhl* mutants compared to controls (Figure 3.6 & 3.7).

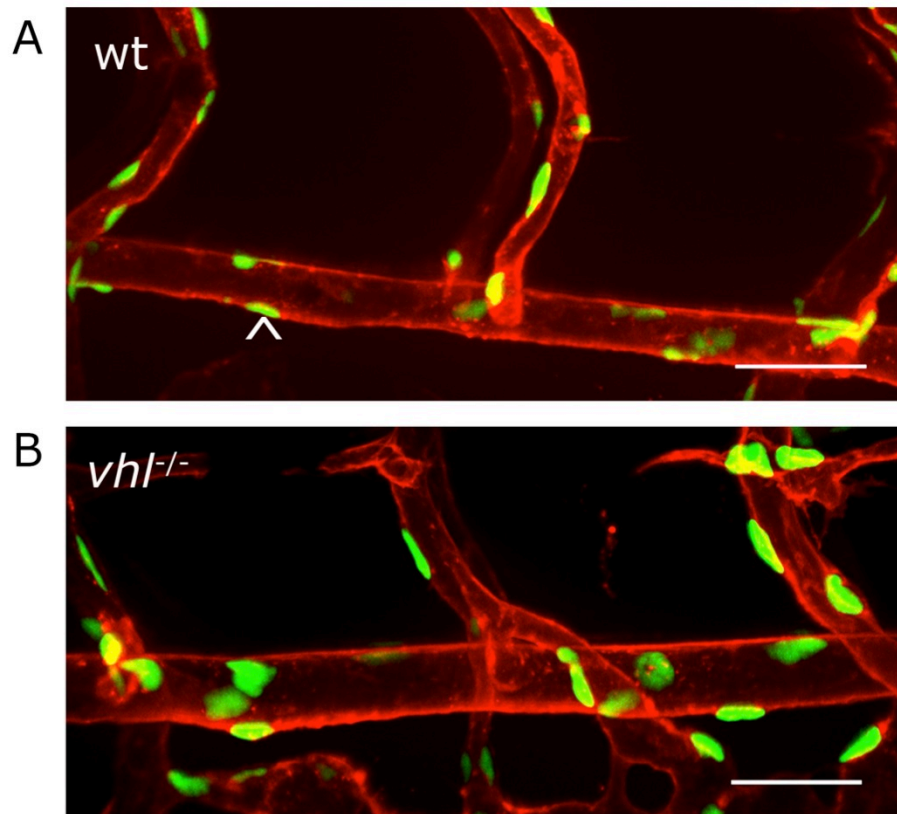


Figure 3.6 Aortic endothelial cell number and aortic diameter in the wt and *vhl*^{-/-} mutant of the mid trunk aorta.

A. The wt aorta with arterial ISV sprouting from the aorta (arrowhead) with the endothelial membrane labelled with red fluorescence, *Tg(kdr-l:HRAS-mCherry)* and the nuclei labelled with GFP *Tg(flk1:eGFP-NLS)*. Scale bar 50 μ m. **B.** Aorta of the *vhl*^{-/-} mutant showing increased number of endothelial nuclei over the 2 somite region using the same dual transgenic.

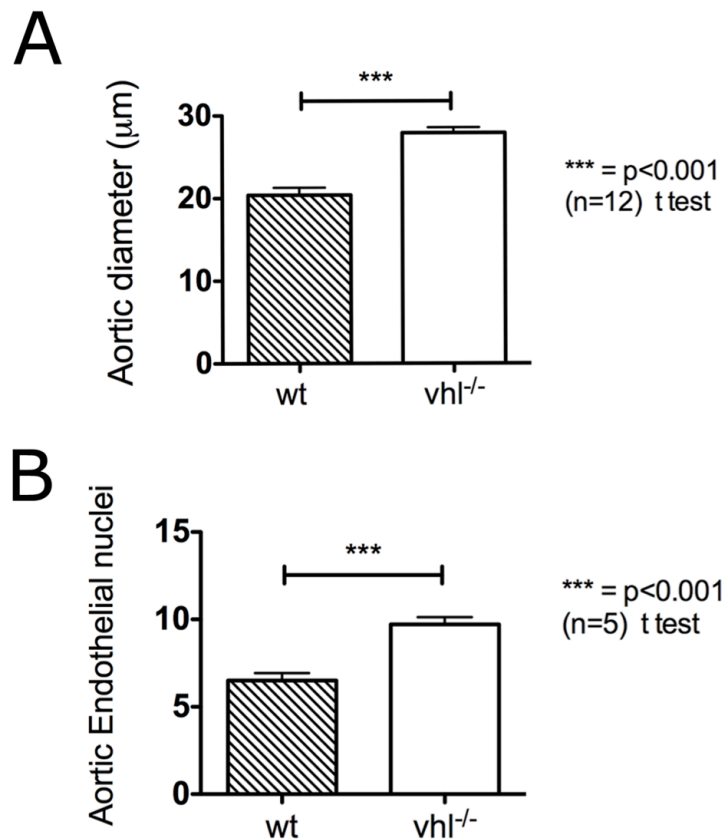


Figure 3.7 Quantification of aortic endothelial cell number and aortic diameter in the wt and *vhl*^{-/-} mutant of the mid trunk aorta.

A. Luminal diameter of the aorta $20.4 \pm 0.9 \mu\text{m}$ in the wildtype and $27.9 \pm 0.6 \mu\text{m}$ in the *vhl*^{-/-} mutant (mean \pm SEM; t test; *** = p<0.001; n=12). Measured using the *Tg(kdr-l:HRAS-mCherry)* line. **B.** Number of aortic endothelial cells in a matched 2-somite region in wt and *vhl*^{-/-} mutants containing; 6.5 ± 0.4 cells in the wt and 9.7 ± 0.4 cells in the *vhl*^{-/-} mutant (mean \pm SEM; t test; *** = p<0.001; n=5) measured using the dual transgenic line *Tg(flk1:eGFP-NLS) Tg(kdr-l:HRAS-mCherry)*.

The two measurements were obtained from different transgenic backgrounds less of the dual transgenics were available for repeated observation due to smaller numbers of co-segregating reporter constructs.

3.2.3.2 Increased aortic diameter in the *vhl*^{-/-} mutant

The *Tg(kdr-l;HRAS-mCherry)* line allows accurate membrane localisation at higher magnification and enabled me to accurately measure luminal size of this vessel. Figure 3.6 shows that the aorta of *vhl* mutants was of significantly larger diameter, an increase of 35% when compared to controls. This is consistent with the increases seen in ISV and DLAV diameter, using the *Tg(fli1:EGFP)* line.

3.2.3.3 Increased endothelial cell number in trunk vessels of the *vhl*^{-/-} mutant

To obtain accurate quantification of the number of endothelial nuclei in the trunk vasculature I used the *Tg(flk1:eGFP-NLS)* line. Spinning disc confocal microscopy provided 2µm Z-stack fluorescence images through the trunk of the developing embryo. The spinning disc microscopy due to its rapid stage movement and Z-stack acquisition allows multiple imaging of embryos of the same developmental stage to be performed. Due to the low numbers of homozygous mutants, (25% from a heterozygous incross) it is important to obtain adequate biological replicates of the mutant group to provide statistical significance. This imaging system provides the fastest, high quality in vivo imaging to make the comparisons required. These sequential images enabled accurate manual quantification of individual endothelial nuclei and confirmation of separate but overlapping nuclei through the trunk and over three ISV and communicating DLAV. Figure 3.8 shows the significantly increased number of endothelial cells in the vessels of the *vhl*^{-/-} mutant compared to the wild type, reflecting an increase of 50% in the number of endothelial cells in *vhl*^{-/-} mutants compared to controls. These data indicates that the enlargement of these vessels and angiogenesis seen in the mutant vasculature is associated with an increase in endothelial cell number.

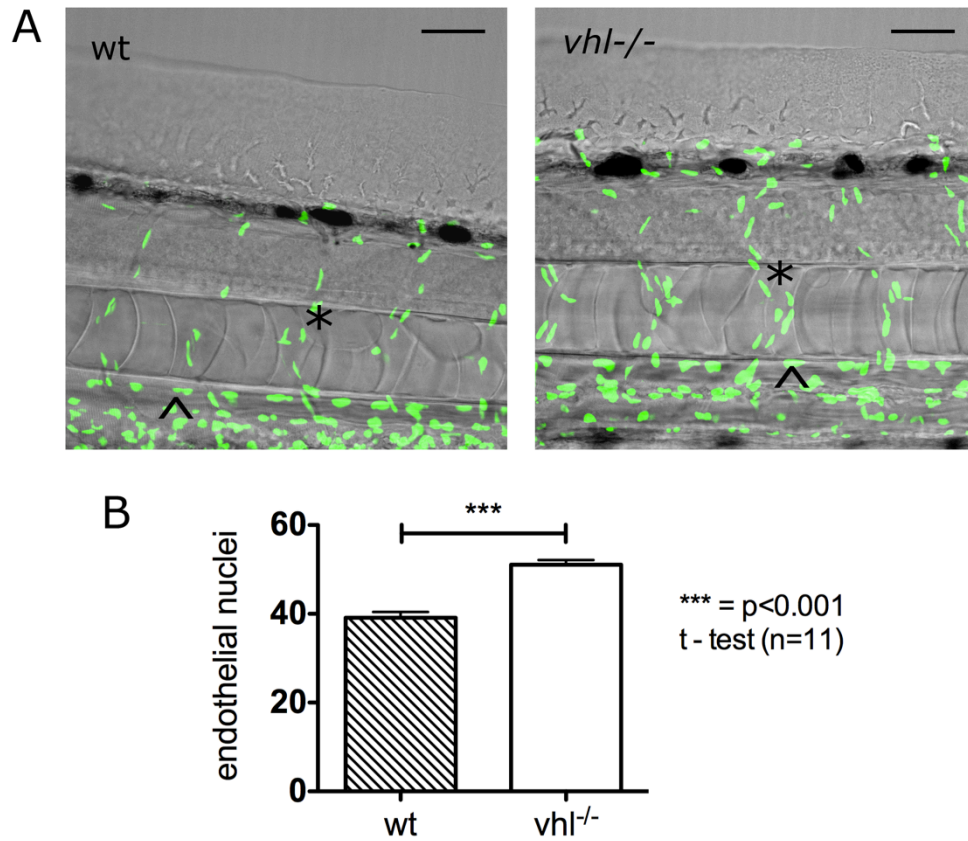


Figure 3.8 Assessment of the endothelial cell number in the vasculature of the wt and *vhl*^{-/-} mutant at 3dpf.

A. *Tg(flk1:eGFP-NLS)* and bright field image overlay of mid trunk in a 3 dpf wt and *vhl*^{-/-} mutant (*=ISV, ^=aorta). Scale bar, 100 μ m. **B.** Endothelial nuclei counts in ISV and DLAV over 2 somites (mean \pm SEM; t test; *** = $p > 0.001$; n=11).

3.2.4 Endothelial tip cell differentiation in the *vhl*^{-/-} mutant

3.2.4.1 Increased number of endothelial cells producing filopodia in the *vhl*^{-/-} mutant

Tip cell and filopodia generation are features of the endothelial tip cell identity driven by local gradients in VEGF-A (Gerhardt 2003). Given the increases in endothelial cell number and vessels in the *vhl*^{-/-} mutant, I expected to see concurrent increases in tip cell population in *vhl* mutants.

To identify tip cells I examined the labelled endothelium for filopodia formation in the ISV of *vhl*^{-/-} mutants using *Tg(kdr-l:H-ras;mCherry)*^{S916} transgenics (Hogan, Bos, et al. 2009a). Given the increased number and size of vessels that I had identified I expected to see increased numbers of tip cells along this vessel. Figure 3.9A shows the labelled membrane of the ISV shown as a grey scale image to enhance membrane contrast and demonstrate tip cell and filopodia morphology. To quantify the difference in the number of tip cells between the wildtype and the *vhl*^{-/-} ISV I looked for membrane projections from the surface of the ISV and the presence of filopodia which confirm active tip cell phenotype. In figure 3.9A there is an increase in angiogenic sprouts from the membrane, there is an associated increase in filopodia seen in the enlarged segment of the ISV (expanded white box in figure 3.9B) seen in the mutant. These angiogenic sprouts with active filopodia were very rare in wildtypes, suggesting an increase in tip cells in the *vhl*^{-/-} mutant at 3 dpf.

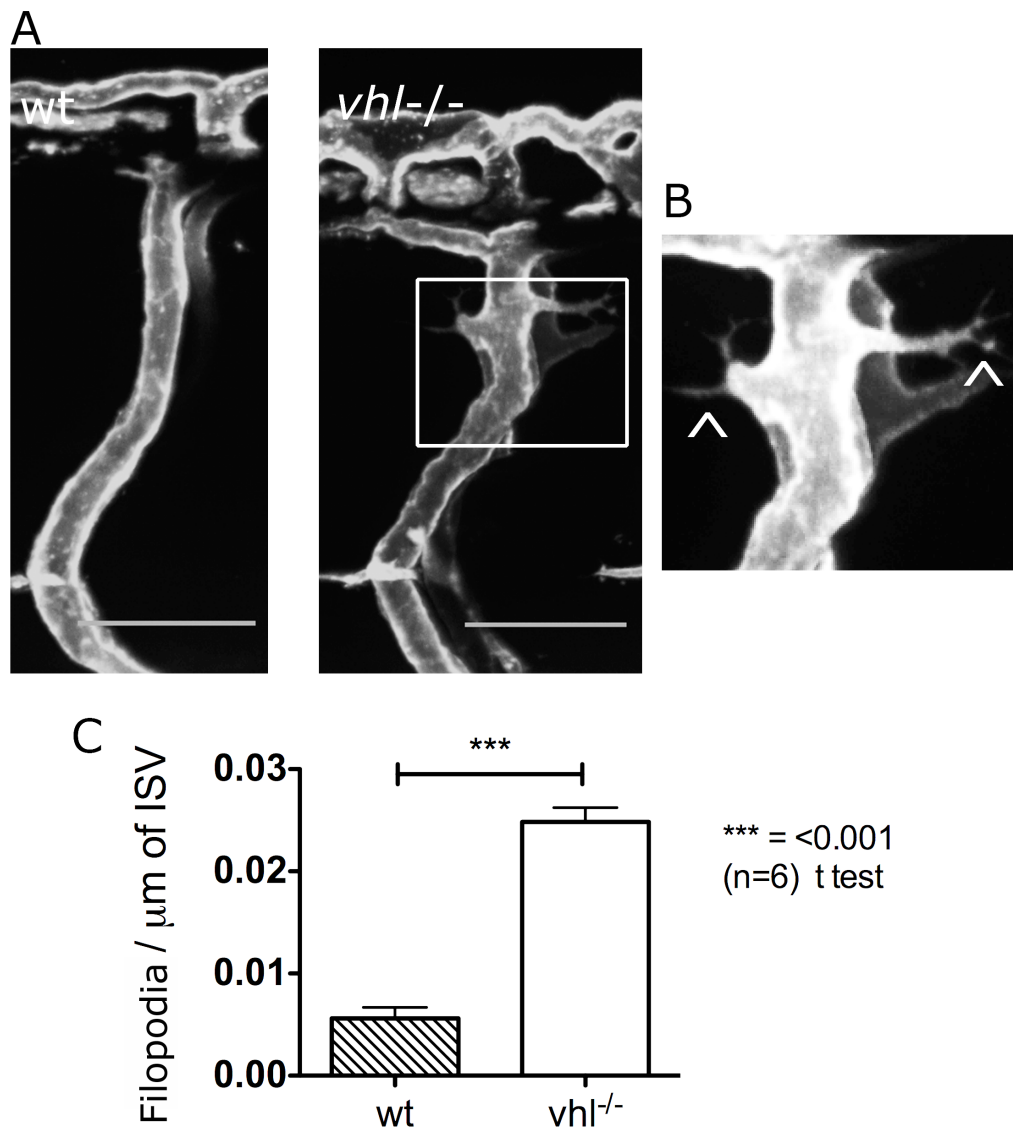


Figure 3.9 Increased filopodia of the endothelial membrane of the ISV in the $vhl^{-/-}$ mutant at 3 dpf.

A. ISV Endothelial morphology and tip cell formation, *Tg(kdr1:HRAS-mCherry)^{s916}* to localise endothelial fluorescence to membrane, scale bar 50μm. In the wt ISV no sprouts are seen, the $vhl^{-/-}$ shows endothelial sprouts with filopodia labelled with the membrane tagged fluorescent *mCherry*.

Figure 3.9 (cont) B. Shows the region of the *vh1^{-/-}* ISV with sprouts and filopodia magnified in 3.9A to show fluorescence of filopodia (arrowheads) in the *vh1^{-/-}* mutant to indicate active angiogenic sprouts possessing tip cells. **C.** Quantification of the number of angiogenic sprouts with filopodia, (labelled on the graph as tip cell) along the ISV, adjusted for total length in the wt and *vh1^{-/-}* mutant (*vh1^{-/-}* 0.025 ± 0.001 wt 0.0056 ± 0.001 , mean number of angiogenic sprouts / μm of ISV \pm SEM; n=7; t test; *** p<0.001).

3.2.5 Is the increase in number of endothelial cells in the *vhl*^{-/-} mutant due to proliferation?

One possible explanation for the difference in endothelial number *vhl*^{-/-} mutants is an increase in endothelial proliferation. This would be consistent with the expansion in endothelial cytoplasm, vessel growth and angiogenic tip cell phenotype seen in the *vhl*^{-/-} mutant (Ellertsdottir et al. 2010).

To assess endothelial cell proliferation I used immunohistochemistry for phosphorylated histone H3 (PH3) to co-localise mitotic cells with endothelial nuclear GFP in the *Tg(flk1:eGFP-NLS)* reporter in the *vhl*^{-/-} and wt backgrounds. Given the increased nuclear number seen in the *vhl*^{-/-} mutant I expected to see increased numbers of endothelial nuclei in the *vhl*^{-/-} mutant co-localise with the PH3 Antibody, indicating actively mitotic cells and thus proliferation.

Despite good tissue penetration with the antibody, resulting in labelled cells in the neural tube, co-localisation with GFP and the fluorescently labelled PH3 antibody (alexa 546) was very rare with only single cells co-localising in the whole trunks of embryos (Figure 3.10). The *vhl*^{-/-} mutant shows continued expansion in the number of endothelial cells over time so we repeated this experiment in *vhl*^{-/-} mutants at 5dpf to see if the greater total number of endothelial cells might enable us to co-localise more endothelial nuclei. Unfortunately I was unable to identify any more than single co-localised nuclei, which was insufficient to detect differences in proliferation in the *vhl*^{-/-} mutant.

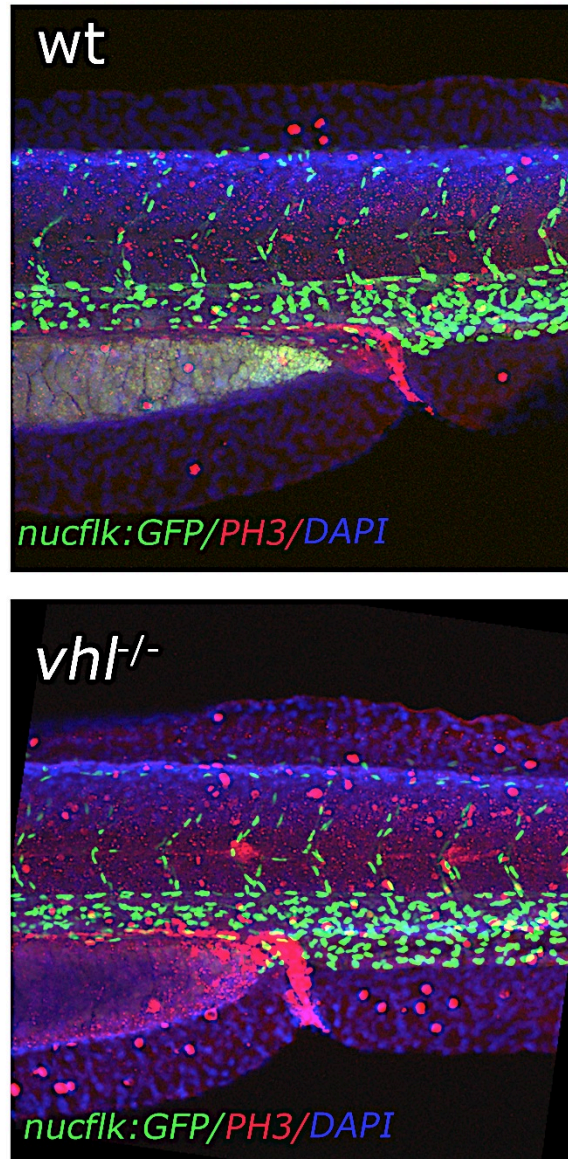


Figure 3.10 Immunohistochemistry of the proliferation marker phosphorylated histone H3 and fluorescent endothelial nuclei in 4dpf *vhl*^{-/-} mutant and wt embryos.

PH3 staining using Alexa 546 nm secondary (red) with endogenous *Tg(flk1:eGFP-NLS)* (green) and nuclear stained with 4',6-diamidino-2-phenylindole (DAPI) (blue) there are no co-localised red and green endothelial nuclei which would appear yellow (red+green) on the compound image even at higher magnification.

3.3 Discussion

The *vhl*^{-/-} mutant displays hypoxic signalling-driven angiogenesis during early embryonic development. This overlaps with normal developmental angiogenesis and vascular patterning. As the zebrafish has numerous advantages for the study of vascular development I wished to characterise in detail the angiogenesis in the *vhl* mutant so it could be used to examine signalling pathways involved in the regulation of angiogenesis.

There is an extensive literature on the features of angiogenesis which has been reviewed extensively (Potente et al. 2011). Angiogenesis is characterised by the differentiation of endothelial cells into tip and stalk cell in the presence of local VEGF gradients. Tip cells produce membrane projections, filopodia which enable path finding to connect with other tip cells to form new vascular connections (De Smet et al. 2009; Gerhardt 2003; Phng & Gerhardt 2009). In addition to the migratory phenotype of the tip cell, stalk cells undergo proliferation and re-organisation to form the stable endothelium of the developing vessels and lumenise via complex processes to form an effective vessel to enable flow of blood (Blum et al. 2008; Herwig et al. 2011; Carmeliet 2000).

In this chapter I have attempted to demonstrate that the aberrant angiogenesis seen in the *vhl*^{-/-} mutant behaves in the same stereotyped way both at a cellular and morphological way as a result of constitutive hypoxic signalling. Previous work has described the angiogenesis seen in the mutant line with particular emphasis on the retinal vasculature and its similarities to human retinal pathology (Van Rooijen et al. 2010). I chose to examine the trunk vessels for this study due to their accessibility and also since these have been used extensively for the study of developmental angiogenesis and endothelial cell behaviour in the zebrafish. This provides comparative data on all aspects of these vessels in the developmental setting.

The *vhl*^{-/-} mutant demonstrated a consistent pattern of aberrant angiogenesis, which was not seen, even at later time points, in the wild type embryo. This additional vessel development was first seen at 3 dpf after the ISV and initial

DLAV connection seemed to form normally. It is not clear why there is a delay in onset of the abnormal angiogenesis. This may represent the time required for accumulation of the HIF transcriptional complex and subsequent protein synthesis in the developing organism. Alternatively there may be an initial contribution from maternal RNA prior to the expression of the zygotic mutant *vhl* transcript (Schier 2007).

I have shown that the abnormal angiogenesis seen in the *vhl*^{-/-} mutant is progressive from 3 dpf until 7 dpf shortly before the embryos die due to high output cardiac failure at 9 dpf (Van Rooijen et al. 2009). There is an expansion in the endothelial cytoplasm and the total area of vessel, in addition to the increased diameter of both the ISV and DLAV from as early as 3 dpf. A potential limitation of this study of the angiogenic morphology is that it is based on vessel morphology, using the endothelial promoter *fli1*. The *fli1* promoter is expressed in both arterial and venous vessels and the differences in vessel morphology do not take into account potentially different vessel responses between the two vessel types. There are differences in the response to VEGF ligands and receptors in arterial and venous angiogenic sprouts (Hogan, Herpers, et al. 2009b) and this could result in differences in an angiogenic response to HIF-1 α signalling. Despite the potential signalling difference I did not see any variation in angiogenesis depending on the arterial or venous origin of the ISV sprout. Also, previous data has also shown an up regulation in all VEGF ligands and receptors as a result of the *vhl*^{-/-} mutation in the developing zebrafish embryo (van Royen et al. 2009).

Tip cells are differentiated endothelial cells stimulated by local VEGF gradient which act in a similar manner to axonal growth cones, for emerging vessels (Potente et al. 2011). Currently there is no single marker of a differentiated tip cell (Phng & Gerhardt 2009). I used an endothelial membrane reporter to show that in the *vhl*^{-/-} mutant there is significantly increased filopodia formation along the length of the ISV. This suggests increases in tip cell population fate in the *vhl*^{-/-} mutant. However, the additional vessels seen in the *vhl*^{-/-} mutant and the increases in filopodia and tip cells suggest the additional vessels are formed by a process of classical tip and stalk cell driven sprouting angiogenesis.

Tip cell formation and angiogenic sprouting is only one of the earliest features of endothelial angiogenesis. The ability of these sprouts to form a vascular lumen from modifications of the stalk cell morphology and expand the endothelial cell number to support this new vessel formation is critical to formation of effective mature vessels. I have shown that the angiogenic sprouts of the *vhl*^{-/-} mutant lumenise early in their formation and there is a concurrent expansion in the number of endothelial cells in the mutant vasculature.

I hypothesised that the increased number of endothelial cells seen in the mutant was due to increased endothelial proliferation. Given the established position of VEGF as a growth factor and endothelial mitogen and the increases demonstrated in the *vhl*^{-/-} mutant. Unfortunately I was unable to demonstrate any differences in active mitosis in the endothelial cells of the mutant using the PH3 antibody. This is likely to be due to technical reasons and I have not confirmed or refuted the presence of increased endothelial proliferation in *vhl* mutants. Two alternative techniques may address this question: One would have been to use the synthetic nucleoside bromodeoxyuridine. This is incorporated into dividing cells and can be identified by immunohistochemistry and co-localised to the endothelium. This would give an indication of the number of endothelial divisions over a period time rather than at single time point, which is a limitation of PH3 immunostaining. The second would be to use time-lapse imaging of endothelial nuclei in the mutant and wildtype backgrounds and use either manual or automated tracking of the nuclei over several hours to quantify number of divisions during time-lapse acquisition. This would also provide information about the origins of these proliferating cells and the sites of active division. It has been shown that the origin of the cells which form the DLAV in the developing embryo emerge from the aorta (Blum et al. 2008), it is possible that the increases in cells seen in this vessels is as a result of aortic proliferation and then migration into the ISV and DLAV as opposed to proliferation in situ.

3.3.1 Is the abnormal vascular phenotype endothelial cell autonomous? (Appendix 1)

In the *vhl*^{-/-} mutant line there is up regulation of hypoxic signalling in all cells. In characterising the angiogenic vessel phenotype of the *vhl*^{-/-} mutant, I was interested to see if increases in hypoxic signalling in only endothelial cells, was sufficient to induce an angiogenic vessel phenotype. Imaging of a double transgenic expressing a dominant active *hif-1ab* protein expressed in the endothelium showed no angiogenic phenotype during the time period observed. WISH experiments to confirm the expression of the transgenes and the GAL4-UAS system indicated that the *fli1GFF-UAS* system was resulting in effective endothelial expression of *kaede* mRNA and protein.

Although there was some global increase in expression mainly in the head of the PHD3 mRNA, (used here as a reporter of HIF signalling) in this endothelial driven hypoxia transgenic, there was not a clear vascular distribution of PHD3 mRNA using WISH. A possible explanation for the lack of clear endothelial UAS-*hif-1ab* expression and angiogenic phenotype, may be due to methylation and silencing of multiple copy insertion of the UAS residue, or potentially its proximity to the modified GAL4 promoter (Akitake et al. 2011). As it is difficult to make strong conclusions from the data (Appendix 1) and I cannot be certain that there is up-regulated endothelial HIF expression it is difficult to comment further on the role of cell autonomous HIF over expression in endothelium and the initiation and production of angiogenesis.

Unfortunately there was insufficient time, within this project, for me to produce the same constitutively active HIF construct with a 4x UAS promoter for the production of a stable transgenic line. This technique may have reduced the effects of any UAS silencing by methylation (Akitake et al. 2011). This area may be of interest for future research as the site of autochrine and paracrine *vegfaa* secretion in the *vhl*^{-/-} mutant or the timing of its onset may begin to explain why there is an observed delay in the development of the angiogenic phenotype in my experiments.

3.3.2 Summary

I have shown that pathological angiogenesis in the *vhl*^{-/-} mutant zebrafish demonstrates phenotypic features consistent with published descriptions of angiogenesis in other models. These models include hypoxia driven angiogenesis in different vessel territories in the zebrafish and developmental models of angiogenesis in both the mouse and zebrafish (Van Rooijen et al. 2010; Potente et al. 2011). Previous work had identified the up regulation of important angiogenic growth factors in the zebrafish mutant line (*vegfa*, *flt1*, *fli1*, *kdr* and *kdr-l*) which have been shown to be critical in the genesis of new blood vessels in a number of models (Phng & Gerhardt 2009; van Royen et al. 2009). The presence of these factors in the *vhl*^{-/-} mutant with the cellular and morphological features of angiogenesis described in this chapter indicate the vessel phenotype of the zebrafish *vhl*^{-/-} mutant trunk is a reliable *in vivo* model of hypoxia driven angiogenesis (Ellertsdottir et al. 2010). These observations enabled me to use this model to investigate cell-signalling pathways regulating the aberrant angiogenesis in *vhl* mutants which I will describe in detail in the following chapters.

**Chapter 4 The role of flow in the
regulation of *vhl*^{-/-} mutant
angiogenesis**

4.1 Introduction

Angiogenesis has been shown to require flow dependent signals in the developing zebrafish vasculature (Nicoli et al. 2010). In addition flow has been shown to regulate formation and the remodelling of the DLAV plexus in concert with VEGF-A signalling (Zygmunt et al. 2012). Despite this understanding of the effect of flow on endothelial behaviour and the regulation of new vessels, there is little information on the role of haemodynamic flow on angiogenesis driven by constitutively active hypoxic signalling or pathological angiogenesis. It has been shown in previous work using the *vhl*^{-/-} mutant zebrafish that the cardiac output and velocity of blood in the aorta is elevated compared with wildtype siblings (Van Rooijen et al. 2009). I hypothesised that this alteration in circulatory force might be permissive to the aberrant angiogenesis described in the previous chapter. In this chapter I therefore examined the effect of altering blood flow on the developing vasculature in *vhl* mutants.

4.2 Results

4.2.1 The effect of absent blood flow on vascular development in *vhl* mutants

4.2.1.1 Genetic manipulation of circulation in the developing *vhl*^{-/-} zebrafish

Using a morpholino antisense oligonucleotide against the sarcomeric protein *troponin t₂*, I was able to block the construction of effective contractile apparatus in the developing embryonic heart to prevent cardiac contraction (Sehnert et al. 2002). I injected this morpholino (MO) into the *Tg(vhl^{hu2117};fli1:eGFP)* transgenic to examine the effect of absent blood flow on the mutant angiogenic phenotype described in the previous chapter. This targeted morpholino blocks the formation of the contractile apparatus of the cardiac myocyte during development. Although the gross anatomy of the heart is preserved, due to the block to transcription of this essential protein cardiac contraction cannot be initiated. Successful knockdown can be identified using simple optical

microscopy where cardiac contraction is identified at about 20-24 hpf and circulating erythrocytes can be observed in real time in the embryos, this is lost in the morpholino injected embryos.

Figure 4.1 shows the stereotyped formation of the ISV and DLAV in the wild type embryo injected with control MO. The vessels are restricted to the somite boundaries and follow a stereotyped pattern (Childs et al. 2002). This pattern is preserved in embryos injected with *troponin t₂* MO, which have never been exposed to circulatory flow. This indicates that these patterned vessels, which emerge from the aorta at a similar time to the onset of circulation, are not dependent on flow for formation. However the additional vessel changes which are seen in the *vhl^{-/-}* mutant, enlargement of the patterned vessels and sprouting of new vessels, are not present in the *vhl^{-/-}* mutant injected with *troponin t₂* MO, which is never exposed to circulation and flow.

In the *vhl^{-/-}* mutant which has endothelium exposed to flow there is about a 50% increase in the diameter of this vessel compared to control, in the *vhl^{-/-}* mutant with absent circulatory flow this is reduced to control levels. The same pattern is seen in the DLAV diameter, which is increased by around 60% in the *vhl^{-/-}* mutant with flow but this highly significant increase is reduced back to control levels in the absence of flow (Figure 4.2 A & B). In both of these measurements, ISV & DLAV diameter, there is no significant change in vessel size in the control group, which is injected with the *troponin t₂* MO thus not exposed to flow.

The total vessel length of a two-somite region and total area of endothelium showed similar patterns to ISV and DLAV diameter in the *vhl^{-/-}* mutant, injected with *troponin t₂* and no flow. The highly significant increases in the *vhl^{-/-}* mutant for vessel length and area of GFP fluorescence are reduced to control levels by the absence of flow. There is no significant difference between the wild type embryos with no flow and the *vhl^{-/-}* with no flow in any of the groups studied. There is a reduction seen in the wildtype embryo with absent flow in the total vessel length and area of endothelial GFP expression, compared to the wild type with normal flow, although a smaller difference than observed in the

mutant. This difference may reflect the smaller size of the somites in the 3 dpf embryo injected with *troponin t₂* MO resulting in the length in vessel and area appearing smaller but the diameter remaining the same.

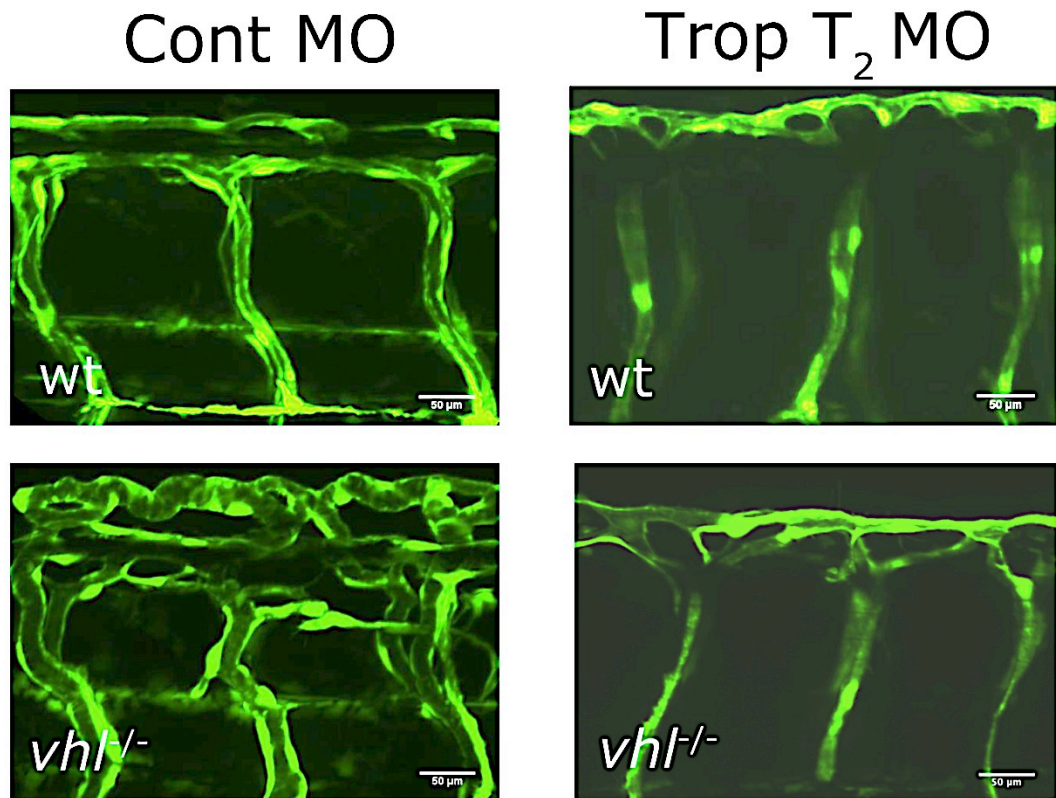


Figure 4.1 The effect of removing circulatory flow from the endothelium of the wild type and *vhl*^{-/-} mutant at 3 dpf.

4dpf *Tg(fli1:eGFP)* embryos injected with control or *troponin t₂* morpholino, essential vascular patterning is preserved with the ISV and DLAV forming despite the absence of circulatory flow in the wt and *vhl*^{-/-}. However the aberrant angiogenesis seen in the *vhl*^{-/-} Control MO embryo is lost in the *vhl*^{-/-} without circulation (*troponin t₂* MO). Scale bar, 50 μm.

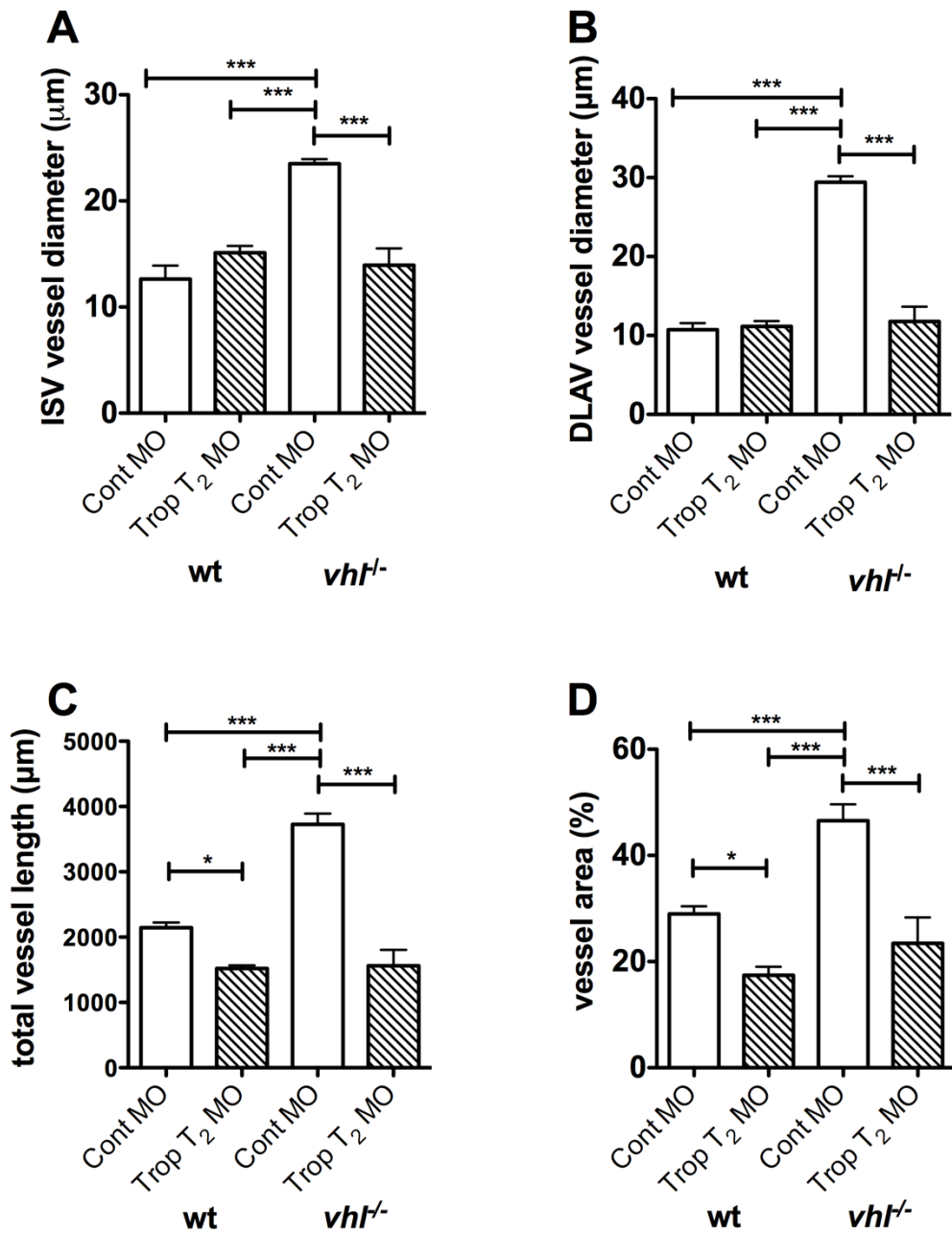


Figure 4.2 Quantification of absent circulatory flow on the hypoxia driven angiogenesis in the $vhl^{-/-}$ mutant.

A. ISV diameter in 4dpf wt & $vhl^{-/-}$ $Tg(fli1:eGFP)$ embryo injected with *troponin t₂* or Control MO. **B.** DLAV diameter in wt & $vhl^{-/-}$ injected with *troponin t₂* or Control MO. **C.** Total vessel length in wt & $vhl^{-/-}$ injected with *troponin t₂* or Control MO. **D.** Vessel area (% area GFP) in wt & $vhl^{-/-}$ injected with *troponin t₂* or Control MO. All groups: 2-way ANOVA; *** $p < 0.001$; $n = 6$.

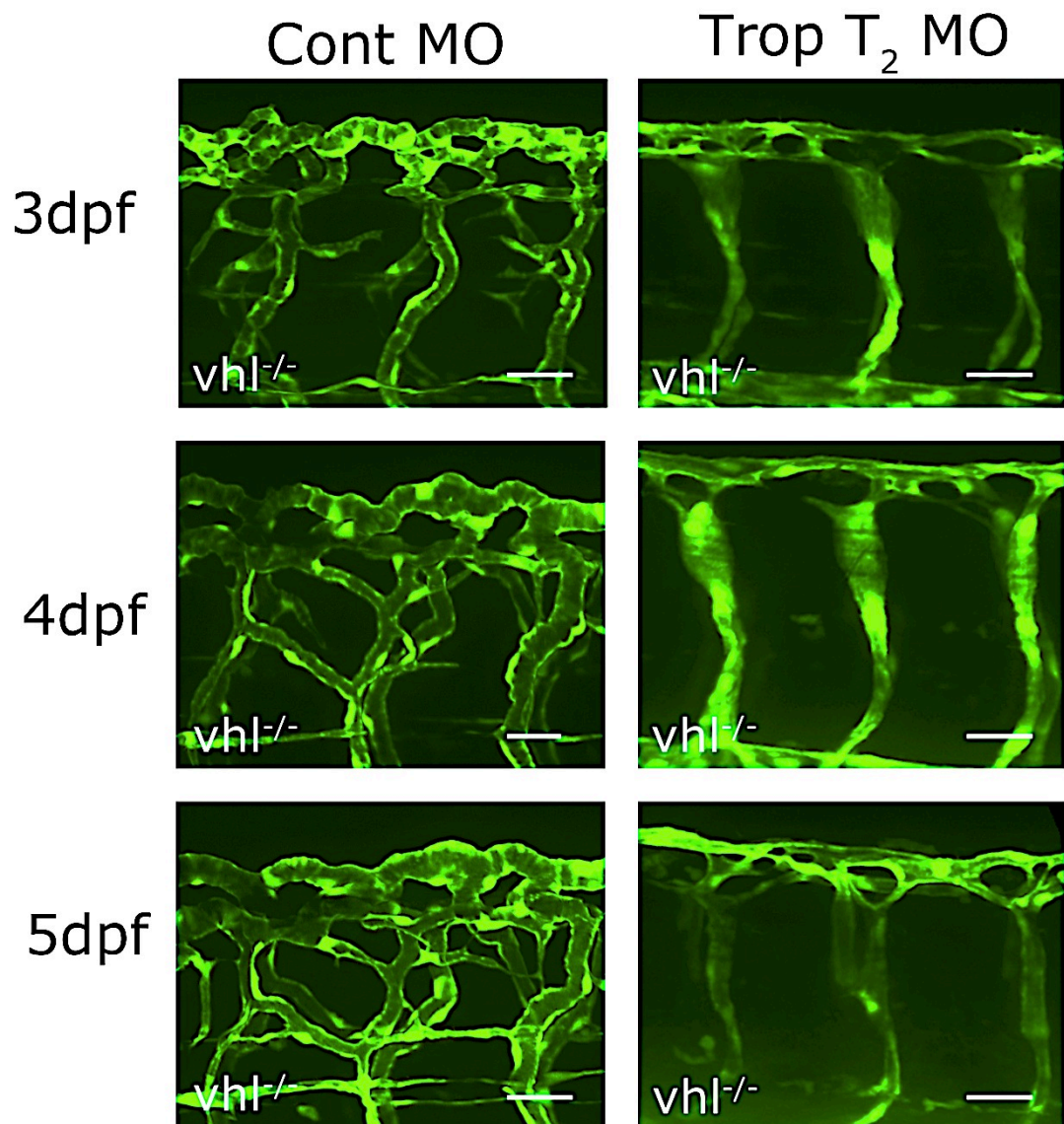


Figure 4.3 Time course of the *vhl*^{-/-} mutant angiogenic phenotype compared with aged matched *vhl*^{-/-} mutants injected with trop t₂ MO.

The angiogenic features previously described in the *vhl*^{-/-} mutant show progression over time (left column photomicrographs). The *vhl*^{-/-} mutant injected with Trop t₂ MO shows none on these features even at later time points (right column). *Tg(vhl^{hu2117};fli1:eGFP)*. Scale bar, 50 μm.

4.2.1.1.1 Does absence of blood flow block the increase in endothelial cell number in *vhl*^{-/-} mutants?

I have previously shown that the *vhl*^{-/-} mutant has an expansion in the number of endothelial cells in its vessels, which corresponds with the morphological changes of angiogenesis. Given the loss of angiogenic changes in the *vhl*^{-/-} mutant in the absence of circulatory flow I expected to see a reduction in the number of endothelial cells in *vhl*^{-/-} mutant injected with *troponin t₂* MO. Figure 4.4 confirmed a significant reduction in endothelial cell number in the ISV and DLAV of the *vhl*^{-/-} mutant injected with the *troponin t₂* MO (Figure 4.5). There was also a reduction in endothelial cell number in the ISVs in wild type embryos in the absence of flow. There was no difference in the endothelial cell number between wild type embryo injected with *troponin t₂* MO and *vhl*^{-/-} mutant embryos injected with *troponin t₂* (Figure 4.5).

The reduction of endothelial cells in the normal patterned vessel in the absence of flow may reflect the shorter length and reduced total area of endothelial tissue induced by the lack of circulation. Alternatively there maybe a reduction in either cell division *in situ* or migration into these vessels from the aorta, where these cells originate (Fouquet et al. 1997; Childs et al. 2002). A limitation of the *Tg(vhl^{hu2117};flk1:eGFP-NLS)* is the lack of concurrent information about vessel morphology. Each individual nucleus is seen in isolation, making accurate assessment about the exact location of individual nuclei difficult, particularly at the junction of vessels and where nuclei are overlaid in close proximity. To overcome this limitation I used the *Tg(vhl^{hu2117};kdr;HRAS-mCherry;flk1:eGFP-NLS)* line for subsequent experimental assessment of nuclei number and vessel morphology.

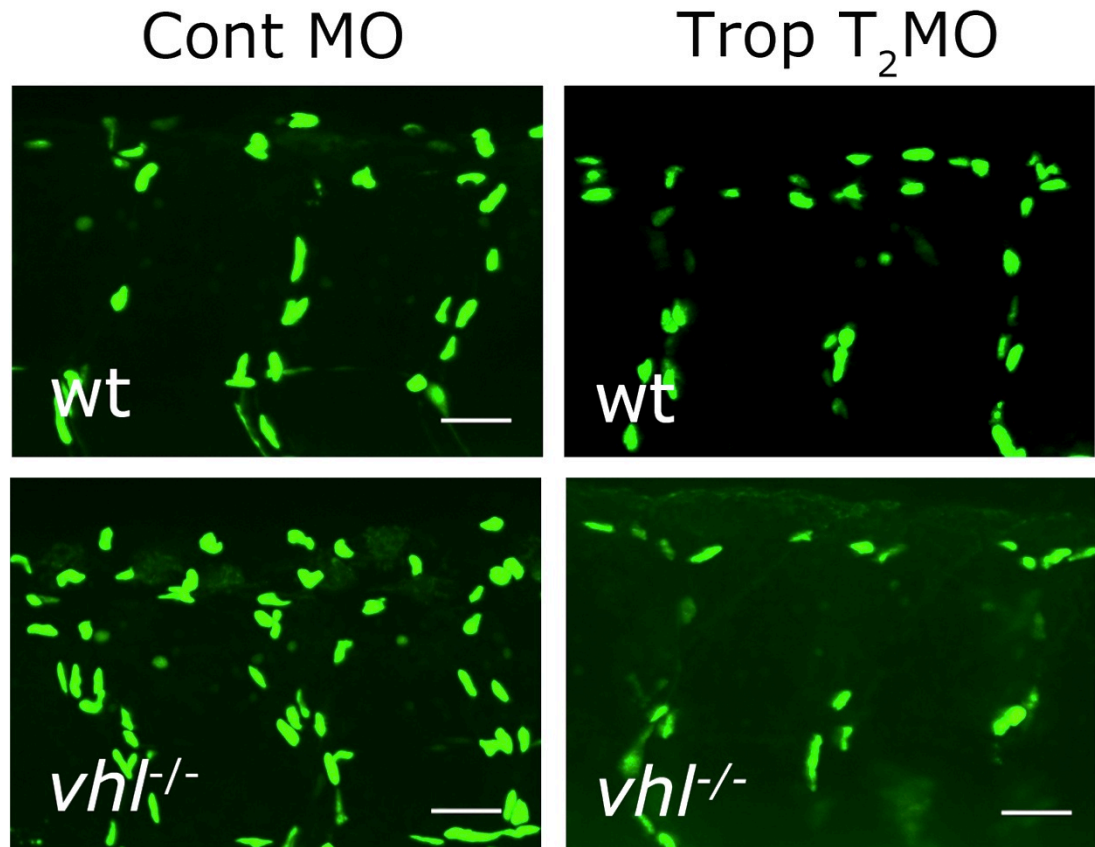


Figure 4.4 Reduction in the endothelial cell number seen in the *vhl*^{-/-} mutant in the absence of circulatory flow.

4 dpf *Tg(vhl^{hu2117};flk1:eGFP-NLS)* injected with either *troponin t₂* MO or control MO and imaged at 4 dpf, photomicrograph of a two somite region of ISV and DLAV at the mid trunk adjacent to the cloaca. *vhl*^{-/-} mutant shows increased endothelial cells in the control injected embryo with a reduction to control levels in the embryo injected with *troponin t₂* MO. Scale bar, 50 μ m.

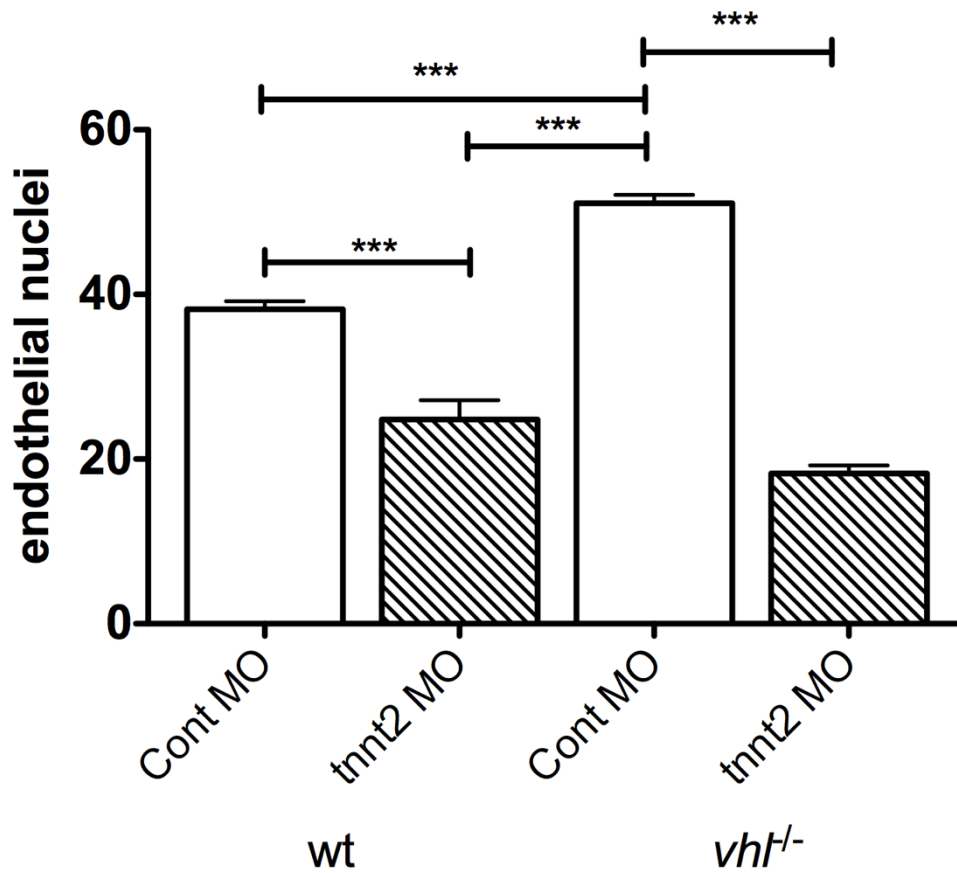


Figure 4.5 Endothelial nuclei counts *vhl*^{-/-} and wild type embryos in the presence of circulatory flow or absence of flow.

Endothelial cell nuclei counts in a two somite region of ISV and DLAV in wt and *vhl*^{-/-} mutant embryos at 4 dpf *Tg(vhl^{hu2117};flk1:eGFP-NLS)*. The significant increase in endothelial cells in the *vhl*^{-/-} is significantly reduced in the *vhl*^{-/-} without flow (trop t₂ MO). 2-way ANOVA Bonferroni post test; *** p<0.001; n=8.

4.2.2 Pharmacological circulatory arrest in the *vhl*^{-/-} mutant

I next sought to determine whether cessation of cardiac contraction by another method similarly reduced angiogenesis in *vhl* mutants. I therefore used the myosin ATPase inhibitor 2,3-butanedione 2-monoxime (BDM) to block cardiac contraction (Jou et al. 2010). This compound was added to the developing embryo at 36 hpf. This agent act to uncouple excitation-contraction of the cardiac myocyte, this is achieved by inhibition of calcium influx into the myocyte resulting in absence of cardiac contraction after treatment (Jou et al. 2010). Since blood flow starts 12 h earlier, this also enabled me to determine if initial exposure to circulation is sufficient to rescue the loss of phenotype induced by *troponin t₂* knockdown.

Circulatory arrest at 36 hpf by application of the BDM compound to the developing embryos blocked the formation of the *vhl*^{-/-} angiogenesis (Figure 4.6). This effect is the same as that of the *troponin t₂* MO injection resulting in normalisation of the ISV and DLAV diameter to that of the wildtype vessel size. The inhibition of cardiac contraction with BDM also reduced the vessel length of the *vhl*^{-/-} mutant (40% longer over a 2 somite region) to the length of wildtype vessels. BDM treatment did not change the diameter or total vessel length in wild type embryos compared with control media treatment as seen in Figure 4.6 & 4.7A, B & C.

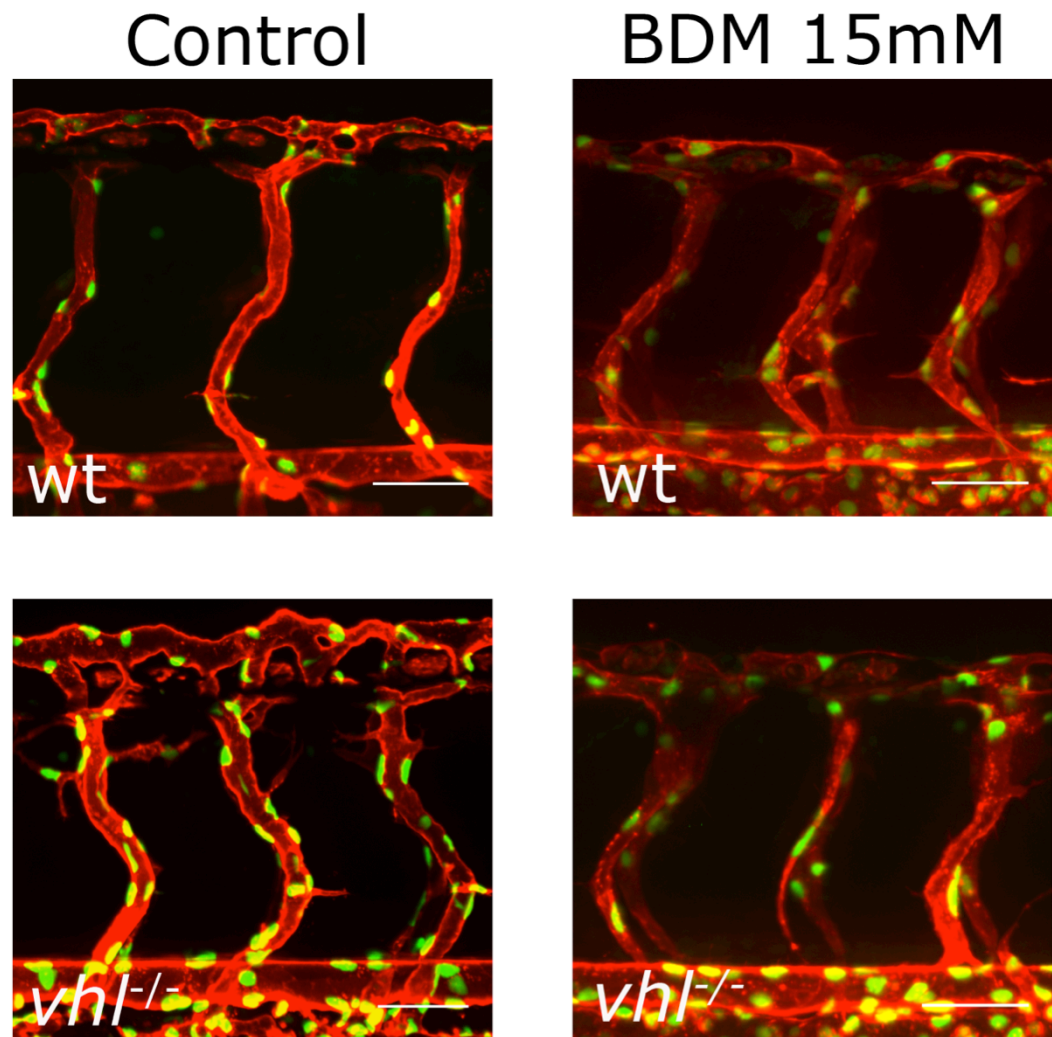


Figure 4.6 Pharmacological inhibition of circulatory flow results in the attenuation of the *vhl*^{-/-} angiogenic phenotype.

3 dpf *Tg(vhl^{hu2117};kdr1;HRAS-mCherry;flk1:eGFP-NLS)* imaged over two somites at the level of the cloaca. Endothelial membrane labelled with red fluorescence and nuclei labelled with green fluorescence. BDM is an inhibitor of cardiac contraction embryos incubated in BDM from 24 hpf until imaging at 72 hpf. Despite the normal developmental angiogenesis in embryos treated with BDM the angiogenesis of the *vhl*^{-/-} mutant is attenuated. Scale bar, 50 μ m.

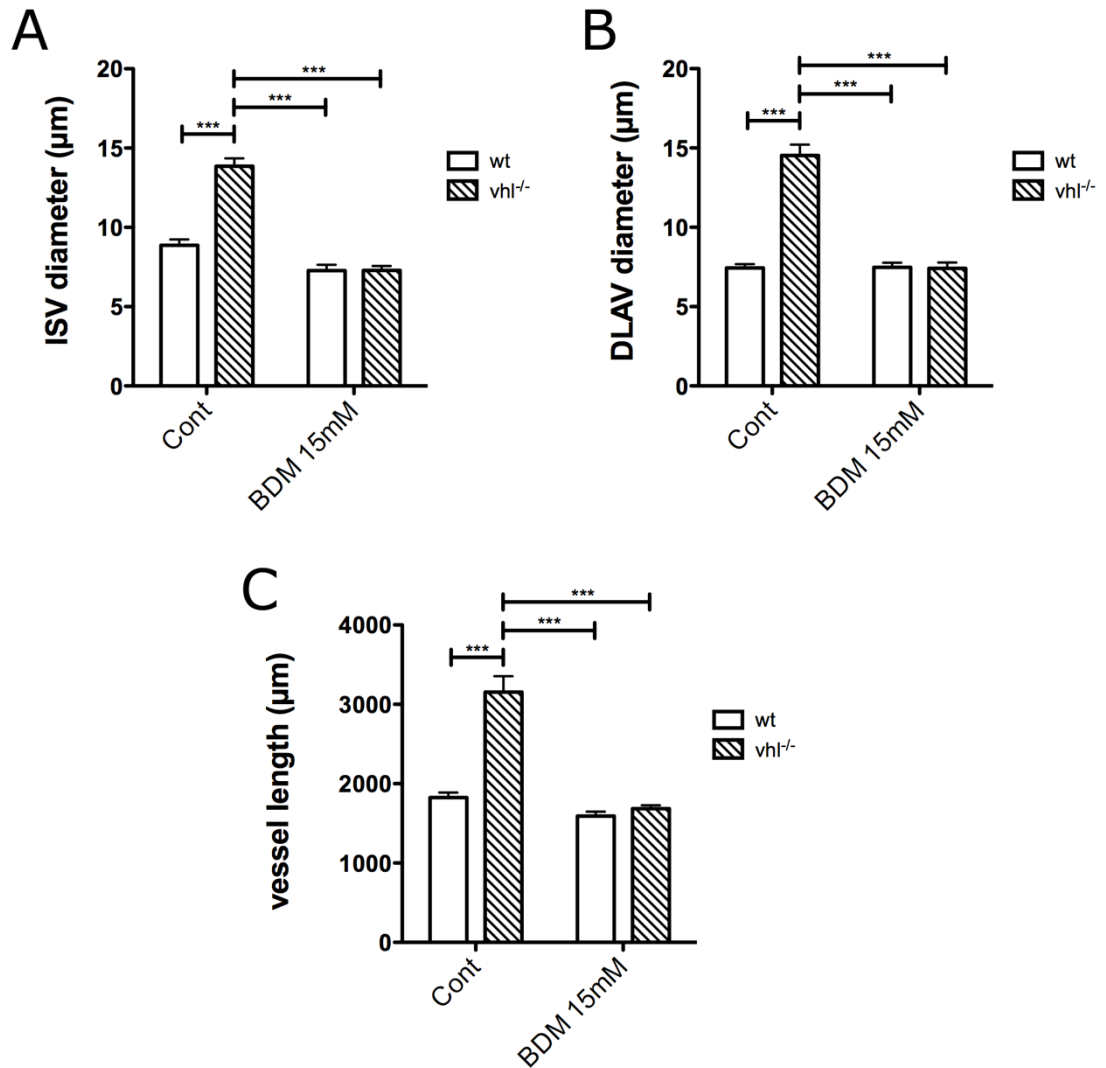


Figure 4.7 Effect of BDM, an inhibitor of cardiac contraction on the quantification of the *vhl*^{-/-} angiogenic phenotype.

A. ISV diameter in the *vhl*^{-/-} and wt treated with BDM 15mM or control from 24hpf until imaging at 72hpf. Treatment with the BDM results in inhibition of cardiac contraction shortly after contraction to enable us to study the effect of cessation of circulation after its onset. **B.** DLAV diameter in *vhl*^{-/-} and wt. **C.** Total vessel length of ISV and DLAV over a 2 somite ROI in *vhl*^{-/-} and wt embryos. All groups mean ± SEM, 2-way ANOVA; Bonferroni post test; *** p<0.001; n=11.

DLAV diameter was increased by about 50% in the *vh1^{-/-}* mutants with circulation compared with wildtypes; this increase is blocked in the *vh1^{-/-}* treated with BDM (Figure 4.7 B) by the removal of flow. There is no significant difference in the DLAV diameter in either wild type or mutant embryos treated with control or BDM.

Figure 4.7 C shows the 50% increase in total vessel length in *vh1^{-/-}* mutants was reduced to wild type levels when treated with BDM. The reduction in total vessel length observed in wild type embryos treated with *troponin t₂* (Figure 4.2 C) was not seen in the BDM treated wild type group (figure 4.7 C), which may relate to the period of circulation prior to circulatory arrest.

Treatment of the *vh1^{-/-}* mutant to remove circulatory flow during vessel development blocks the formation of the hypoxic signalling-induced angiogenic response. This appears to be blood flow dependent and occurs despite initial exposure of endothelium to a flow signal in the *vh1^{-/-}* mutant.

The increase in endothelial nuclei in the ISV and DLAV of the trunk vessels of the *vh1^{-/-}* mutant is normalised to control levels in *vh1^{-/-}* mutant treated with BDM from 36hpf (Figure 4.8). In these experiments there was no statistically significant difference in the number of endothelial nuclei in the wild type control, wild type BDM and *vh1^{-/-}* BDM groups. This is at odds with the data on endothelial cell number after injection of *troponin t₂* in the wild type to block circulation (shown in Figure 4.5). With the *troponin t₂* MO knockdown there was a significant decrease in the number of endothelial cells in wild type embryos injected with the MO, a decrease of 27%. It is possible that loss of circulation at a later stage in development in the BDM experiment may account for this difference. It is also possible this is due to a flow-dependent effect on endothelial proliferation during this early period of circulation, prior to circulatory arrest in the BDM treatment group.

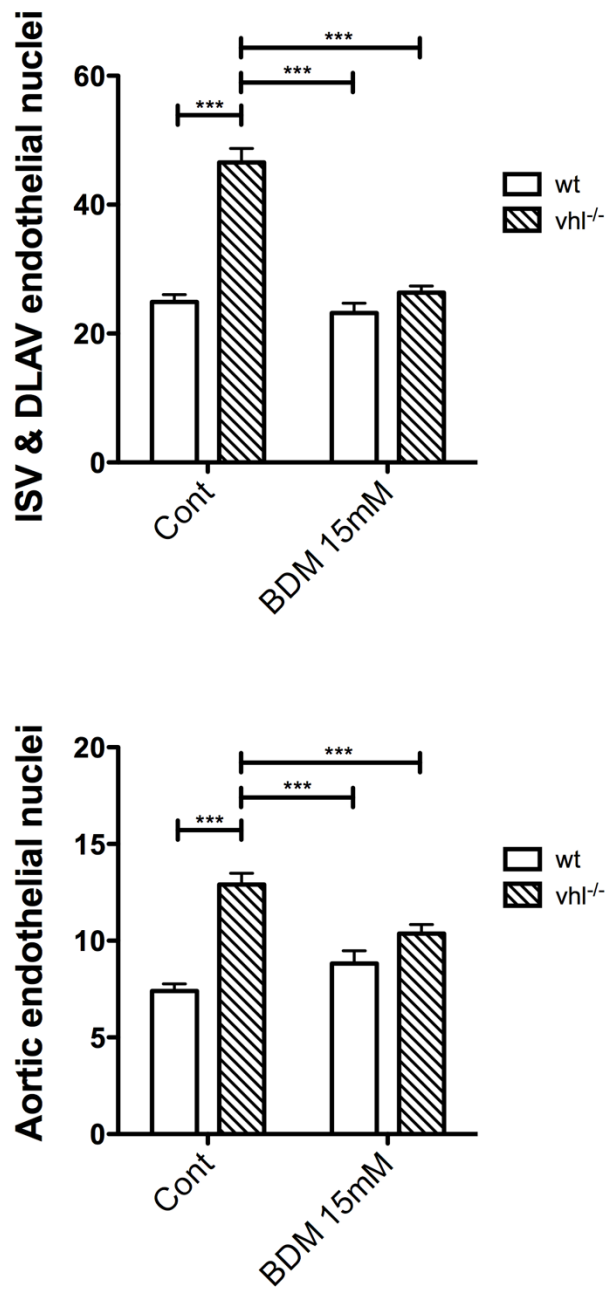


Figure 4.8 Effect of pharmacological inhibition of cardiac contraction on endothelial number in the *vhl*^{-/-} aorta (A) and trunk vessels (B).

A. Number of endothelial nuclei in the ISV and DLAV of a 2 somite ROI adjacent to the cloaca in *vhl*^{-/-} and wt 3 dpf embryos treated with BDM 15 mM or control media. **B.** Endothelial nuclei in the aorta of 2 somites in *vhl*^{-/-} and wt 3 dpf embryos treated with BDM 15 mM or control media. All groups: Mean ± SEM; 2-way ANOVA; Bonferroni post test; *** p<0.001; n=11.

4.2.3 Are the increases in the number of erythrocytes in the *vhl* mutant required for development of the angiogenic phenotype?

The *vhl*^{-/-} mutant has increased red cell production as a result of increased in hypoxic signalling (Van Rooijen et al. 2009). Since this increase precedes the changes in the vasculature I was interested to study the effects of this erythrocytosis on angiogenesis. Previous work in our laboratory has shown that the *vhl*^{-/-} mutant has increased red cell velocity and cardiac output which precede the angiogenesis. In addition to these increases, I have previously shown that there is early lumenisation of the angiogenic sprouts of the *vhl*^{-/-} mutant (Figure 3.6). Therefore increased force exerted on the endothelium from increased numbers of red cells may play a role in the angiogenic phenotype. To examine red cells prior to the initiation of the angiogenic phenotype I used *Tg(fli1:eGFP;gata1a:dsRed)* embryos with dsRed-labelled erythrocytes. The dense columns of red fluorescence seen within the green endothelium in the *vhl*^{-/-} mutant (Figure 4.9) suggest more erythrocytes passing through these vessels at the same developmental stage in the mutant angiogenic phenotype compared to the vessels of the wild type.

4.2.3.1 Does early venesection reduce red cell density in the *vhl*^{-/-} mutant?

I developed a technique for venesectioning the developing embryo at 48hpf using a micropipette and micromanipulator, which uses the embryo's heartbeat to drive erythrocytes and plasma from the circulation into the surrounding agarose. Then by imaging the aorta I was able to quantify the number of erythrocytes in a fixed volume of aorta, based on measurements of aortic length and diameter and an assumption of a cylindrical tube for the aorta, enabling me to calculate a red cell density. Figure 4.10A shows that although red cell density is reduced in *vhl*^{-/-} mutants after the procedure, by 5 dpf the density of red cells has recovered to the same levels as seen in non-venesectioned *vhl*^{-/-} mutants.

4.2.3.2 Does venesection alter red cell velocity in the vessels of the *vh1^{-/-}* mutant?

Despite the recovery in the density of red cells back to non-venesected levels in the *vh1^{-/-}* mutant by 5 dpf there is still a measurable effect on aortic velocity seen in figure 4.10B. This shows that at 5 dpf the velocity in the aorta as a result of venesection is reduced, compared to the sham procedure. As this reduction of aortic velocity may represent a difference in the flow in the developmental vessels and angiogenic vessels I wanted to see if this change led to an alteration in the *vh1^{-/-}* mutant vessel phenotype.

4.2.3.3 Does venesection in the *vh1^{-/-}* mutant block the angiogenic phenotype?

I performed venesection on 2 dpf mutant and wildtype embryos. Figure 4.11 shows that venesection had no effect on the angiogenic phenotype of the *vh1^{-/-}* mutant as previously described in this chapter. Due to the technical difficulties in performing this procedure on a 48 hpf embryo and the individual mounting and manipulation it is difficult to perform this procedure in large numbers.

Post-hoc power calculations for the *vh1^{-/-}* mutant groups were performed based on a significant difference between groups of $p \leq 0.05$, the power calculation for ISV diameter calculates that the power is 0.309. This indicates that the number of observations in this experiment is inadequate to conclude that reducing aortic velocity by venesection has no effect on the mutant phenotype. To achieve power of > 0.8 would require an $n > 12$ for the expected effect size. For DLAV and vessel length the power is even lower and would require group sizes of > 40 embryos to achieve a power of > 0.8 . Given I have only demonstrated a modest reduction in aortic velocity after venesection in the mutant and no change in erythrocyte density at 5 dpf, such large experiments were not feasible during this study.

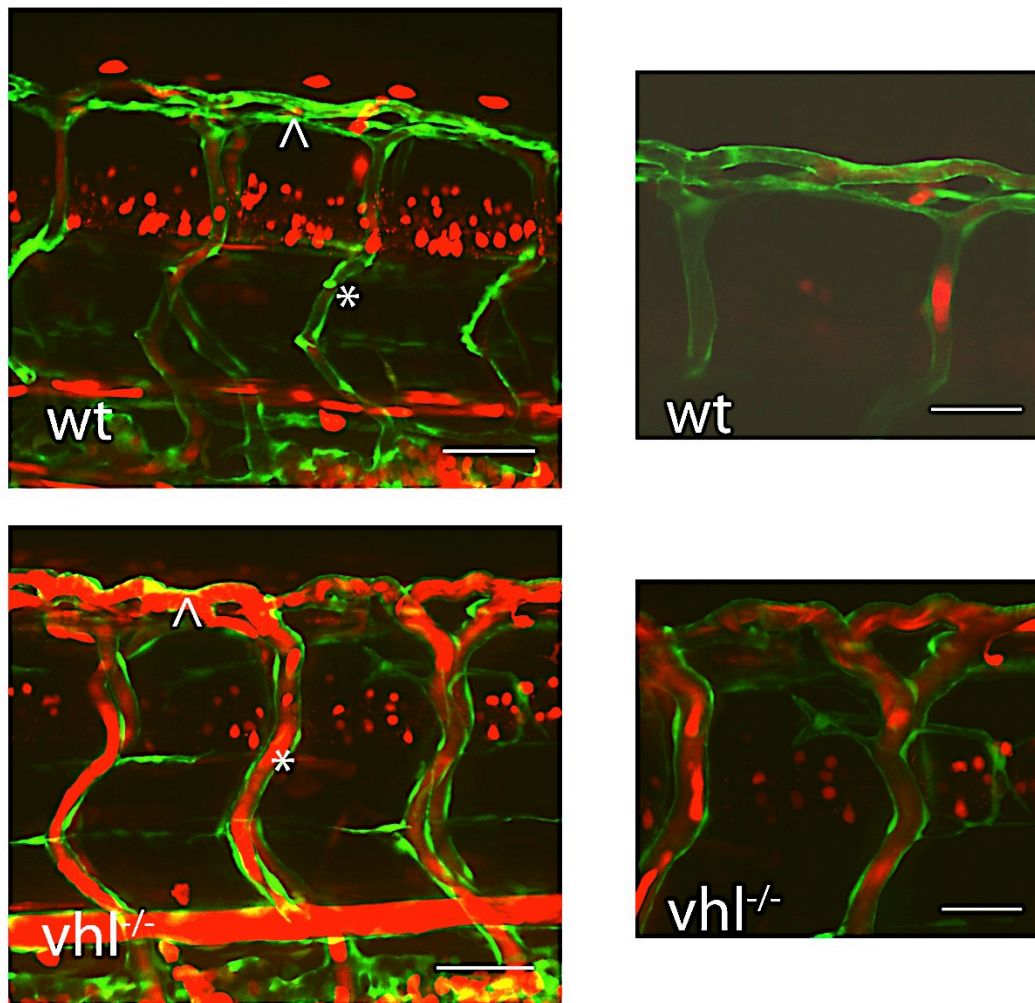


Figure 4.9 Polycythaemia of *vhl*^{-/-} mutants and the resulting increased erythrocyte flow in the developing and constitutive hypoxia driven angiogenic vessels.

Tg(vhl^{hu2117};fli1:eGFP;gata1a:dsRed) 3dpf embryos were imaged using spinning disc confocal microscopy endothelium is labelled with green fluorescence and the red fluorescence shows the path of labelled red cells. The intensity of the red fluorescence is dependent on the number of red cells passing through the vessel during Z-stack acquisition. (asterisks=ISV, arrowhead=DLAV). Expanded image shows the increased red fluorescence seen in the ISV and DLAV in the *vhl*^{-/-} and wt. Scale bar, 50 μ m.

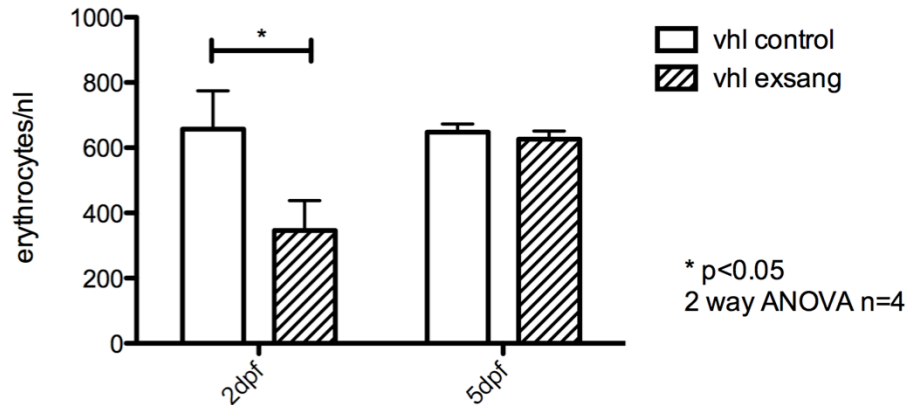
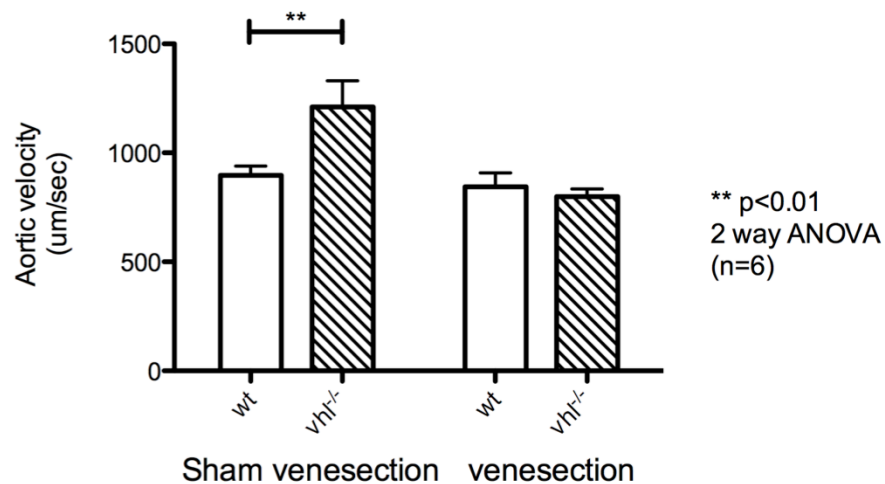
AEffect of venesection on erythrocyte density in *vhl* mutants**B**Effect of hypovolaemic anaemia on systolic aortic erythrocyte velocity in the *vhl* mutant and wt sibling at 5dpf

Figure 4.10 Effect of venesection on the erythrocyte density and its effect on the aortic erythrocyte velocity in the *vhl*^{-/-} mutant.

A. Venesection of *vhl*^{-/-} mutants by injury with a micropipette at the duct of Cuvier at 2 dpf reduces the erythrocyte density under circulatory force, but this density is back to the same levels as control *vhl*^{-/-} mutants by 5 dpf. **B.** The venesection reduces the aortic velocity to wild type levels in the *vhl*^{-/-} mutant by 5 dpf. All groups: Mean ± SEM; 2-way ANOVA; Bonferroni post test; * p < 0.05, ** p < 0.01; n annotated on the graph.

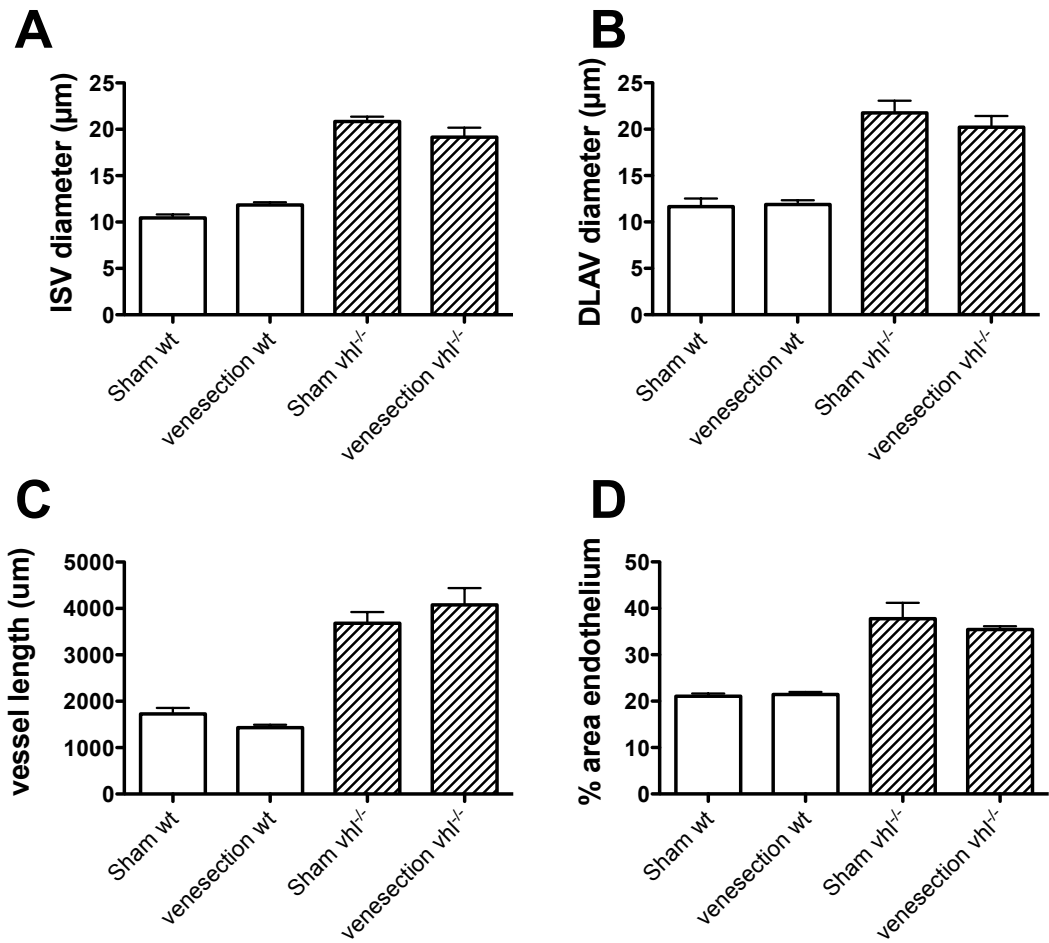


Figure 4.11 Venesection at 2 dpf to reduce aortic velocity in the *vhl*^{-/-} mutant does not change the angiogenic phenotype at 5dpf.

A. Effect of venesection at 2 dpf on *vhl*^{-/-} and wt embryos with quantification of ISV diameter in *Tg(fli1:eGFP)* in a 2 somite ROI at the level of the cloaca. **B.** Effect of venesection on the DLAV diameter in *vhl*^{-/-} and wt at 5 dpf. **C.** Effect of venesection at 2 dpf on *vhl*^{-/-} and wt embryos with quantification of total vessel length of ISV and DLAV in *Tg(fli1:eGFP)* in a 2 somite ROI at the level of the cloaca. **D.** Effect of venesection on the total area of GFP expressing endothelium in the same ROI in *vhl*^{-/-} and wt at 5 dpf. All groups mean ± SEM; 2-way ANOVA; all groups ns; n=4.

4.3 Discussion

Extensive research has shown that the differentiation, behaviour and morphology of endothelial cells is altered in different types of circulatory flow, in particular shear stress (Boon & Horrevoets 2009; Davies 2008). In addition recent work in the zebrafish has identified a mechanism for flow dependent regulation of developmental angiogenesis (Nicoli et al. 2010). I wanted to use the zebrafish model of constitutively active, HIF-driven angiogenesis to address the question of whether altering flow in the presence of increased hypoxic signalling alters angiogenic behaviour *in vivo*.

I have shown that removing flow in the developing *vhl*^{-/-} mutant leads to attenuation in all of the features of the angiogenic phenotype described in the previous chapter. Of particular interest is that the phenotype is returned to control levels by the injection of the *troponin t*₂ MO, as opposed to a partial reduction. This suggests that flow is a requirement for development and may lie downstream of the increases in VEGF-A signalling present in the mutant (Van Rooijen et al. 2009). To confirm this it would be necessary to look at the different levels of zebrafish *vegf* isoforms and their expression by WISH in the *vhl*^{-/-} and wildtype embryos in the presence and absence of flow.

In the developmental setting the absence of flow results in the loss of the accessory 5th aortic arch in the zebrafish. There are similarities with the observation that the aberrant angiogenesis of the *vhl*^{-/-} mutant is lost in the absence of flow. Given that the developmental regulation of this flow dependent angiogenesis is regulated by mirRNA-126 and alteration of endothelial *vegf* sensitivity, it would be interesting to look at expression levels of mirRNA-126 in the endothelium of the aberrant mutant vessels and how its expression responds to the loss of flow. The technique of WISH for microRNAs is becoming increasingly available in the zebrafish model (Lagendijk et al. 2012), assessment of the role of this and other microRNAs in the *vhl* mutant phenotype would clearly be of great interest.

An additional striking feature of the experiments in the *vhl*^{-/-} mutant with and without circulatory flow is the differential response of vessels to flow. In the *vhl*^{-/-}

mutant there is complete attenuation of the angiogenic phenotype in the absence of flow. However the early developing vessels which form by sprouting angiogenesis, (ISV and DLAV) are preserved and pattern normally in both the wild type and the *vh1^{-/-}* mutant despite the removal of flow. This indicates that early developmental angiogenesis is independent of endothelial flow sensing but that hypoxia signalled angiogenesis requires flow. Also the on going detection of flow is essential for the continued development of the *vh1^{-/-}* phenotype, as indicated by the BDM experiments, in which flow was removed only after 12 hrs. The differential regulation of angiogenesis based on sensitivity of the endothelium to flow signals and the mechanism by which the angiogenesis is stimulated (developmental or hypoxia signalling) has not been previously reported.

Although apparently novel, this differential regulation may not be so surprising given that the early formation of developmental vessels occurs before, or at the onset of circulation. These primitive vessels are required to form the stereotyped trunk vessels often before flow has been established outside the aortic loop. Hypoxia-driven angiogenesis however is a physiological adaptation to reduced oxygenation and thus intuitively may require the presence of flow, as there is little value in the production of novel vessels to overcome hypoxia, if there is no flow of oxygenated erythrocytes in these vessels. However, this remains only a hypothesis.

Although antisense oligonucleotide morpholinos are an effective tool for the temporary knockdown of zebrafish genes in development they have been shown to cause off target effects (Nasevicius & Ekker 2000) potentially via p53 activity (Bill et al. 2009). Despite the simple readout of gene knockdown (visual confirmation of lack of circulation) of *troponin t₂* knockdown in my experiments there remains the possibility that this MO has off-target effects leading to loss of the *vh1^{-/-}* angiogenic phenotype. I used the chemical BDM which uncouples excitation and contraction in the contractile apparatus (Jou et al. 2010), resulting in the arrest of cardiac contraction in the developing zebrafish. Despite the different mechanism of arresting flow in the developing embryo, the effect on the *vh1^{-/-}* angiogenic phenotype was the same as when induced by *troponin*

t_2 MO injection. This probably confirms that the development of the angiogenic vessel morphology in the *vhl*^{-/-} mutant is flow-dependent.

The increase in the number of endothelial cells in the *vhl*^{-/-} mutant was blocked by both genetic knockdown of *troponin t₂* and BDM treatment. However even in wildtypes, *troponin t₂* injected embryos showed lower numbers of endothelial nuclei than controls. This difference in endothelium was not seen in the group treated with BDM. This may suggest that the difference is due to the short period of flow, which occurs between 24 and 36 hpf in the BDM treatment group. Unfortunately I do not have data to look at the number of endothelial cells in the aorta prior to formation of the ISV and DLAV. This data would correspond to the period of aortic flow in the BDM group but not in the *troponin t₂* MO group. This may enable us to explain the difference in cell number in the endothelium never exposed to flow compared to endothelium initially exposed to flow prior to its arrest.

It is possible that changes in the number of endothelial cells in the aorta, prior to their migration into the ISV and DLAV, may subsequently affect the population of cells available to migrate from the aorta to form these vessels (Childs et al. 2002; Blum et al. 2008). This may explain the lower numbers of cells seen in the ISV and DLAV in embryos never exposed to flow, as migration from the aorta drives normal patterning preceding any significant *in situ* proliferation in these vessels (Zygmunt et al. 2012).

Alternatively it has been previously established that there is a flow dependent population of haematopoietic stem cells in the ventral wall of the aorta from 30hpf which migrate and proliferate in response to flow (North et al. 2009). These cells would express endothelial markers at this stage in development and the number of this subset of endothelial cells would be reduced in the absence of flow (North et al. 2009). A similar mechanism may influence aortic endothelium and permit normal migration and proliferation in preparation for ISV and DLAV formation at the point of aortic flow, in a similar manner to the haematopoietic stem cell (HSC) population. To address this experimentally it would be interesting to look at the endothelial cells of the aorta and their

migration patterns after *troponin t₂* knockdown or BDM treatment over a series of time points. It would be possible to track the migration and also image proliferation of these cells from the aorta to the ISV and DLAV in a similar manner to the demonstrated by (Blum et al. 2008), This tracking of individual endothelium could be achieved using transgenic *kaede* (photo-convertible) endothelial cells and time-lapse imaging to track individual endothelial cells from there origin to sites of mitosis in both the wild type and the *vhl*^{-/-} mutant.

4.3.1 Summary

I have shown that circulatory flow is required for the initiation and maintenance of the *vhl*^{-/-} angiogenic phenotype. This attenuation of the *vhl*^{-/-} mutant phenotype is established as a result of cessation of flow even after its onset and not merely the absence of flow throughout development. Changes in endothelial cell number are consistent with those seen in vessel morphology in response to absent flow in the mutant vessels. These changes in response to a flow signal of endothelial angiogenic behaviour have not been previously described.

The possibility that alteration in the circulation of soluble angiogenic growth factors like VEGF-A and NO which have been shown to be modified by up-regulated HIF signalling may mediate flow and thus the aberrant angiogenesis I have described. I have undertaken a detailed study of the role of the vascular growth factors and cell signalling molecules, which have been shown to alter their expression and effect on the endothelium, in the next chapter.

Chapter 5 Examination of the interactions between blood flow, Notch and nitric oxide signalling in wildtype and *vhl* mutant zebrafish

5.1 Introduction

In the previous chapter I described my discovery that blood flow is required for aberrant angiogenesis seen in the trunk vessels of homozygous *vhl* mutants. In this chapter I summarise my attempts to identify mechanisms that underlie this flow-dependent angiogenesis. Specifically, I aimed to examine whether alterations in Notch and / or NO signalling might contribute to this phenomenon.

5.2 Results

5.2.1 Identification of changes in endothelial Notch signalling in response to flow using a novel Notch reporter transgenic

As discussed in Chapter 1, Notch signalling plays a central and complex role in the initiation and co-ordination of angiogenesis. Given that reduction of Notch signalling has been shown to block angiogenesis I wanted to see if alterations in endothelial Notch signalling regulated the response to flow seen in the *vhl*^{-/-} mutant without haemodynamic flow. It (notch signalling) therefore appeared a good candidate pathway to examine in this model.

To identify changes in Notch signalling I used a novel transgenic zebrafish *Tg(CSL:venus)* kindly provided by Martin Gering (University of Nottingham, UK). All canonical Notch signalling occurs by activation of the CSL transcriptional binding complex in the presence of the NICD. This transgenic line uses a multiple repeat of the CSL binding domain to activate expression of the modified green fluorescent protein (GFP) molecule, venus. In this transgenic the fluorescent protein expression is a result of activation of canonical Notch signalling pathway and can be observed in cells with increased Notch activity as fluorescence. The modified GFP (venus) used for this transgenic has been shown to have more rapid protein synthesis, folding and improved stability, improving real time visualisation of Notch-dependent cellular signals (Nagai et al. 2002).

5.2.1.1 Morpholino knockdown of *troponin t₂* increases endothelial Notch signalling in the developing aorta

To examine whether prevention of blood flow altered vascular Notch signalling, I knocked down *troponin t₂* (in the same manner as in the previous chapter) in *Tg(CSL:venus)* embryos and visualised reporter expression.

Figure 5.1 shows the trunk region of representative 48 hpf control and *troponin t₂* morphants. I found that *troponin t₂* knockdown increased fluorescence in the aorta and a number of ISVs at 48 hpf and 72 hpf. There is greater fluorescence of the aorta in the 72 hpf *troponin t₂* morphant embryos compared with 48 hpf *troponin t₂* morphants. I quantified aortic fluorescence in groups of embryos (Figure 5.2). This showed *troponin t₂* knockdown increased aortic fluorescence by about 40% at 48hpf and around 300% at 72hpf. The increase in fluorescence seen in some of the ISV was not seen in all intersegmental vessels and the level of intensity in these vessels varied in the embryos. This variation may reflect the smaller numbers of endothelial cells in these vessels or that they overlie the neural tube which demonstrates high levels of Notch signalling in the *Tg(CSL:venus)* line. These limitations make further fluorescence analysis of this particular vascular tissue difficult. As a result analysis of notch reporter expression was focused on the aortic endothelium, which showed consistent changes in Notch signalling in response to flow.

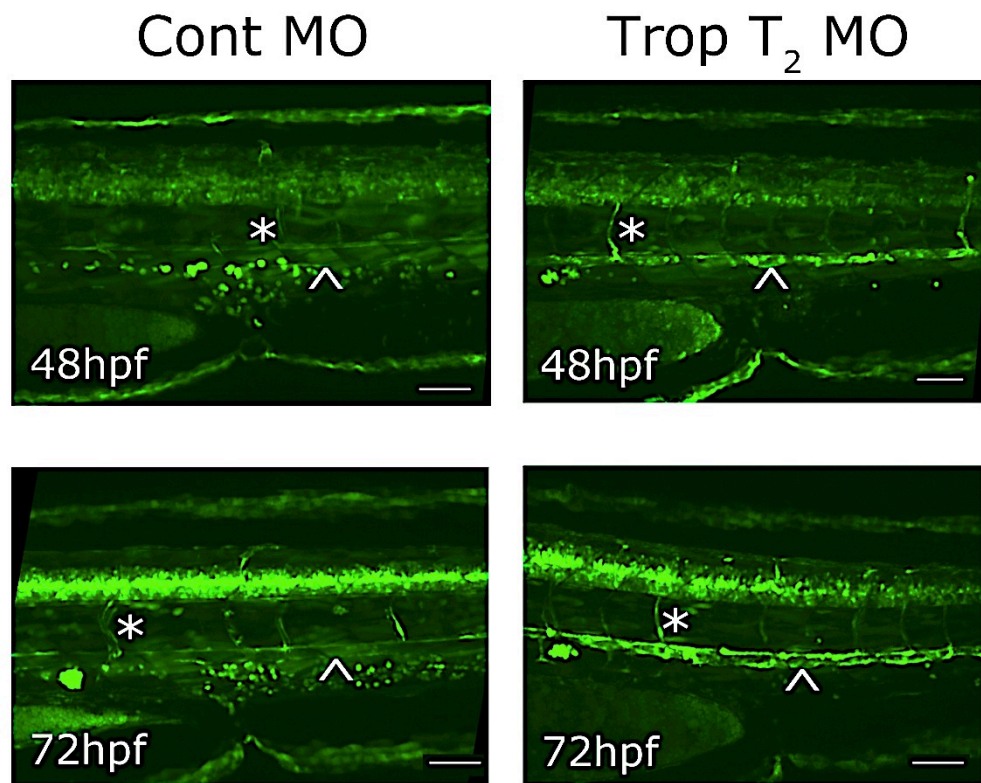


Figure 5.1 Flow dependent changes in aortic endothelial Notch signalling as a result of troponin t_2 MO knockdown at 48 hpf and 72 hpf.

Troponin t_2 and Control MO injection of *Tg(CSL-venus)^{qmc61}* embryos, fluorescence shows areas of Notch signalling mediated by the CSL transcription factor. Top panels show the increased Notch-dependent fluorescence in the aorta (arrowhead) and ISV (asterisk) in the mid-trunk of 48 hpf embryos injected with *troponin t_2* MO not exposed to circulatory flow (see Fig 5.9 for expanded detail of the aorta reporter expression). This Notch reporter line is not restricted to endothelial tissue so Notch mediated fluorescence can be seen in neural tube, yolk sac and the developing fin edge. In the top panels the aortic tissue (arrowhead) contains more green fluorescence in the embryo without circulatory flow. Lower panels show increased CSL signal in the aorta in the absence of flow compared to the earlier time point. There is also an increase in neural tube signal at 72 hpf compared to 48 hpf. Scale bar, 200 μ m.

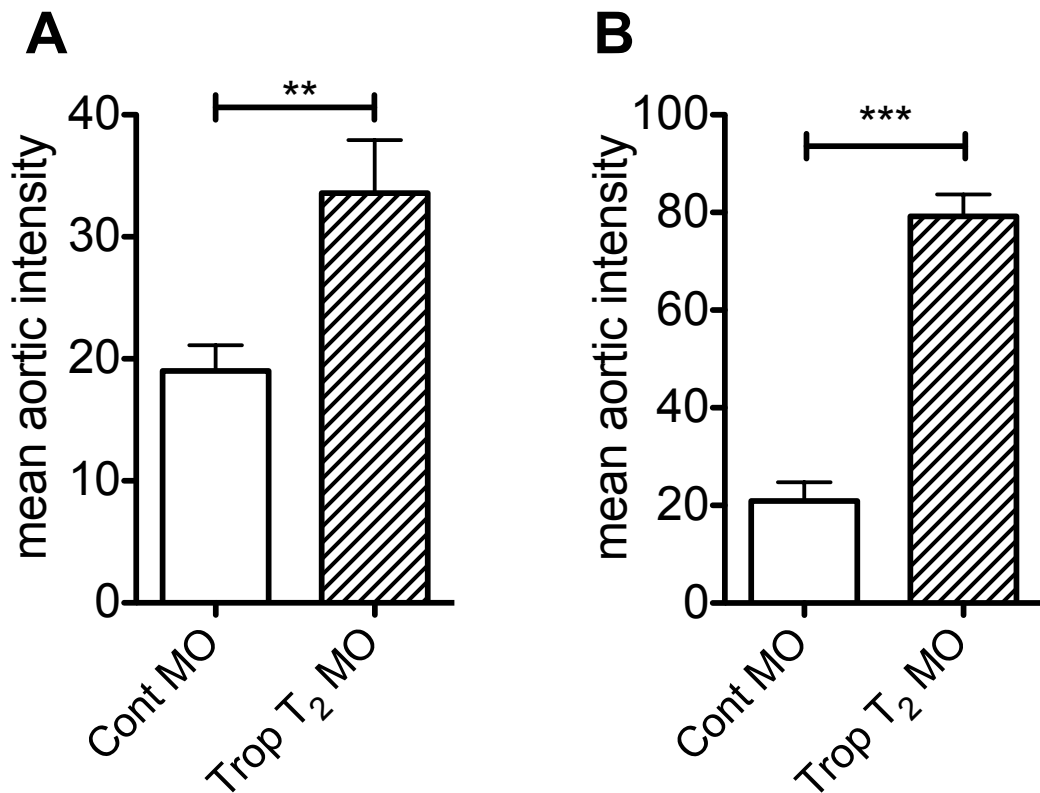


Figure 5.2 Quantification of endothelial notch signal at 48hpf (A) and 72hpf (B) in the presence of flow or absence (Trop T₂), due to injection with *troponin t₂* MO.

The overall aortic fluorescence was measured by obtaining the mean aortic fluorescence along the dorsal aortic wall using a line tool in imageJ drawn through the dorsal aorta endothelium in the *Tg(CSL-venus)^{qmc61}* notch reporter line injected with control or *troponin t₂* MO. This technique overcomes the cellular variability in CSL expression by averaging the fluorescence through the tissue. There is a significant increase in aortic endothelial fluorescence in the endothelium of embryos not exposed to flow (*troponin t₂* MO) at 48hpf (A) By 72hpf (B) this the difference in fluorescence is increased. All groups, mean \pm SEM; unpaired two-tailed t test; ** = $p < 0.01$; *** = $p < 0.001$; $n = 9$.

5.2.1.2 Pharmacological induced circulatory arrest leads to increases in endothelial notch expression

The previous experiments showed that complete prevention of cardiac output by *troponin t₂* knockdown led to increases in Notch signalling in the developing vasculature. Although *troponin t₂* is not expressed outside the heart (Sehnert et al. 2002), it is possible these observed effects were not caused by the absence of blood flow. I therefore treated *Tg(CSL:venus)* embryos with the myosin ATPase inhibitor BDM as in the previous chapter. Developing embryos were treated with BDM from 36hpf (after onset of cardiac contraction) until imaging at 72hpf. Cessation of cardiac contraction and circulatory flow was confirmed by microscopy at several stages throughout drug incubation and before imaging.

Figure 5.3A shows representative photomicrographs demonstrating that BDM treatment increased reporter expression in the aorta and ISVs; mean aortic fluorescence was increased by 45% in BDM-treated embryos (Figure 5.3B). Therefore, complete prevention of cardiac output (by *troponin t₂* knockdown) or pharmacologic cessation of blood flow after onset of circulation (by BDM treatment) both lead to increased Notch signalling in the aortic endothelium.

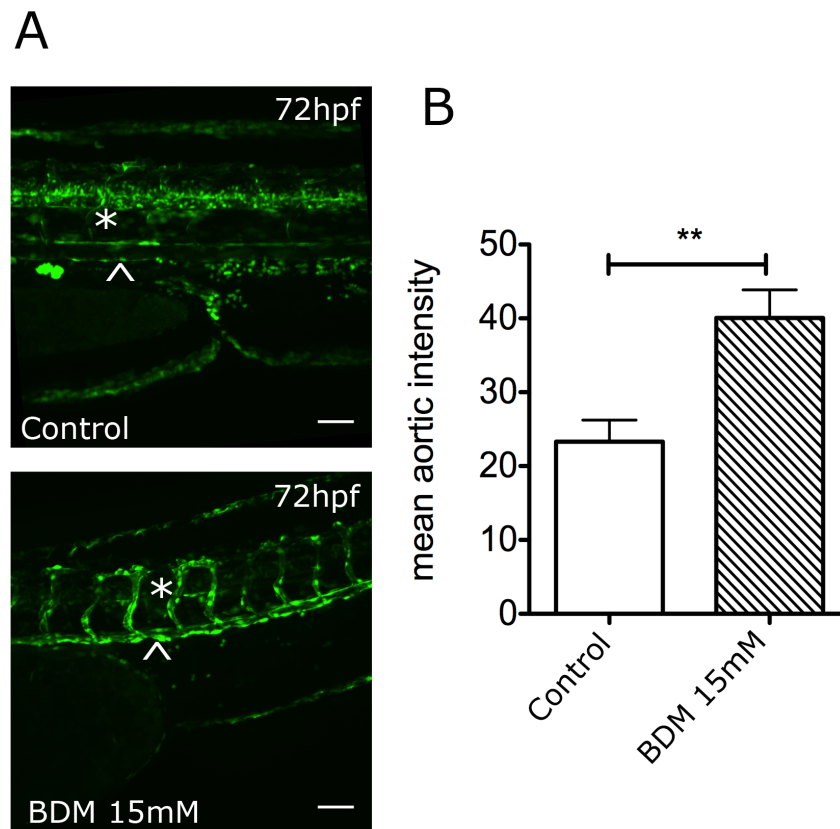


Figure 5.3 Effect of pharmacological induced circulatory arrest with BDM (15mM) at 36hpf on endothelial Notch signalling imaged at 72 hpf.

Aortic fluorescence in the *Tg(CSL-venus)^{qmc61}* Notch reporter line treated with BDM 15 mM or control E3 media from 36 hpf until 72 hpf. There is a clear increase in aortic endothelial notch signal in the embryos not exposed to flow (BDM 15 mM) at 72 hpf aorta (arrowhead) and ISV (asterisk) (**A**). This difference in aortic fluorescence is significantly increased in the BDM group compared to control embryos (**B**). All groups: Mean \pm SEM; unpaired two-tailed t test; ** = $p < 0.01$; $n = 8$.

5.2.1.3 Confirmation that increased endothelial Notch signalling is mediated by a classical Notch ligand-receptor interaction

Notch signalling is mediated by expression of a ligand on the surface of the signalling cell, which binds to a receptor on an adjacent cell. This receptor-ligand complex is then cleaved at the cell membrane of the transducing cell and then the ligand-receptor complex is internalised to activate signalling in the receiving cell by direct promotion of numerous gene targets.

To examine whether the increase in aortic Notch signalling seen in response to absent blood flow shown above results from this classical or canonical Notch signalling, I treated *Tg(CSL:venus)* embryos injected with the *troponin t₂* morpholino with the γ -secretase inhibitor DAPT. This blocks cleavage of the ligand-receptor complex at the cell membrane before internalisation and activation of Notch signalling targets in the nucleus by NICD binding to the CSL complex.

Control *troponin t₂* morphant *Tg(CSL:venus)* embryos treated with DAPT (see methods section 2.10.2.1) showed no difference in aortic reporter expression, consistent with the generally low level of reporter expression in these embryos (Figure 5.4 and 5.5). It is possible that the fluorescent protein that is clearly seen in the endothelium, but at lower levels may still be present in the tissue due to expression at an earlier time point, prior to DAPT exposure, a phenomenon known as perdurance. Perdurance is the persistence of a reporter fluorophore, due to the stability of the reporter in the cytoplasm, after the expression of the driving transcription factor or gene has ceased. This phenomenon results in the appearance of continuing gene expression with *in vivo* imaging. This is a well described limitation of single time point observation of transgenic lines and a well described issue with stable fluorophores like GFP (Wells et al. 2011; Vitorino et al. 2009). However, the increases in reporter expression induced by *troponin t₂* knockdown, was completely abolished by DAPT treatment. This indicates that the increase in Notch signalling induced by absence of blood flow is dependent on NICD formation from the extracellular Notch receptor. If this is due to canonical Notch signalling, this may be due to the effect of blood flow on Notch at a ligand / receptor level. However, the

possibility remains that the effect is via a non-canonical pathway resulting in modification or stabilisation of the NICD protein, which would lead to the same result.

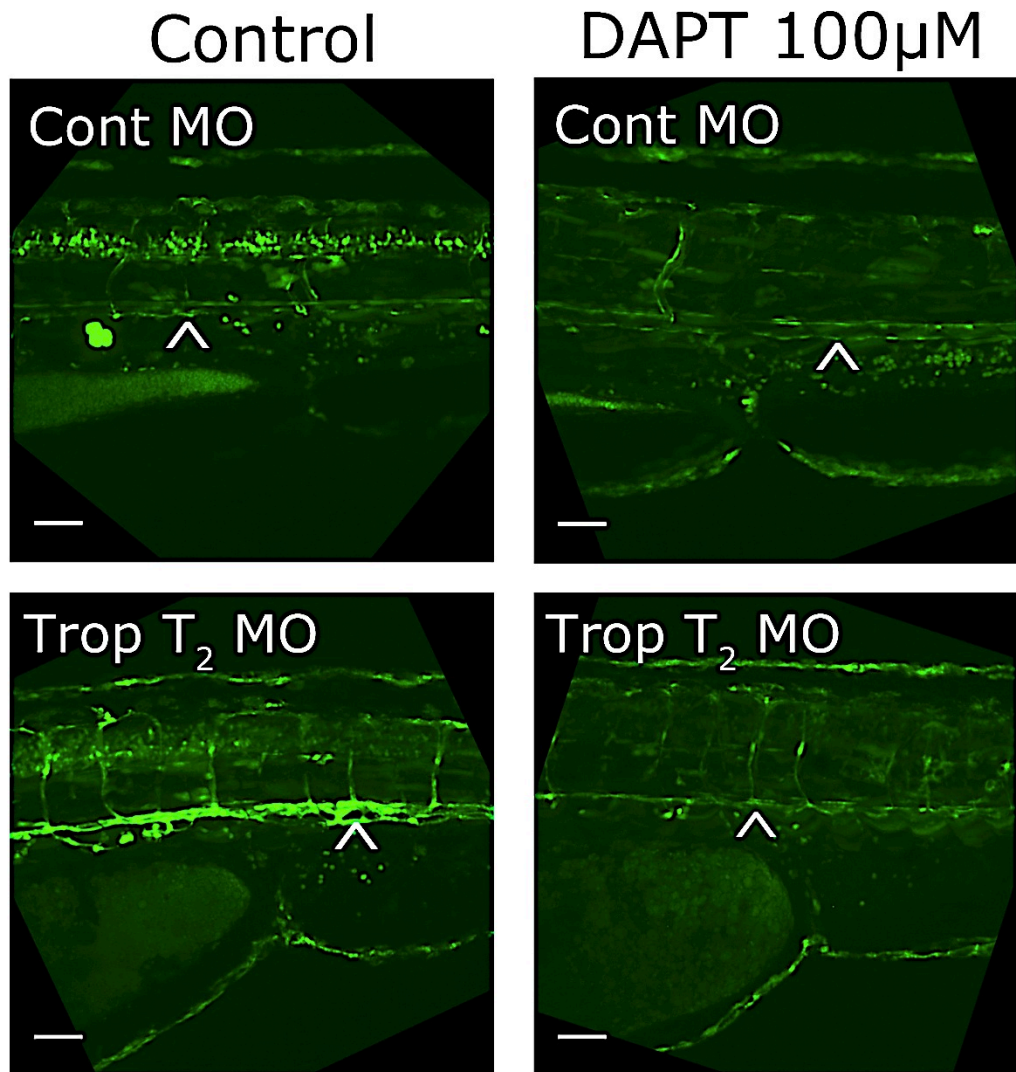


Figure 5.4 Effect of a pharmacological Notch signalling inhibitor on the flow dependent increase in CSL-venus fluorescent signal.

Troponin t₂ and Control MO injection of *Tg(CSL-venus)^{qmc61}* embryos, right panels incubated with the Notch inhibitor DAPT in E3 media, left panels incubated in control media. The increased aortic (arrowhead) fluorescence induced by *troponin t₂* MO injection is reduced to control levels by Notch inhibition. Scale bar, 100 µm.

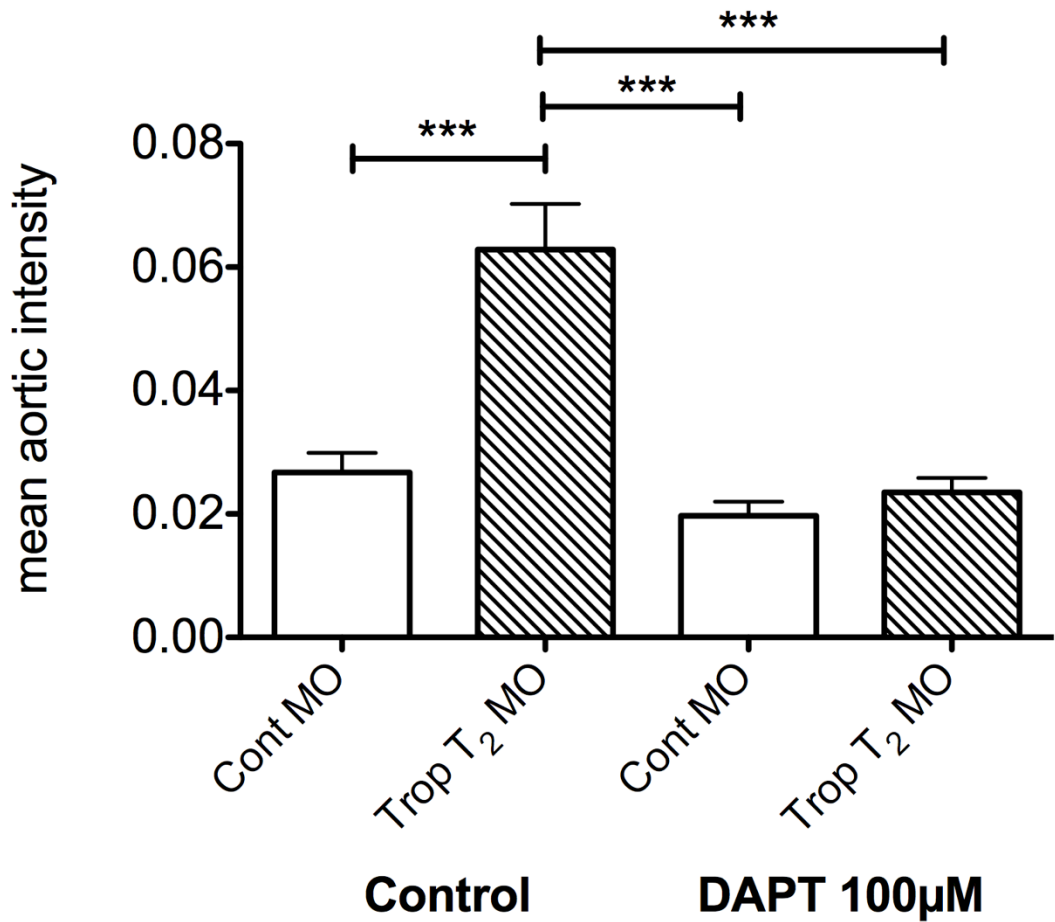


Figure 5.5 Quantification of the mean aortic CSL-venus fluorescence in embryos injected with *troponin t₂* MO and the effect of DAPT.

Quantification of the mean aortic fluorescence in *troponin t₂* and Control MO injected *Tg(CSL-venus)^{qmc61}* embryos either treated with control E3 media or incubated in DAPT 100 µM (Notch inhibitor) from 48-72 hpf. The significant increase in CSL fluorescence in *troponin t₂* MO injected embryos can be blocked by incubation with DAPT. All groups: Mean ± SEM; two way ANOVA; *** = p<0.001; n=10.

5.2.2 Identification of Notch signalling components differentially expressed in endothelial cells in the absence of circulatory flow

Since the above studies suggested that blood flow regulates endothelial Notch signalling via ligand/receptor interactions, I examined whether blood flow alters expression of these molecules.

I therefore used RT-qPCR to quantify expression of a range of Notch ligands, receptors and downstream targets (*vegfab*, *vegfc*, *kdr/flk1*, *kdr-*l*/flt1*, *flt4*, *ephrinB2*, *her6*, *her12*, *notch3*, *nrarpa*, *dll4*, *cxcr4a*, β -actin2) in RNA extracted from the trunk of developing embryos with and without blood flow (due to *troponin t₂* knockdown), at 48 hpf and 72 hpf. Differential expression was normalised to expression of β -actin.

Figure 5.6 shows expression of each of these genes in 48 hpf control or *troponin t₂* morphant embryos. Our group previously showed that *cxcr4a* expression increases in *troponin t₂* morphants (Packham et al. 2009), and this was confirmed in my experiments, thus acting as a positive control. From the genes I examined, only the notch ligand *dll4* was significantly differentially regulated in trunk tissue in response to flow. *dll4* expression was increased 2.5-fold in the absence of flow (induced by *troponin t₂* knockdown). There was no significant differential expression of the *vegfab* and *vegfc* ligands or of *kdr* and *flt4* (*vegfb*) receptors. There was also no significant alteration in the expression of the notch receptor *notch3* or the downstream Notch targets *her12* and *ephrin-b2a* (figure 5.6).

At 72 hpf the only significantly differentially expressed gene in the absence of flow was *cxcr4a* (Figure 5.7), which was increased 3-fold compared to the control MO injected group. There was increased expression of *dll4* at this time point but this was not statistically significant (Figure 5.7) after normalisation to β -actin.

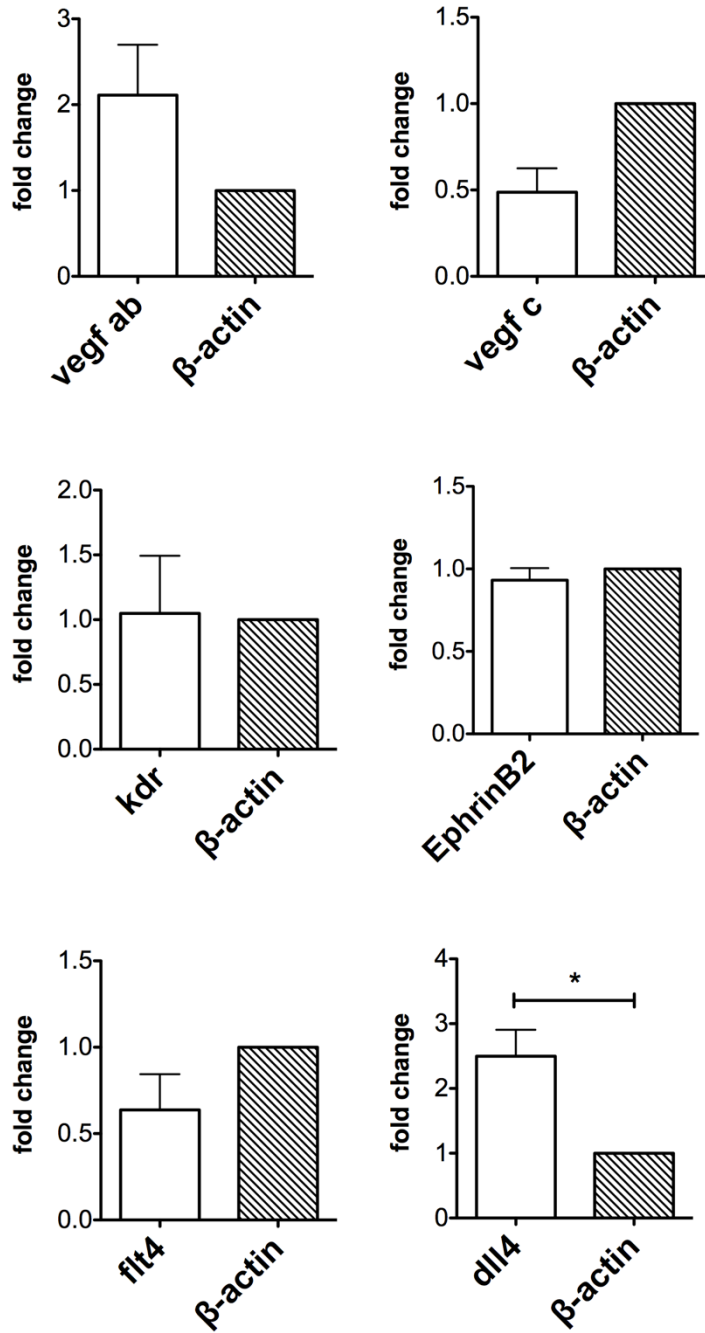


Figure 5.6 RT-qPCR of trunk tissue from 48 hpf embryos comparing the relative expression of known angiogenic genes, Notch ligands, receptors and notch signalling targets in *troponin t₂* MO injected embryos.

Graphs show the fold change of mRNA transcripts in the *troponin t₂* MO treated group (n=30 embryos) normalised to the expression of β -actin as housekeeper

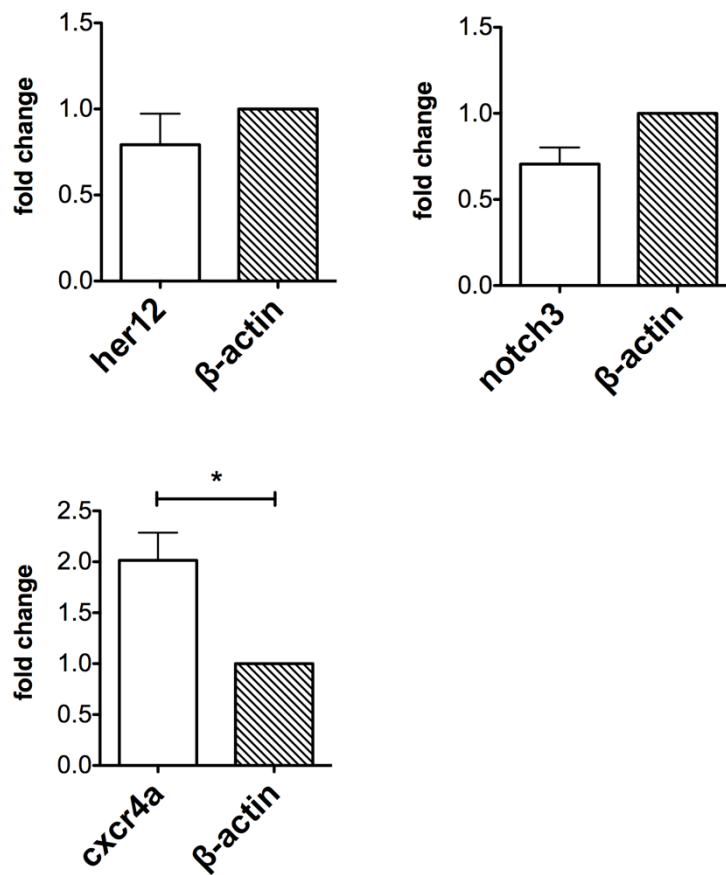


Figure 5.6 (cont)

All experiments performed in triplicate with 3 biological replicates (3 separate pools of 30 embryos). Mean \pm SD; * = $p < 0.05$; t test; $n = 3$.

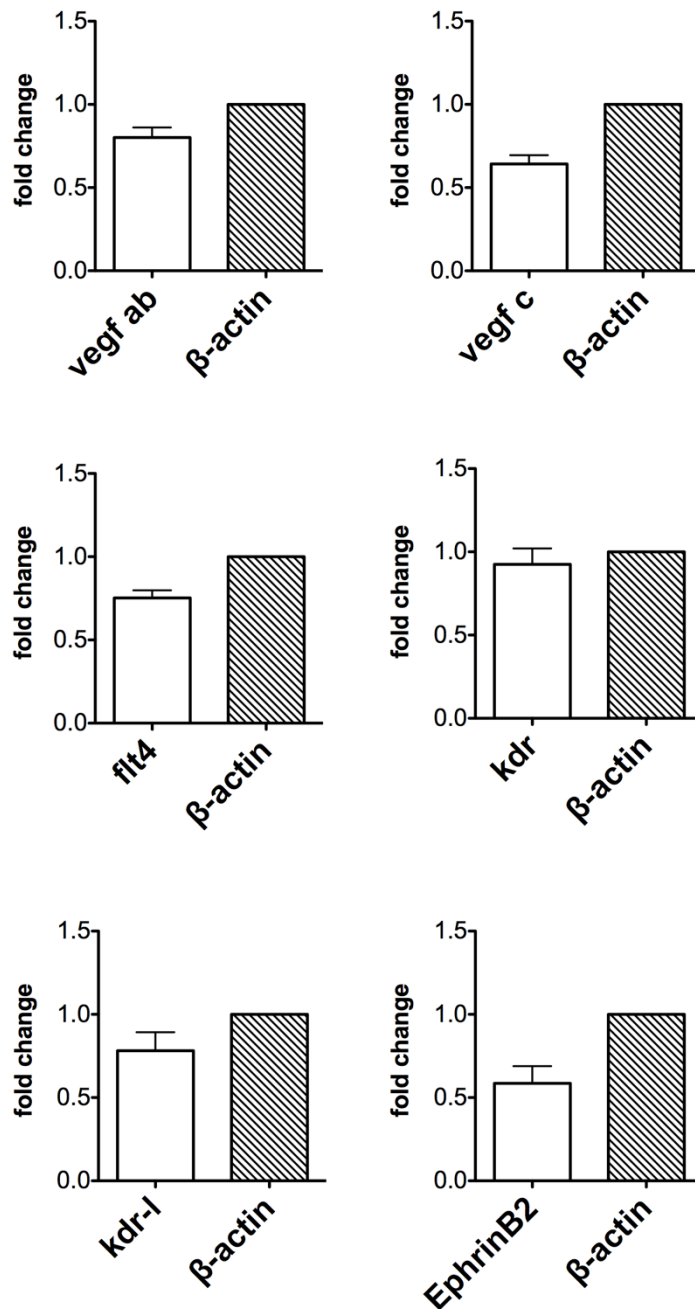


Figure 5.7 RT-qPCR of trunk tissue from 72 hpf embryos comparing the relative expression of known angiogenic genes, notch ligands, receptors and notch signalling targets in *troponin t₂* MO injected embryos.

Graphs show the fold change of mRNA transcripts in the *troponin t₂* MO treated group (n=20 embryos) normalised to the expression of β -actin as housekeeper gene in *troponin t₂* injected embryos.

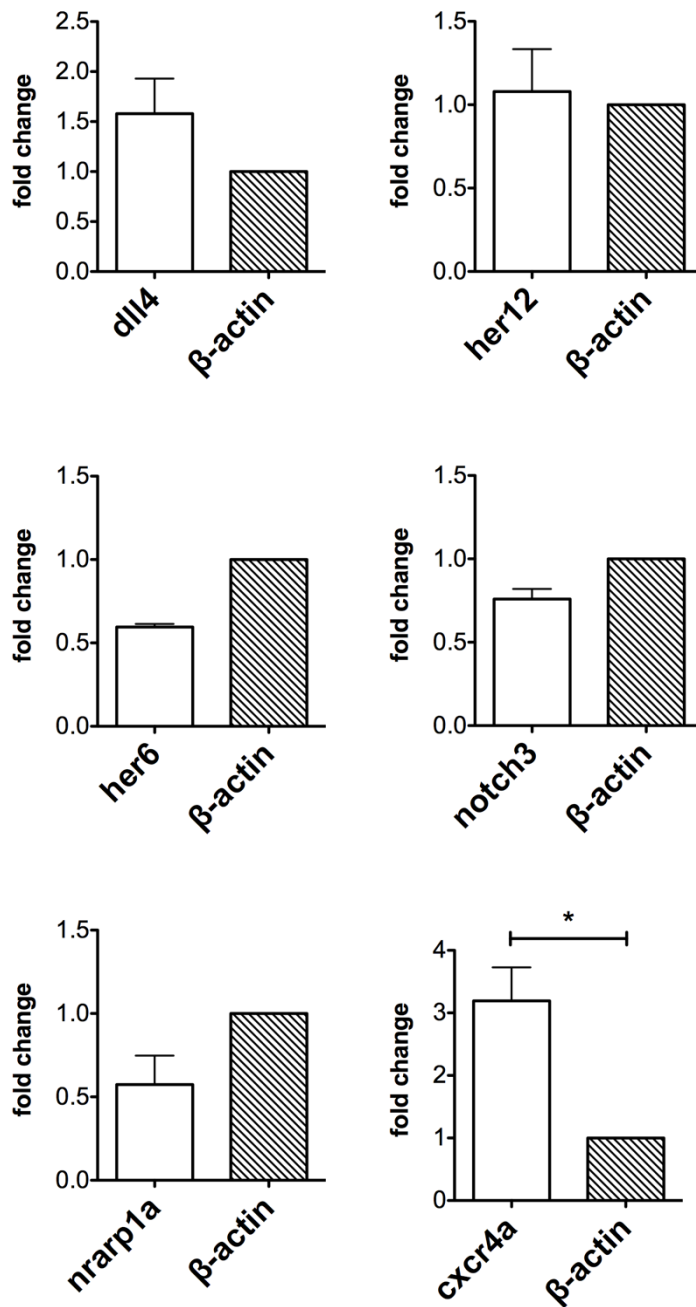


Figure 5.7 (cont)

All genes run in triplicate with 3 biological replicates (3 separate pools of 20 embryos). The only significant differential regulation is the up regulation of *cxcr4a* in the *troponin t₂* injected embryos at 72 hpf. Mean \pm SD; * = p < 0.05; t test; n=3.

5.2.2.1 Confirmation that differential expression of *dll4* in response to flow is an endothelial specific change in expression

RT-qPCR enables quantification of differential expression of RNA transcripts in the tissue of embryos in response to flow but does not provide information about spatial restriction of expression. I therefore next performed whole mount in situ hybridisation for *dll4* in control and *troponin t₂* morphants.

In control morphants, I demonstrated vascular *dll4* expression at 36 hpf, which appeared to diminish by 48 hpf and was not detectable at 72 hpf (Figure 5.8). However, in *troponin t₂* morphants, *dll4* expression was more strongly detected at 36hpf and persisted even at 72 hpf (Figure 5.8).

5.2.2.2 Knockdown of *dll4* blocks the endothelial increase in notch expression seen in response to absent flow

Data from the qPCR analysis and the transgenic notch reporter lines suggested that the notch ligand *dll4* may mediate the flow dependent up regulation of notch signalling in the endothelium of the developing zebrafish. To confirm the role of *dll4* I used a MO against the ATG site of *dll4* (Geudens et al. 2010) in the *Tg(CSL-venus)* line and measured the aortic fluorescence as a measure of endothelial notch signalling.

Figure 5.9A shows the increase in aortic endothelial notch signal in the absence of flow after injection of *troponin t₂* MO. This is an increase in venus aortic expression of around 65%, due to the absence of flow after *troponin t₂* MO injection. Co-injection of a *dll4* MO in the presence of flow does not alter the levels of venus expression but in the absence of flow *dll4* knockdown blocks the increase in notch signal (Figure 5.9B).

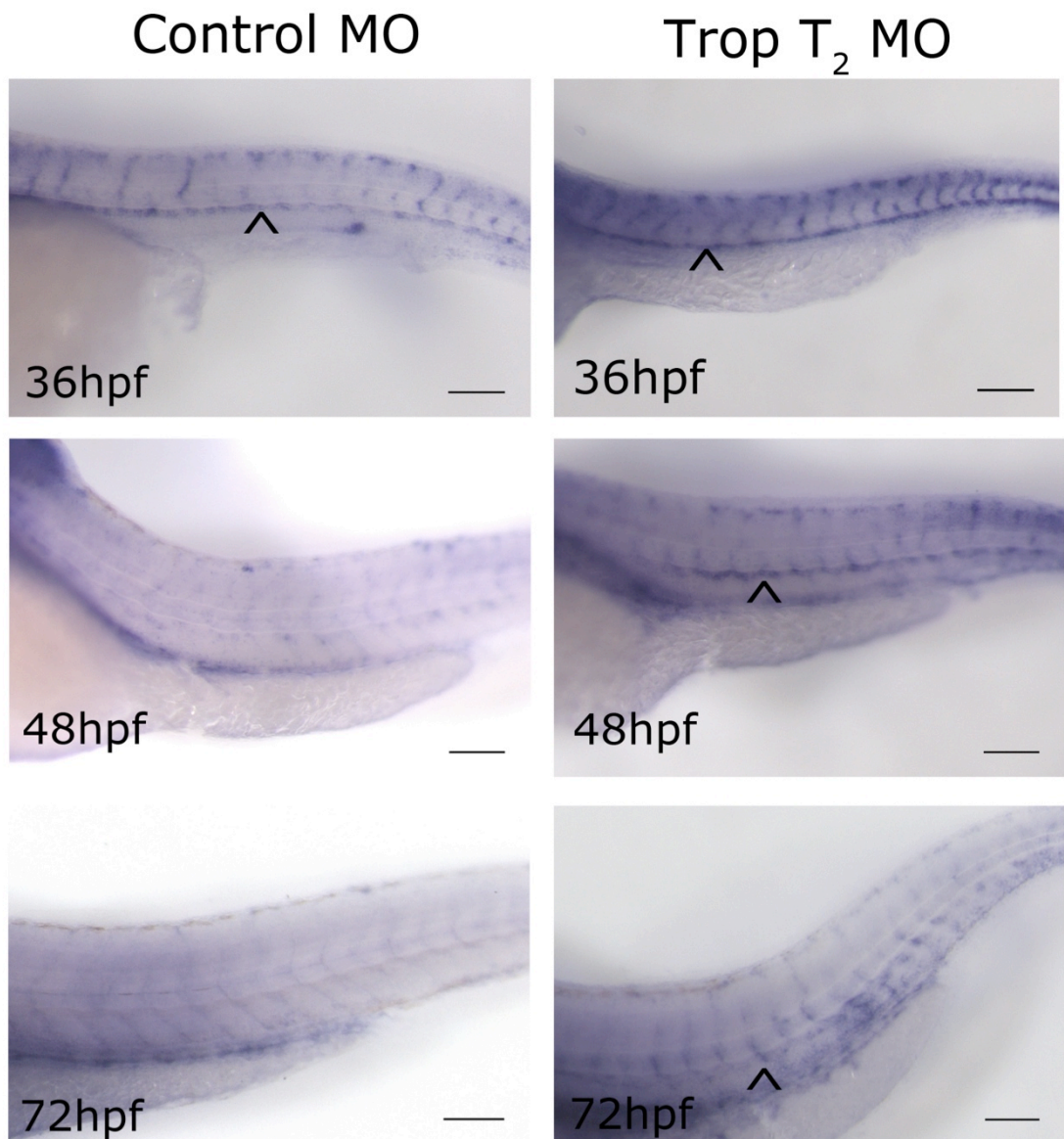


Figure 5.8 Whole mount in situ hybridisation of *dll4* mRNA expression in embryos exposed to circulatory flow and without (*troponin t₂* MO injection)

Top panels show the expression of *dll4* in the aorta (arrowhead) and ISV of the 36 hpf embryo with increased expression in these vessels in the embryos without flow. There is increased expression of *dll4* in the embryo injected with *troponin t₂* at 48 hpf and 72 hpf although the overall expression declines over time. Scale bar, 200µm.

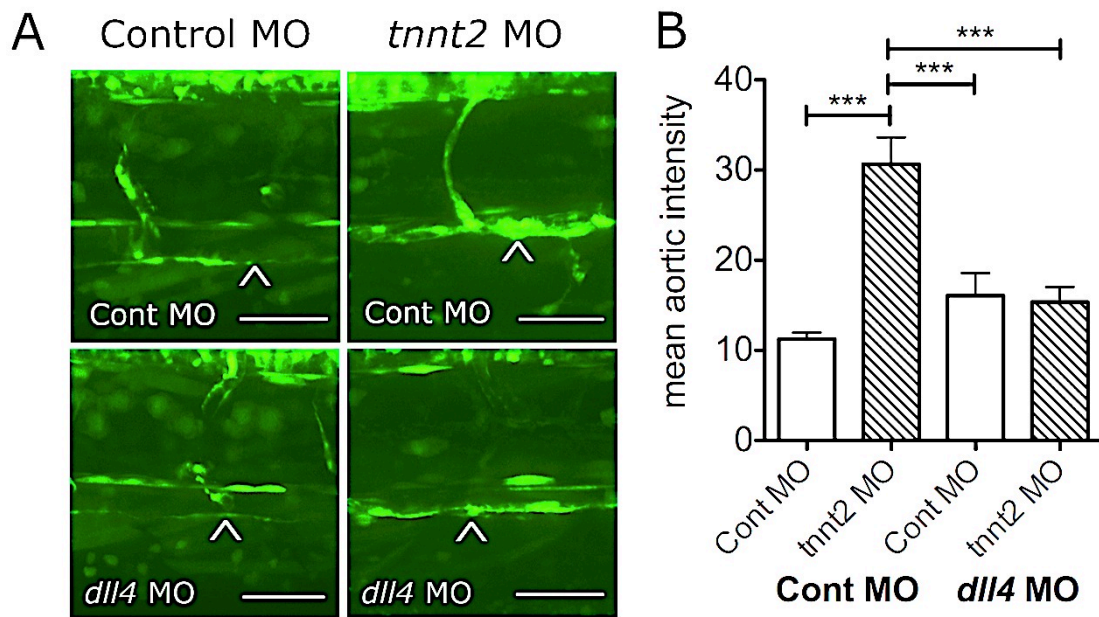


Figure 5.9 Effect of *dll4* MO knockdown on the flow dependent increase in notch signalling in the CSL:venus transgenic reporter.

A: *dll4* MO knockdown on notch reporter expression in 72hpf *Tg(CSL-venus)^{qmc61}* embryos with and without blood flow by *troponin t₂* MO injection. B: Mean aortic fluorescence in control (n=18) and *dll4* morphant (n=19) 72hpf *Tg(CSL-venus)^{qmc61}* embryos with and without blood flow due to *troponin t₂* knockdown (n=11). Mean \pm SEM; *** = $p > 0.001$; 2 way ANOVA all other groups ns.

5.2.3 Effect of manipulating NO signalling on the development of the *vhl*^{-/-} mutant vessel phenotype

5.2.3.1 The effect of NOS inhibition on angiogenesis in the *vhl*^{-/-} mutant

NO regulates many processes in vessel biology. I therefore attempted to determine if NO production contributed to the aberrant angiogenesis in the *vhl*^{-/-} mutant. L-NAME is a non-specific inhibitor of all isoforms of NO synthase and has been shown in other mammalian models to effectively inhibit eNOS. I incubated *vhl*^{-/-} embryos (in a *Fli1:eGFP* transgenic) background in [1mM] L-NAME from 24 hpf until 96 hpf and examined the effect on vascular development.

Figure 5.10 shows the trunk vessels of wild type and *vhl*^{-/-} mutants at 4 dpf treated with or without L-NAME. The characteristic angiogenic phenotype previously described in *vhl* mutants is apparent. I found no effect of L-NAME on the formation or appearance of the aorta, ISVs or DLAV in either wildtype or *vhl* mutants. Figure 5.11 shows quantification of the total vessel area, ISV diameter, DLAV diameter and total vessel length, incubation with L-NAME at 1 mM has no effect on any of these measurements in either *vhl*^{-/-} or wildtype embryos.

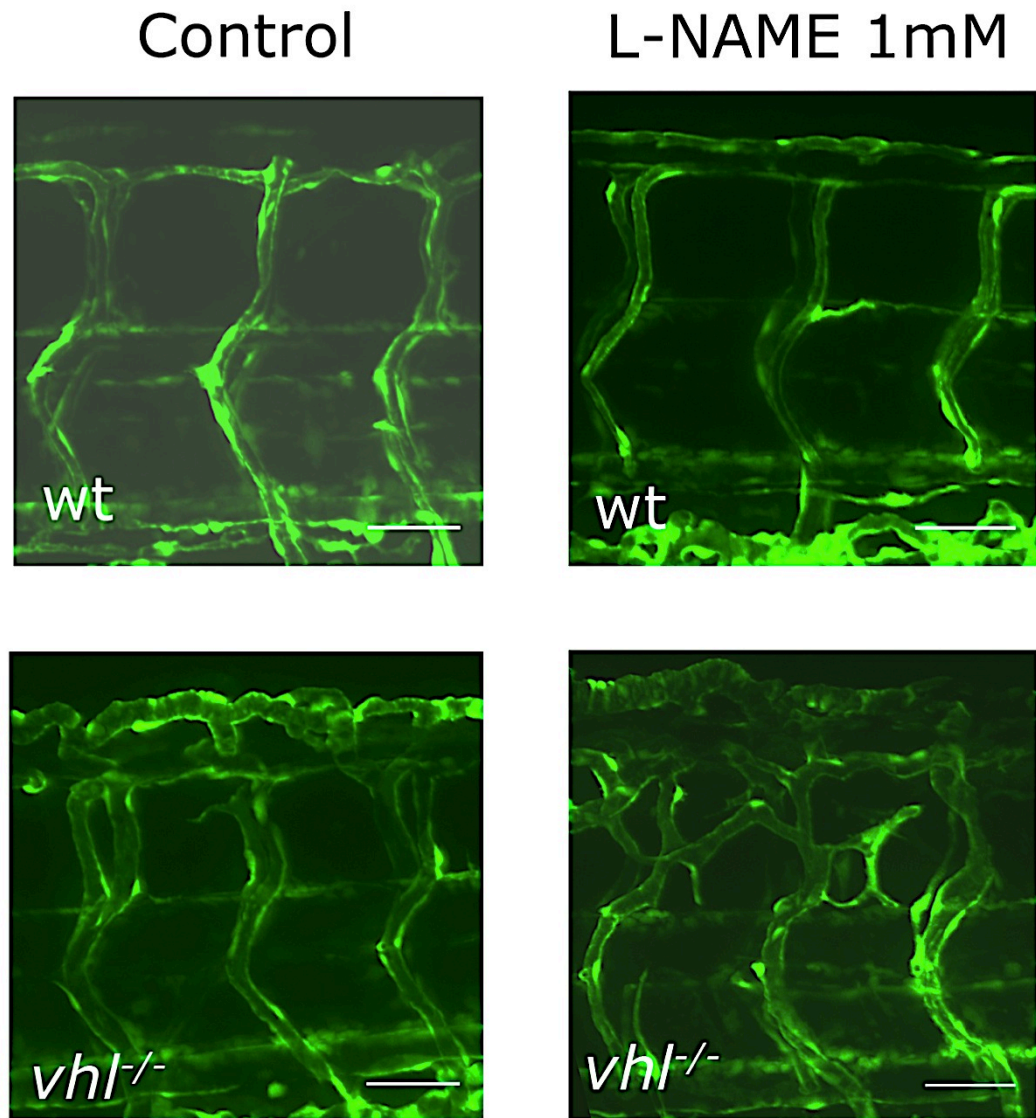


Figure 5.10 Effect of NO inhibition by L-NAME on the *vhl*^{-/-} mutant angiogenic phenotype.

4 dpf wild type and *vhl*^{-/-} mutants in the Tg(*fli1*:eGFP) background treated with control media or L-NAME a NO synthase inhibitor from the onset of cardiac contraction until imaging at 4 dpf. Photomicrographs of the mid trunk region. There is no change in the *vhl*^{-/-} angiogenic phenotype after incubation with this NO inhibitor. Scale bar, 100 μm.

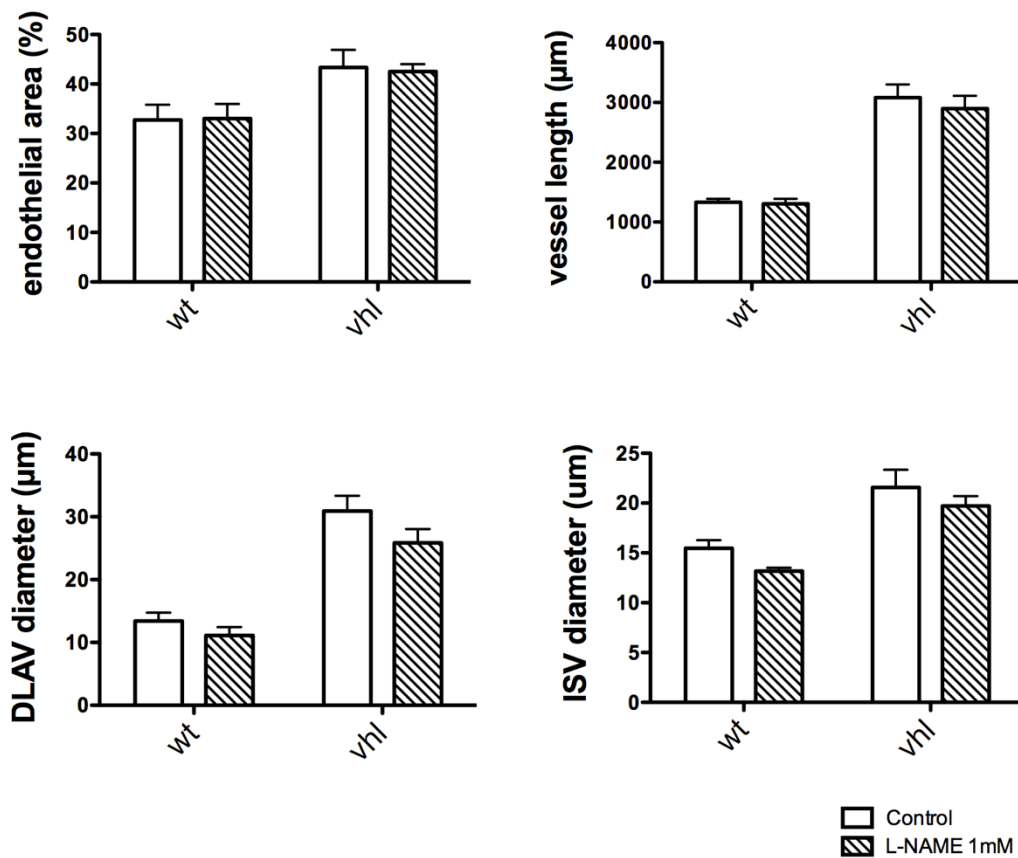


Figure 5.11 Quantification of vessel diameter, endothelial area and vessel length in wt and the *vhl*^{-/-} mutant treated with L-NAME NO synthase inhibitor.

4dpf wild type and *vhl*^{-/-} mutants in the *Tg(fli1:eGFP)* background treated with control media or L-NAME a NO synthase inhibitor from the onset of cardiac contraction until imaging at 4dpf. Measurement of the ISV and DLAV diameter show no differences in the L-NAME and control treated groups. There is no difference in the total vessel length and area of endothelium. All graphs mean ± SEM; 2-way ANOVA; all groups ns; n=5.

5.2.3.2 Effect of manipulation of NO on the aortic size in the *vhl*^{-/-} and wild type embryo

L-NAME has previously been shown to alter vascular tone and vessel diameter in the developing zebrafish at similar times to the experiments I performed in the *vhl*^{-/-} and wildtype embryos. I had hypothesised that changes in vessel diameter and tone may alter endothelial force which may lead to attenuation of the *vhl*^{-/-} angiogenic phenotype which shows increased vessel size in the trunk and has previously been shown to have increases in cardiac output (Van Rooijen et al. 2009). Differences in the aorta diameter in response to L-NAME have been shown in vessel physiology experiments (Fritsche et al. 2012) and in experiments on flow dependent migration of haematopoietic stem cells (North et al. 2009).

To confirm the results of my earlier experiments looking at the effect of NO synthase inhibition on the *vhl*^{-/-} mutant phenotype, I looked to see if L-NAME was effective in altering aortic diameter. Identification of a change in vascular reactivity would show that L-NAME at this dose has vasoactive effects in the zebrafish embryo as previously published, confirming that the compound is able to penetrate into the vascular tissue. This would lend further support to my conclusion that inhibition of NO signalling does not alter the *vhl*^{-/-} mutant vessel phenotype, confirming the negative result in figures 5.10 and 5.11.

Figure 5.12 shows that the size of the aorta in the age matched *vhl*^{-/-} mutants compared to wild types. The diameter of the aorta was not altered by L-NAME (1mM) treatment or by exposure to the NO donor SNP (100 µM). Although the SNP treatment suggests an increased diameter, which was the effect seen in other published studies this did not reach statistical significance in my experiments.

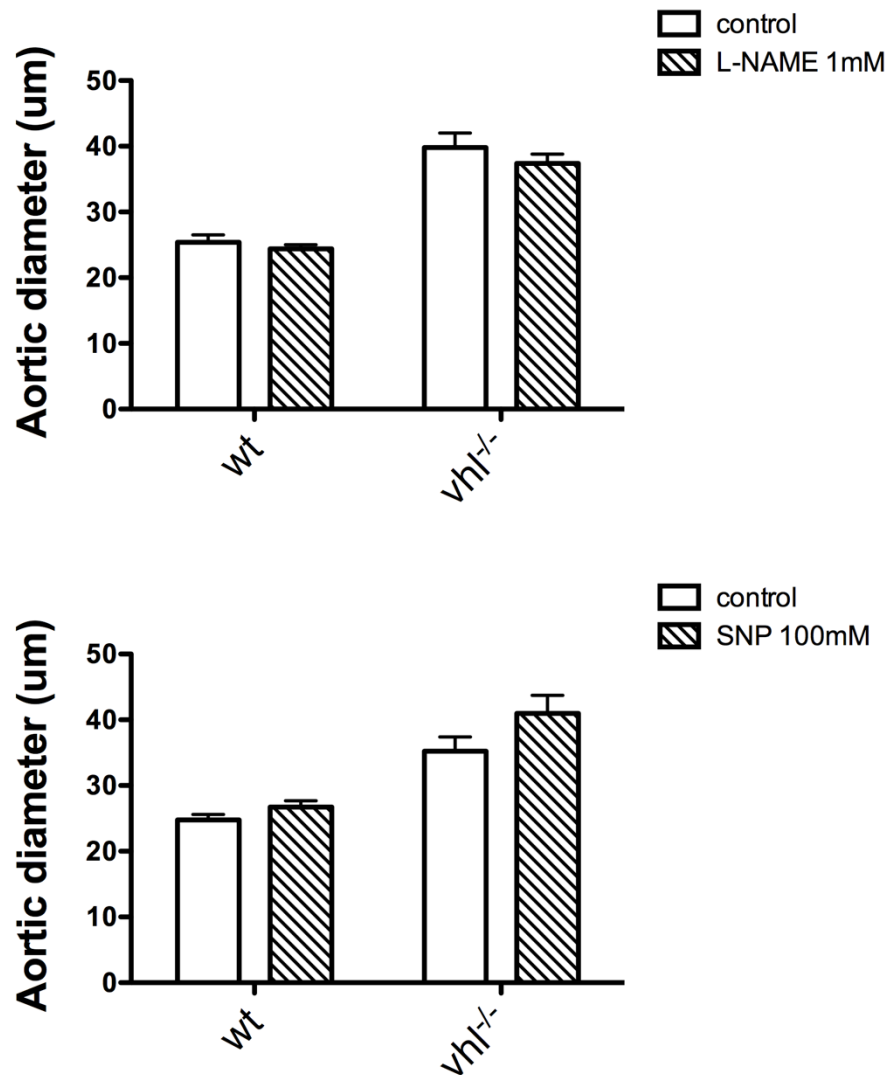


Figure 5.12 Effect of L-NAME and SNP on the aortic diameter in the *vhl^{-/-}* mutant and wt embryo at 4dpf.

Measurement of the aortic diameter in the *Tg(fli1:eGFP)* background in both the *vhl^{-/-}* mutant and wildtype embryo. L-NAME (1mM) and SNP (100mM) incubated in embryo media from 24hpf until imaging at 4dpf. The *vhl^{-/-}* mutant shows enlarged aortic diameter at the same embryonic stage however inhibition or donation of NO does not alter the aortic diameter significantly. All graphs mean \pm SEM; 2-way ANOVA; all groups ns; n=7.

5.2.3.3 Total embryo NO signalling using the fluorophore DAFF-FM

In addition to the effects of NO signalling on vessel size, quantification of NO signalling directly has been previously demonstrated directly using a fluorophore activated by the presence of NO (Lepiller et al. 2007). Given my difficulty in replicating published effects of NO manipulation in the developing zebrafish I wanted to see if either L-NAME or SNP were able to alter embryo levels of NO. I compared the total level of NO signalling in the *vhl*^{-/-} mutant and wild type, and looked at the effect of L-NAME and SNP on the total NO signal in both of these genotypes. Figure 5.13 shows a whole mount photomicrograph of overlaid bright field and fluorescence images of DAFF-FM, which labels NO signalling and its distribution in the embryo in both the wild type and *vhl*^{-/-} mutant and in both cases incubated in the NO synthase inhibitor L-NAME or the NO donor SNP.

The levels and distribution of fluorescent signal in the embryos in fig 5.13 shows little difference in the amount or distribution of the NO signal in wild type and *vhl*^{-/-} mutant embryos. The tissue distribution of the NO signal at this developmental stage is consistent with published data (Lepiller et al. 2007), indicating high levels of signal in the bulbus arteriosus, notochord and caudal fin edge. Figure 5.14 shows there is no change in the DAFF-FM signal in the L-NAME treated embryos, either wild type or *vhl*^{-/-} mutant. The NO donor SNP incubation resulted in a significant increase in NO derived DAFF-FM fluorescent signal of about 2-fold in the wild type and of about 1.6 fold in the *vhl*^{-/-} mutants. Interestingly there was a smaller increase in the level of NO in the *vhl*^{-/-} mutants compared with the wild type embryos, however there was no difference between these groups when treated with L-NAME.

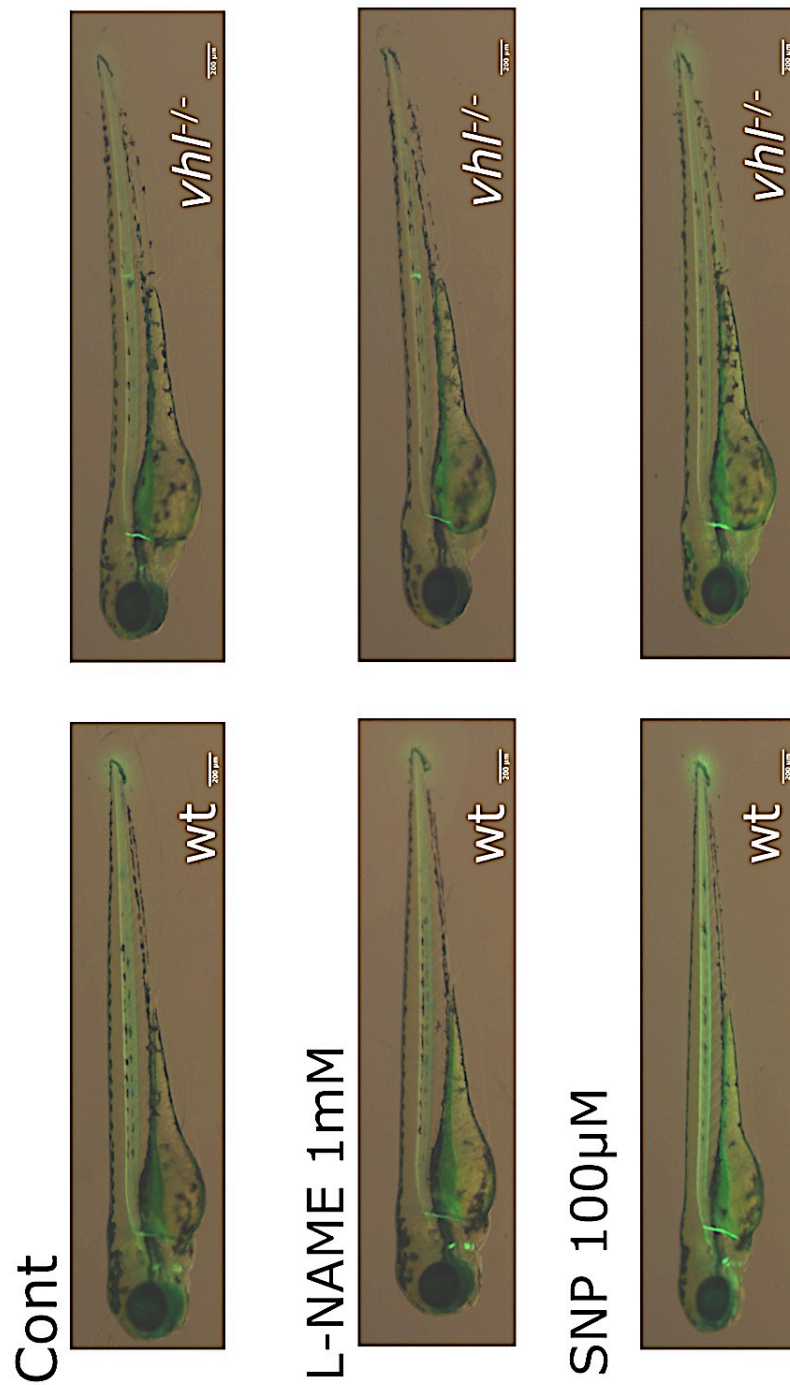


Figure 5.13 DAFF-FM fluorescence in 4 dpf wildtype and *vhl*^{-/-} mutant embryos incubated with L-NAME or SNP.

Fluorescence and bright field overlay images of DAFF-FM, which fluoresces on contact with NO. There is increased fluorescence in the embryos treated with SNP (100 mM) but no reduction in the embryos treated with L-NAME (1 mM) compared to controls. There is no difference in wt and *vhl*^{-/-} DAFF-FM signal.

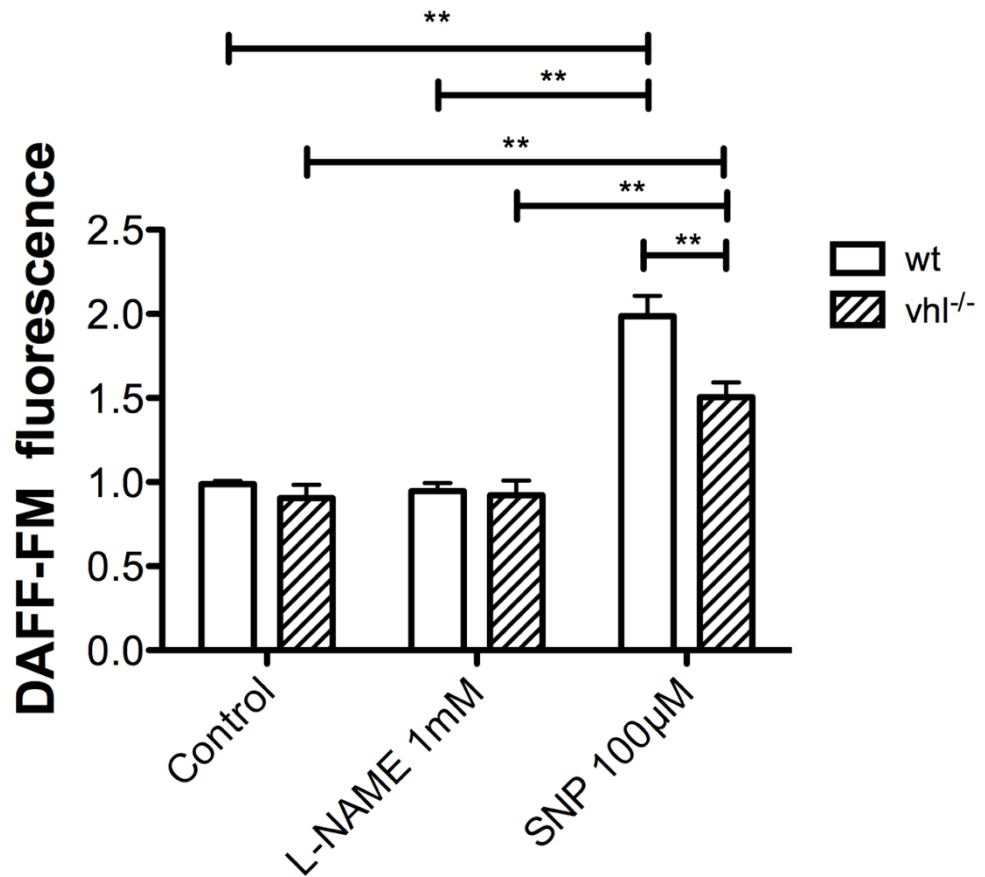


Figure 5.14 Quantification of whole mount DAFF-FM fluorescence at 4 dpf in wt and *vhl*^{-/-} mutant embryos treated with SNP or L-NAME.

Whole mount fluorescence in 4 dpf wt or *vhl*^{-/-} embryos adjusted to wt control levels. There is no effect on the NO fluorescent reporter after treatment with L-NAME (1 mM) however there is increased fluorescence in the groups treated with SNP (100 µM) in both wt and *vhl*^{-/-} background. All graphs mean ± SEM; 2-way ANOVA; ** = p<0.01; n=5.

5.3 Discussion

In this chapter I investigated two signalling pathways of particular relevance to endothelial behaviour; Notch signalling and NO signalling. Both have been shown to regulate angiogenesis, vasculogenesis and in the case of NO, endothelial responses to flow (Phng & Gerhardt 2009; Fritsche et al. 2012; Sessa 2009).

To study the effects of flow on the notch signalling pathway I used a zebrafish transgenic reporter line of notch activity *Tg(CSL:venus)*. This allowed me to use genetic knockdown and pharmacological manipulation of the heart to regulate blood flow. Blocking onset of circulation in the developing zebrafish by knockdown of *troponin t₂* resulted in clear up regulation of notch signalling in the aortic endothelium. The same increase was seen when the circulation was stopped at 36hpf, using BDM. This indicates that the increases in notch observed in the endothelium of the transgenic are as a direct result of changes in flow resulting in increased expression of the CSL transcriptional apparatus. The observation of suppression of notch signalling in endothelial cells by the absence of blood flow has not been previously described.

The transgenic used for these experiments acts as a notch-signalling reporter producing fluorescent venus expression as a direct result of activation of the DNA binding site of the notch transcriptional apparatus CSL. I wanted to confirm this increase in notch dependent fluorescence due to changes in endothelial notch signalling not via an indirect mechanism altering binding of CSL. Clarification of this was important as a number of notch receptor and CSL-independent signalling pathways have now been described in the literature (Bray 2006; Martinez Arias et al. 2002). The increases in CSL seen in the transgenic were blocked by incubation with the DAPT indicating that the increase in the notch transcriptional activator CSL is as a result of increased intracellular NICD signalling which may be derived from changes in ligand-receptor interactions although the possibility of an indirect activation of CSL transcriptional activity has not been entirely excluded.

Having established the increase in notch signalling in endothelium in response to flow I wanted to look at the individual signalling components to identify the component or components of the pathway which were differentially regulated by changes in endothelial detection of circulatory flow. I looked at the expression of mRNA in the trunk of the developing embryo using RT-qPCR. One limitation of this technique is that I was unable to isolate only endothelial cells from the zebrafish to assess changes in transcription. I used trunk tissue which has the advantage of removing brain tissue transcripts from the assay, as this is known to contain large amounts of active notch signalling during development (Cau & Blader 2009). Also by isolating only the trunk tissue we are only looking at the tissue specific regulation of angiogenesis in the vessels studied. This also minimised the effect of other vascular tissues already shown to regulate angiogenesis in response to haemodynamic signals in particular the cerebral vessels (Bussmann et al. 2011).

Despite the use of this mixed tissue in the RNA extraction process I was able to show that *dll4*, a notch ligand which has been previously shown to influence endothelial angiogenesis in the developmental setting (Siekman & Lawson 2007b; Leslie et al. 2007), is differentially regulated at a transcriptional level by flow. RT-qPCR showed a significant up regulation of the *dll4* transcript in the absence of circulatory flow by *troponin t₂* genetic knockdown. Subsequently I demonstrated that this differential regulation seen in trunk tissue is restricted to the endothelium between 48 hpf and 72 hpf. The levels of expression change in *dll4* are consistent with the changes in *cxcr4a* which has been previously shown to differentially regulated in the absence of circulatory flow (Packham et al. 2009).

Many of the target genes used for my RT-qPCR did not demonstrate any differential expression at either 48 hpf or 72 hpf, which would have provided additional evidence that the notch pathway is strongly implicated in the regulation of flow dependent endothelial regulation. This may be due to the selection of qPCR genes of interest. This was based on previously published notch receptors, ligands and transcriptional targets and the validation of suitable primer probes. This process is time consuming and inherently biased, thus the

lack of notch target hits may just reflect the fact I have not selected the correct gene targets for assay. One possible technique with which to address this experimental difficulty may be to use a microarray technique on isolated endothelium, which would provide an unbiased approach to this problem. However, isolation of endothelium from the in vivo model is likely to alter transcriptional profiles and cultured endothelium may not demonstrate the in vivo sensitivity to notch signalling I have described.

Notch signalling has been shown to be regulated on various levels and is very dependent on the signalling context, timing and cell type in the production of its signalling output (Andersson et al. 2011; Bray 2006). This in combination with the large number of notch signalling ligands, receptors, co-factors and target genes makes this a difficult and time consuming undertaking. However there are some genes on which any future study would need to focus. The notch ligand *jagged1* has been shown to have opposing effects on angiogenesis to *dll4* (Benedito et al. 2009). Unfortunately I was unable to optimise this particular primer set for adequate amplification of mRNA transcripts in my extracted RNA. Another potential notch target gene is Enhancer of split. This may be differentially regulated by flow, which would add to the evidence for the role of *dll4* in activation of the canonical notch-signalling pathway in response to flow.

The increase in *dll4* expression in response to loss of flow is attractive as a mechanism for the regulation of hypoxic signalling dependent angiogenesis in the *vh1^{-/-}* mutant. *dll4* is known to act as a repressor of angiogenesis in the vascular development of the zebrafish (Leslie et al. 2007). Clearly if this is up regulated in response to reduced flow this may be a potential mechanism by which *vh1^{-/-}* mutant angiogenesis is repressed in the absence of flow.

Despite extensive testing I have been unable to rescue the *vh1^{-/-}* mutant phenotype by down regulation of notch signalling in the absence of flow. To approach this I have used either troponin gene knockdown or BDM circulatory arrest by which to block flow in the mutant. In combination with either DAPT or *dll4* gene knockdown by morpholino to block endothelial Notch signalling. Despite altering the timing and doses of co-injection of morpholino and the

exposure to BDM I have failed to show rescue of the *vhl*^{-/-} mutant vessel phenotype. Isolated knockdown of *dll4* or troponin t₂ does not result in the same level of toxicity that was seen in the co-injection group or dual treatment group suggesting that the combination of knockdown results in excessive mortality, which requires further investigation.

One experimental system which may be able to address this difficulty would be a Cre/lox transgenic which by using tamoxifen induction of Cre recombination would allow for a endothelial restricted knockdown of the *dll4* transcript and control over the timing of this knockdown, tools for the production of such a transgenic are now established (Mosimann & Zon 2011). This would minimise any off target toxicity on the other developmental processes in my zebrafish developmental model, which may be the cause for the high mortality I have experienced in my rescue experiments to date. This technique has been effectively used in the mouse retinal model of angiogenesis to elucidate the balance of *dll4* and *jagged1* on angiogenesis (Benedito et al. 2009). Unfortunately such a complex transgenic system was outside the scope and timescale of this project.

The experiments performed to identify a role for NO signalling in the production of the flow sensitive angiogenesis in the *vhl*^{-/-} mutant were negative. I was not able to demonstrate any change in the angiogenic phenotype of the *vhl*^{-/-} mutant after inhibition of the NO synthase enzyme. However it is difficult to be certain of this as a true negative experimental result due to the absence of physiological effect of the compound L-NAME at similar doses and exposures to previously published positive studies into manipulation of NO in the developing zebrafish embryo. These studies showed aortic constriction and reduction in erythrocyte flow after treatment with L-NAME and reduced migration of haematopoietic stem cells (North et al. 2009; Fritsche et al. 2012).

Given the large body of published literature on the effects of NO synthase inhibition on blood vessels in the zebrafish model it would seem likely that the lack of effect of L-NAME in my experiments is due to a problem with the experimental system. The most likely explanation is a problem with the

compound or its preparation however attempts to resolve this by using new preparations resulted in the same negative results. It is also possible that differences in the E3 media used in my experimental setup led to the precipitation or inhibition of the L-NAME causing the discrepancy in my results and those published by other groups. Alternative NO synthase inhibitors exist however these are thought to have more specific effects on the various NOS subtypes which would be expected to reduce the effect of these compounds e.g. L-NMMA compared to L-NAME (Alderton et al. 2001). I was unable during this project to assess the reasons for these negative results. Further experiments looking at NO synthase inhibition and the effect on hypoxia-stimulated angiogenesis would focus on the lack of activity of L-NAME in our experimental setup. Simple controls like assessment of the pH of the media, rate of degradation of the compound and penetration of the embryo by the compound would all have to be assessed before the negative result could be confirmed that blocking NO does not inhibit the formation of *vh1*^{-/-} dependent angiogenesis.

In addition a more thorough study of the role of NO signalling in hypoxia signalled angiogenesis would need to look at the expression patterns and activity of the NOS orthologues in the zebrafish and there overlapping effects (Lepiller et al. 2009) in comparison with the established effects of mammalian eNOS, iNOS and nNOS. This would also need to be assessed in the vessels of the *vh1*^{-/-} mutant. Established MO have been published against nNOS have been described and the developing technique of TALEN mutagenesis may allow stable mutants in the NOS family with which to further study this interaction of flow and *vh1*^{-/-} dependent angiogenesis.

5.3.1 Summary

I have identified a flow dependent suppression of endothelial *dll4* expression, which in the absence of blood flow leads to increased endothelial notch signalling. This observation suggests that endothelial cells require a flow signal which is permissive to angiogenesis mediated by suppression of notch signalling in the presence of a local VEGF gradient, stimulated by hypoxic signalling. This may be expected to affect the angiogenic phenotype of the *vh1*^{-/-}

mutant, which I have previously demonstrated is flow dependent. Unfortunately I have been unable to show that by blocking *dll4* dependent notch signalling I can rescue the loss of *vh1*^{-/-} vessel phenotype seen in the absence of flow. However the presence of an endothelial flow stimulus, which is capable of modulating endothelial behaviour via notch signalling, is a novel observation and may lead to a better understanding of angiogenic regulation.

If angiogenesis driven by hypoxia has sensitivity to flow, mediated by notch signalling this presents novel mechanisms which could manipulate pathological angiogenesis. In the field of oncology the regulation of angiogenesis is a key target for therapeutics to arrest the metastatic spread of cancers. The success of the VEGF inhibitors in oncology has not been as successful as initially hoped. If it were possible to locally regulate flow at the site of malignancy either pharmacologically or physically with surgical intervention this would be a potential adjunct to established anti-angiogenic therapies, without the prolonged process of novel drug discovery. The additional target of notch signalling for regulation of pathological angiogenesis is another potentially attractive translational finding as the gamma-secretase inhibitors have already been used in clinical trials, (Purow 2012) providing established tools to take these findings forward to therapeutic intervention in human disease.

Chapter 6 General discussion

The *vhl*^{-/-} mutant zebrafish has the unique advantage of enabling the study of both developmental and hypoxic signalling driven angiogenesis concurrently, *in vivo*. I have characterised in detail the aberrant vessel development in the trunk of the mutant in the early part of this study. The angiogenesis stimulated by the *vhl*^{-/-} mutation demonstrates conserved features of endothelial behaviour and signalling, which have been described in both cell culture and other higher mammalian models. My observations indicate that the vessel growth I have described acts as a reliable model of angiogenesis with which to investigate the role of flow and its endothelial signalling effects. Establishing this conservation of behaviour and signalling is important to the translation of any potential therapeutic observations into other models and potentially man.

During the characterisation of the *vhl*^{-/-} induced angiogenesis I observed that aberrant angiogenesis follows a stereotyped pattern, despite the apparent chaotic vessel appearance compared with the controls. The earliest changes are seen in the dorsum of the embryo, then over time additional vessels and sprouts emerge more proximally closer to the aorta. Although I have described endothelial cell number changes in the aorta it is noteworthy that no additional angiogenic sprouts were seen, suggesting that the factors determining development of the paired intersegmental vessels that run between each somite are not affected by increased hypoxic signalling. It is possible that the process of vasculogenesis and the other roles of the aorta in development (e.g. haematopoietic stem cell production) may protect it from additional angiogenic sprouting driven by hypoxic signalling. Alternatively the early resistance of this vessel to sprouting behaviour may be due to changes in timing of as yet unknown endothelial signals, or a contribution of maternal RNA that prevents hypoxic signalling from occurring until after these vessel sprouts are specified.

To speculate on the mechanism for this stereotyped sprouting pattern and its distribution, it is possible that there is overlap of the initial developmental signals, which pattern the vasculature into its stereotyped form, including potentially the plexins-semaphorins family and their downstream targets (Torres-Vázquez et al. 2004; Zygmunt et al. 2011). These molecules may be at higher concentrations in proximity to the aorta in order to tightly limit the

angiogenic sprouts to the somite borders. Or it is possible these signals are at a lower concentration along the dorsum of the embryo or that the timing of expression declines as the levels of hypoxic signals accumulate. Further study into how the up-regulated hypoxic signals are able to overcome these developmental pathways and produce the extensive angiogenic networks seen in the mutant would be necessary to understand the differential regulation of these processes. The ability to target angiogenesis to a particular vascular bed or site would have particular relevance in overcoming the occlusive vascular diseases like stroke and heart disease.

During this study I was unable to spend sufficient time to fully address the role of endothelial specific hypoxic signalling in initiation of angiogenesis in the *vh1* mutant. Clearly this would be of great interest in terms of the initiation and maintenance of the angiogenesis seen in the *vh1*^{-/-} mutant. The mutant has clear upregulation of hypoxic signalling (Van Rooijen et al. 2009) throughout its tissues, one consequences of this being the aberrant vessel development which I have described. The transgenic that I generated using the modified GAL4:UAS construct to increase HIF1 signalling in only endothelial cells *Tg(fli1:GFF;UAS:kaede, UAS; da-hif-1ab-IRES-GFP)*²¹⁸ showed no increase in endothelial angiogenic behaviour (Appendix 1). This would be consistent with the established literature; the autocrine expression and secretion of VEGF is felt to maintain endothelium in a state of quiescence (Warren & Iruela-Arispe 2010). Only when local gradients of this growth factor (VEGF) are established in the surrounding tissues is there adequate stimulus for angiogenesis. Unfortunately my experiments were inadequate to make categorical conclusions about the effect of endothelial up regulation of hypoxic signalling and angiogenesis. However this system of targeted expression of angiogenic ligands using the modified yeast GAL4:UAS system in the zebrafish would be an powerful tool with which to study this in the future.

An additional question arising from the characterisation of the *vh1*^{-/-} mutant vasculature relates to the site of endothelial migration, proliferation and potentially apoptosis. Previous literature has shown the dynamic reorganisation of the ISV and DLAV in terms of the individual endothelial cells (Blum et al.

2008) and the role of arterial specified cells in the formation of the DLAV (Zygmunt et al. 2012). It is possible that this particular vessel bed in the developing embryo has a particular sensitivity to the accumulation of hypoxic signals resulting in the earliest vessel changes appearing in this region of vasculature before more proximal vessels. Using a nuclear-labelled vascular reporter in conjunction with a different endothelial membrane reporter in the same transgenic line would enable detailed time-lapse imaging to track the migration and nuclear division *in vivo*. The transgenic line Tg(*flk1:eGFP-NLS;kdr-I;HRAS-mCherry*) is already established in our laboratory but due to the amount of time required to develop and perform these experiments I have not been able to address these questions in this study. Clearly the differential regulation of the developmental and pathological angiogenesis seen in this zebrafish mutant embryo is an important to understanding how to target angiogenic vessels with a view to therapeutic manipulation.

The identification of flow sensitivity in the aberrant angiogenesis of the *vhl*^{-/-} mutant is potentially the most exciting observation from this project. I have demonstrated that removing flow in the developing *vhl*^{-/-} mutant embryo, prior to and shortly after the onset of circulation blocks the formation of new vessels and the expansion in endothelial cell number. These experiments demonstrated a differential sensitivity to flow of developmental angiogenesis required for formation of the ISV and DLAV when compared to hypoxic signalling-stimulated angiogenesis. I limited my study to the early development of these vessels however it is not clear if the aberrant angiogenesis seen in the mutant demonstrates flow sensitivities at a later stage, or if this process inhibits only the initiation of new vessel sprouts. It is possible that removal of flow at a later developmental stage may lead to regression of *vhl*^{-/-} induced angiogenesis. Recent developments in morpholino technology mean that there are now photosensitive morpholino oligonucleotides, which could be used to knockdown an essential cardiac protein like troponin, but at a later time point to enable the study of the timing effects of removal of flow on hypoxic signalling induced angiogenesis.

One particular area not addressed in this study is the mechanism by which the endothelium is able to transduce the flow signal. There is no consensus on the mechanism for flow transduction in the endothelial cell in the literature, however transcription factors like *klf2a* have been shown to be differentially regulated by alterations in haemodynamic flow (Lee et al. 2006), which result in alterations in *vegfaa* sensitivity in limited endothelial territories in the developing zebrafish (Nicoli et al. 2010). A detailed study of the mechanism of endothelial flow transduction was outside the scope of this study. Given the data available on developmental flow sensitivity (Nicoli et al. 2010) in the zebrafish it would be interesting to look at the effects of knockdown of *klf2a* and miRNA-126 in the *vhl*^{-/-} mutant. It is not necessarily the case that this regulatory pathway is preserved in the aberrant angiogenic endothelium particularly given the differential sensitivity to flow of developmental and pathological angiogenesis that I have demonstrated.

Further study is also required to address the issue of what threshold of flow is required for hypoxic signalling mediated angiogenesis. In vessels of the size studied in the *vhl*^{-/-} mutant the lumen of the ISV and DLAV is only the size of a single red cell; as a result much of the physical force on the endothelium at this developmental stage is derived from physical deformation of the endothelium. This is of particular interest in the *vhl*^{-/-} mutant due to its increased red cell mass as a consequence of increased *epo* expression (Van Rooijen et al. 2009). It is notable that the onset of angiogenesis in the mutant is delayed until 2-3dpf, the time when expression levels of both *vegfa* and *epo* are increased. If additional studies were to implicate a role for erythrocyte density in the response of endothelium to flow this would be of significant translational interest. As established clinical tools are established to manipulate red cell number within modern haematology practice; including venesection and drugs like hydroxyurea to reduce red cell number and also medications to activate bone marrow production of red cells. It is tempting to suggest that such therapies might be useful as potential adjunctive therapies to influence angiogenic behaviour in diseases dependent on angiogenesis like cancer and macular degeneration

There remain questions about how manipulation of *dll4* and subsequently notch signalling in the endothelial cell alters angiogenic behaviour in response to flow. My experiments have shown that the notch ligand *dll4* is regulated by flow in the endothelium of the developing zebrafish (summarised in Figure 6.1), it is not clear from my experiments how the alteration in this ligand is transduced by the endothelial cell. There is data indicating that the microRNA-30 family are involved in the post-transcriptional regulation of *dll4* in zebrafish (Bridge et al. 2012). Clearly examination of the expression of these regulatory RNAs and the response to flow would be future experiments to clarify the signalling pathway activated by changes in flow sensing by endothelial cells. Alternatively screening a number of mirRNAs may identify novel regulators of endothelial response to flow in these cells, given the increasing literature indicating their role in endothelial flow transduction and response (Nicoli et al. 2010; Bridge et al. 2012).

I was unable to show that manipulation of *dll4* in the *vhl*^{-/-} mutant without flow is able to rescue the loss of angiogenic vessels despite various approaches.. This finding would link the flow sensitive aberrant angiogenesis seen in the mutant with the alteration of *dll4* in endothelial cells in response to flow. An alternative approach to this important question would be the use of a system where expression of *dll4* could be regulated, for example a Cre/Lox system. Using such a system, where the levels of *dll4* expression could be manipulated in only endothelial cells and at a specific time point, minimising any off target toxicity from notch signalling alterations in the presence of the background *vhl* mutation may be a solution to the experimental difficulties to date. Alternatively these experiments could be performed in established mouse retinal models of angiogenesis, where the molecular machinery and assays are already established (Benedito et al. 2009).

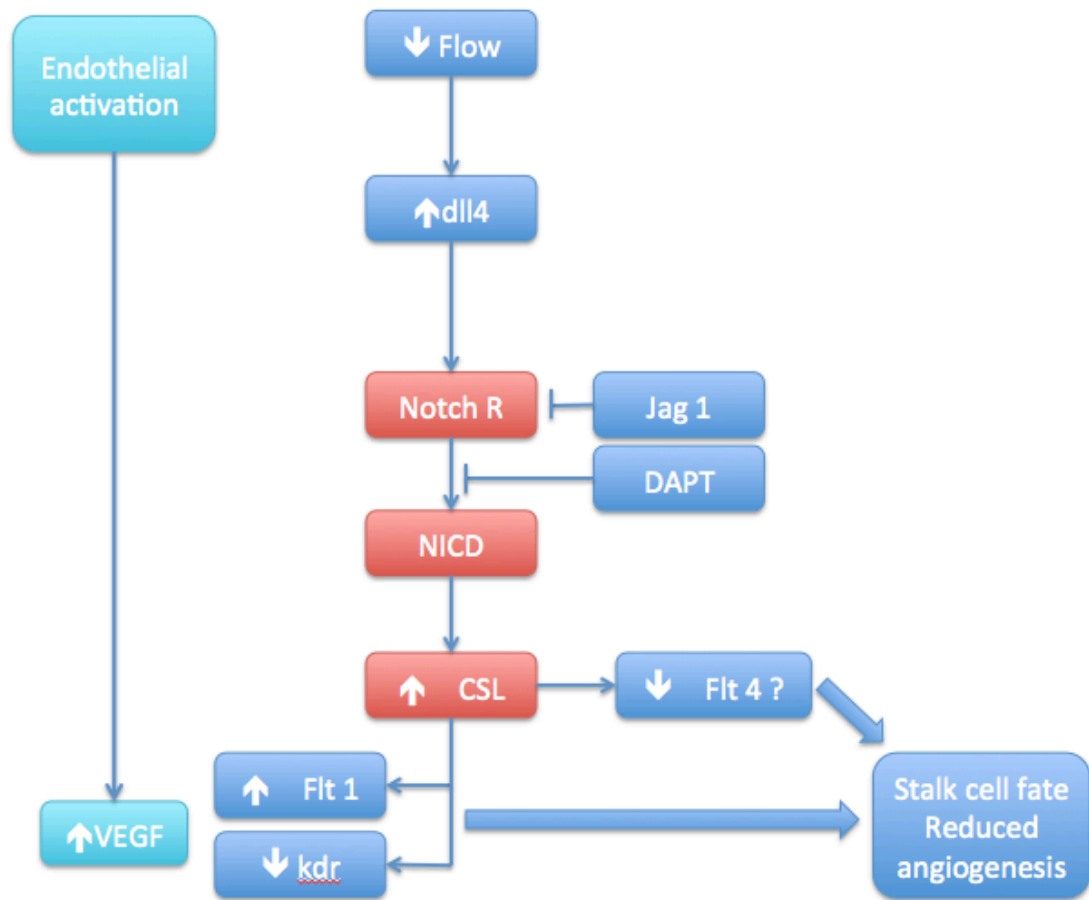


Figure 6.1. Summary of the role of Notch signalling and *dll4* on the angiogenic phenotype in the presence of endothelial activation.

Summary diagram indicating the potential role of Notch signalling and the ligand *dll4* on established angiogenic growth factors like *vegfaa / ab* and the receptor population. In the *vhl^{-/-}* mutant the endothelial activation is a result of up-regulated HIF-1 α signalling which increase levels of *vegfaa / ab* despite the increased expression of these vascular growth factors the absence of endothelial flow stimulus blocks the formation of new vessels via Notch signalling.

A potential limitation of my study is that all of the experiments have been performed in zebrafish. Although the advantages of this model have enabled the detailed assessment of the angiogenic process *in vivo* and in addition to the ease of manipulation of genes of interest, translating the experiments to other models would indicate that the regulation of notch signalling by endothelial *dll4* expression in response to flow is a conserved signalling pathway. This could be achieved using the mouse retinal model or using cultured human umbilical vein cells (HUVECS) which could be exposed to varying levels of flow in the presence of up regulated HIF1 signalling to look at the effect on notch signalling assayed by RT-qPCR.

Angiogenesis is a critical process in both the development of a complex organism and the initiation and maintenance of disease. There are common signaling processes involved in both pathology and development; in this study I have used an embryonic zebrafish model, which enables the study of both processes. Pathological angiogenesis driven by hypoxia plays a critical role in the development of cancer and understanding the behaviour of endothelial cells in this process may enhance our ability to influence this process therapeutically. Initial attempts to regulate tumour growth by halting angiogenesis have yielded somewhat disappointing results clinically (Potente et al. 2011), any additional mechanisms, which may enhance the effects of established clinical anti-VEGF agents could have significant therapeutic impact. Also any novel insights into the regulation of angiogenesis may also have additional benefits outside the cancer field. The ability to target vessel growth might enable initiation of new vessels to circumnavigate occlusion or to perfuse hypoxic tissue. This is of particular relevance in a number of human diseases like stroke and heart disease, pathological consequences of vessel blockage and damage.

To conclude, I have discovered novel interactions between blood flow, hypoxic-signalling regulated angiogenesis, and Notch signalling. Further work is likely to reveal much more about the complex regulation of blood vessel formation in development and disease.

Chapter 7 Appendix 1

7.1 Endothelial cell constitutive hypoxic signalling and the initiation of an angiogenic phenotype

The *Tg(UAS:da-hif-1ab-IRES-GFP)ⁱ²¹⁸* line was crossed with the *Tg(fli1:GFF;UAS:kaede)*, positive double transgenics were identified by endothelial KAEDE expression and expression of GFP in the eye to identify carriers of the da-hif construct. These embryos were compared to GFP negative fish, which lack the dominant active HIF construct. In three separate crosses no angiogenic phenotype was identified in the double transgenic by 4 dpf (Figure 7.1). We considered that endothelial hypoxia may not give as dramatic a phenotype as that seen with the *vhl⁻* mutant line but further observations at 7dpf revealed no morphological changes in the endothelium.

To confirm that there was up regulated hypoxia signalling in the endothelium of the double mutants we looked at expression patterns in the double transgenics of a validated hypoxia signalling transcriptional target propyl-hydroxylase 3 (PHD3) and KAEDE fluorescent protein expression. It was hoped that a clear vascular expression pattern of both of these by whole mount in situ hybridisation would confirm that the expression of the endothelial promoter and effective GAL4 and UAS expression in the double transgenics. Figure 7.2 shows the clear expression of the *kaede* mRNA in a classical vascular distribution both in the head and trunk of the selected double transgenic embryo. However there is no vascular distribution to the PHD3 mRNA expression, although there is some expression in the head but this does not appear to be clear endothelial distribution expected.

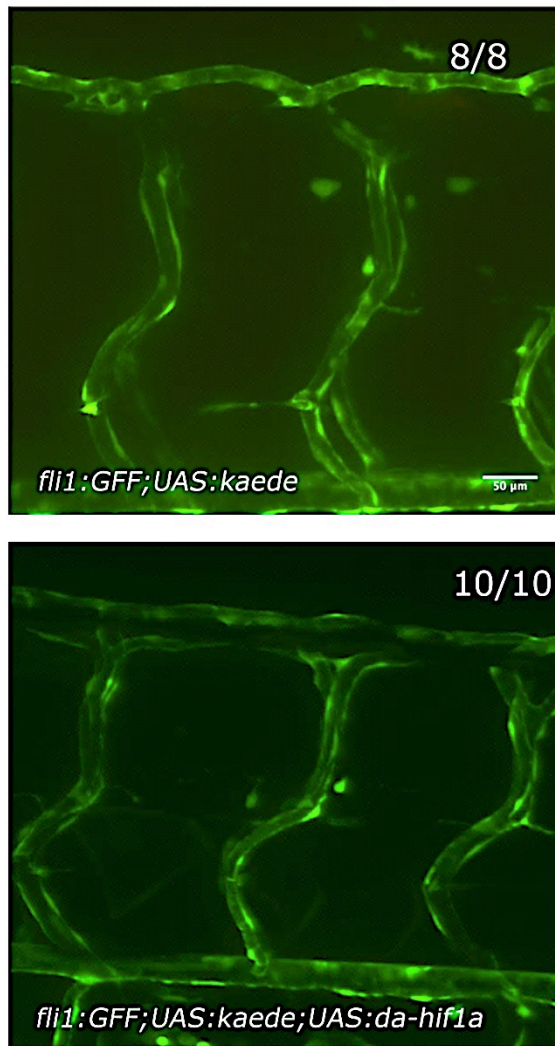


Figure 7.1. Effect of up regulated HIF-1 α signalling in the endothelium of 3 dpf embryo labelled with *Tg(fli:GFF;UAS:kaede)*

Top panel shows the normal vascular pattern seen at 72 hpf with paired ISV and the DLAV remodelling into a single longitudinal vessel. Lower panel shows representative photomicrograph of embryo selected for endothelial *kaede* expression and a constitutively active mutated HIF construct both driven by the *fli1* promoter. All embryos showed the same vessel morphology in both groups

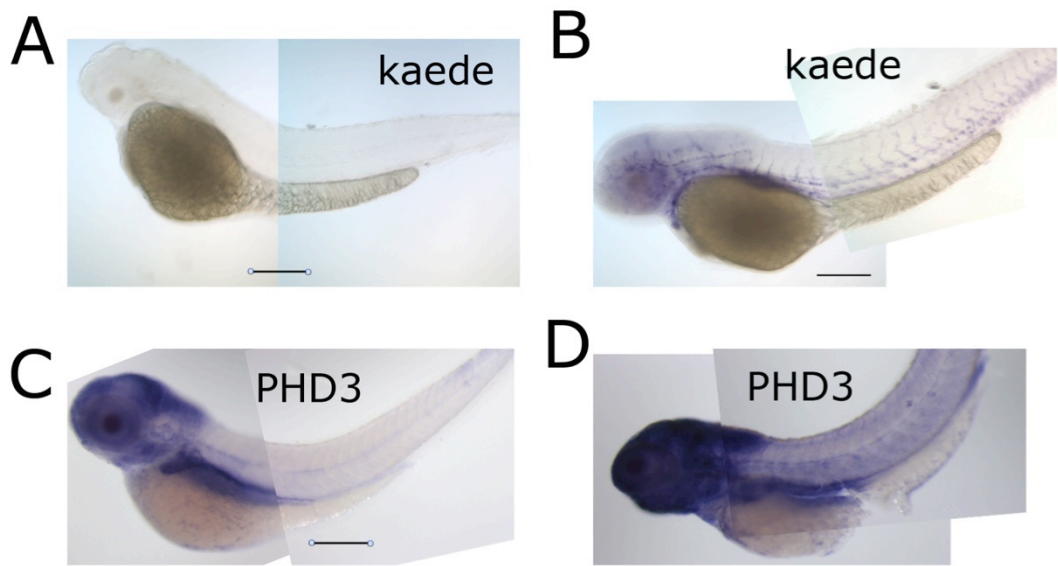


Figure 7.2. WISH expression of *kaede* and *phd3* genes in double transgenics and controls to confirm expression of the *fli1*:GFF promoter and the downstream UAS:*kaede* and UAS:*da-hif-1ab*-IRES-GFP constructs

A. Expression of *kaede* detected by WISH antisense probe at 72 hpf in *Tg(fli1:GFF;UAS: da-hif-1ab-IRES-GFP)^{j218}* embryos, there is no expression as this a promoted transgene with no endogenous expression **B.** Expression of *kaede* in double fluorescence selected *Tg(fli1:GFF;UAS:kaede, UAS; da-hif-1ab-IRES-GFP)* showing staining in an endothelial distribution **C.** Expression of PHD3 by WISH in 72 hpf embryos selected for *Tg(fli1:GFF;UAS:kaede)* showing some endogenous expression in the head **D.** Expression of PHD3 in double transgenic fluorescence selected *Tg(fli1:GFF;UAS:kaede,UAS; da-hif-1ab-IRES-GFP)* with increased expression in the head above the endogenous levels and in the somites but with no endothelial expression pattern seen in the trunk. Scale bar, 400µm. Although there is increased staining in the head in **D.** this is likely to be due to trapping of the stain and a result of over exposure. To

ensure that no endothelial stain is seen in the trunk vessels the development time is left longer, as the tissue of the head is better permeabilised by the process then increased variability in head staining can be seen despite the same process of treatment in both **C & D**. Despite the differences in stain the distribution suggests that there is no specific endothelial increase in *phd3* expression in the trunk vasculature.

Chapter 8 References

- Adams, R.H. & Alitalo, K., 2007. Molecular regulation of angiogenesis and lymphangiogenesis. *Nature reviews. Molecular cell biology*, 8(6), pp.464–478.
- Akitake, C.M. et al., 2011. Transgenerational analysis of transcriptional silencing in zebrafish. *Developmental biology*, 352(2), pp.191–201.
- Alderton, W.K., Cooper, C.E. & Knowles, R.G., 2001. Nitric oxide synthases: structure, function and inhibition. *The Biochemical journal*, 357(Pt 3), pp.593–615.
- Andersson, E.R., Sandberg, R. & Lendahl, U., 2011. Notch signaling: simplicity in design, versatility in function. *Development*, 138(17), pp.3593–3612.
- Armer, H.E.J. et al., 2009. Imaging transient blood vessel fusion events in zebrafish by correlative volume electron microscopy. *PloS one*, 4(11), p.e7716.
- Arroyo, A.G. & Iruela-Arispe, M.L., 2010. Extracellular matrix, inflammation, and the angiogenic response. *Cardiovascular research*, 86(2), pp.226–235.
- Artavanis-Tsakonas, S., Rand, M.D. & Lake, R.J., 1999. Notch signaling: cell fate control and signal integration in development. *Science (New York, N.Y.)*, 284(5415), pp.770–776.
- Asakawa, K. et al., 2008. Genetic dissection of neural circuits by Tol2 transposon-mediated Gal4 gene and enhancer trapping in zebrafish. *Proceedings of the National Academy of Sciences of the United States of America*, 105(4), pp.1255–1260.
- Bedell, V.M. et al., 2012. In vivo genome editing using a high-efficiency TALEN system. *Nature*, 491(7422), pp.114–118.
- Benedito, R. et al., 2009. The Notch Ligands Dll4 and Jagged1 Have Opposing Effects on Angiogenesis. *Cell*, 137(6), pp.1124–1135.
- Bill, B.R. et al., 2009. A primer for morpholino use in zebrafish. *Zebrafish*, 6(1), pp.69–77.
- Blum, Y. et al., 2008. Complex cell rearrangements during intersegmental vessel sprouting and vessel fusion in the zebrafish embryo. *Developmental biology*, 316(2), pp.312–322.
- Boon, R.A. & Horrevoets, A.J.G., 2009. Key transcriptional regulators of the vasoprotective effects of shear stress. *Hämostaseologie*, 29(1), pp.39–40–41–3.
- Bray, S.J., 2006. Notch signalling: a simple pathway becomes complex. *Nature reviews. Molecular cell biology*, 7(9), pp.678–689.
- Bridge, G. et al., 2012. The microRNA-30 family targets DLL4 to modulate

- endothelial cell behavior during angiogenesis. *Blood*, 120(25), pp.5063–5072.
- Brown, L.A. et al., 2000. Insights into early vasculogenesis revealed by expression of the ETS-domain transcription factor Fli-1 in wild-type and mutant zebrafish embryos. *Mechanisms of development*, 90(2), pp.237–252.
- Bruick, R.K. & McKnight, S.L., 2001. A conserved family of prolyl-4-hydroxylases that modify HIF. *Science (New York, N.Y.)*, 294(5545), pp.1337–1340.
- Bussmann, J. et al., 2008. Zebrafish VEGF receptors: a guideline to nomenclature. *PLoS genetics*, 4(5), p.e1000064.
- Bussmann, J., Wolfe, S.A. & Siekmann, A.F., 2011. Arterial-venous network formation during brain vascularization involves hemodynamic regulation of chemokine signaling. *Development*, 138(9), pp.1717–1726.
- Carmeliet, P., 2000. Mechanisms of angiogenesis and arteriogenesis. *Nature medicine*, 6(4), pp.389–395.
- Carmeliet, P. & Jain, R.K., 2011. Molecular mechanisms and clinical applications of angiogenesis. *Nature*, 473(7347), pp.298–307.
- Cau, E. & Blader, P., 2009. Notch activity in the nervous system: to switch or not switch? *Neural development*, 4, p.36.
- Chico, T.J.A., Ingham, P.W. & Crossman, D.C., 2008. Modeling cardiovascular disease in the zebrafish. *Trends in cardiovascular medicine*, 18(4), pp.150–155.
- Childs, S. et al., 2002. Patterning of angiogenesis in the zebrafish embryo. *Development*, 129(4), pp.973–982.
- D'Souza, B., Meloty-Kapella, L. & Weinmaster, G., 2010. Canonical and non-canonical Notch ligands. *Current topics in developmental biology*, 92, pp.73–129.
- Davies, P.F., 2008. Hemodynamic shear stress and the endothelium in cardiovascular pathophysiology. *Nature clinical practice Cardiovascular medicine*, 6(1), pp.16–26.
- De Smet, F. et al., 2009. Mechanisms of Vessel Branching: Filopodia on Endothelial Tip Cells Lead the Way. *Arteriosclerosis, Thrombosis, and Vascular Biology*, 29(5), pp.639–649.
- Egginton, S., 2011. In vivo shear stress response. *Biochemical Society Transactions*, 39(6), pp.1633–1638.
- Eisen, J.S. & Smith, J.C., 2008. Controlling morpholino experiments: don't stop

- making antisense. *Development*, 135(10), pp.1735–1743.
- Elks, P.M. et al., 2011. Activation of hypoxia-inducible factor-1 (Hif-1) delays inflammation resolution by reducing neutrophil apoptosis and reverse migration in a zebrafish inflammation model. *Blood*, 118(3), pp.712–722.
- Ellertsdottir, E. et al., 2010. Vascular morphogenesis in the zebrafish embryo. *Developmental biology*, 341(1), pp.56–65.
- Elvidge, G.P. et al., 2006. Concordant regulation of gene expression by hypoxia and 2-oxoglutarate-dependent dioxygenase inhibition: the role of HIF-1 α , HIF-2 α , and other pathways. *The Journal of biological chemistry*, 281(22), pp.15215–15226.
- Firth, J.D. et al., 1994. Oxygen-regulated control elements in the phosphoglycerate kinase 1 and lactate dehydrogenase A genes: similarities with the erythropoietin 3' enhancer. *Proceedings of the National Academy of Sciences of the United States of America*, 91(14), pp.6496–6500.
- Flamme, I., Breier, G. & Risau, W., 1995. Vascular endothelial growth factor (VEGF) and VEGF receptor 2 (flk-1) are expressed during vasculogenesis and vascular differentiation in the quail embryo. *Developmental biology*, 169(2), pp.699–712.
- Fong, G.-H., 2008. Mechanisms of adaptive angiogenesis to tissue hypoxia. *Angiogenesis*, 11(2), pp.121–140.
- Fong, G.-H., 2009. Regulation of angiogenesis by oxygen sensing mechanisms. *Journal of Molecular Medicine*, 87(6), pp.549–560.
- Fong, G.-H. & Takeda, K., 2010. Role and regulation of prolyl hydroxylase domain proteins. *Cell death and differentiation*, 15(4), pp.635–641.
- Fouquet, B. et al., 1997. Vessel patterning in the embryo of the zebrafish: guidance by notochord. *Developmental biology*, 183(1), pp.37–48.
- Fritsche, R., Schwerte, T. & Pelster, B., 2012. Nitric oxide and vascular reactivity in developing zebrafish, *Danio rerio*. *American journal of physiology Regulatory, integrative and comparative physiology*, 279(6), pp.R2200–7.
- Furchgott, R.F. & Zawadzki, J.V., 1980. The obligatory role of endothelial cells in the relaxation of arterial smooth muscle by acetylcholine. *Nature*, 288(5789), pp.373–376.
- Gentile, C., Muise-Helmericks, R.C. & Drake, C.J., 2013. VEGF-mediated phosphorylation of eNOS regulates angioblast and embryonic endothelial cell proliferation. *Developmental biology*, 373(1), pp.163–175.
- Gerhardt, H., 2003. VEGF guides angiogenic sprouting utilizing endothelial tip cell filopodia. *The Journal of Cell Biology*, 161(6), pp.1163–1177.

- Geudens, I. et al., 2010. Role of Delta-like-4/Notch in the Formation and Wiring of the Lymphatic Network in Zebrafish. *Arteriosclerosis, Thrombosis, and Vascular Biology*, 30(9), pp.1695–1702.
- Goldberg, M.A. & Schneider, T.J., 1994. Similarities between the oxygen-sensing mechanisms regulating the expression of vascular endothelial growth factor and erythropoietin. *The Journal of biological chemistry*, 269(6), pp.4355–4359.
- Goldberg, M.A., Gaut, C.C. & Bunn, H.F., 1991. Erythropoietin mRNA levels are governed by both the rate of gene transcription and posttranscriptional events. *Blood*, 77(2), pp.271–277.
- H William Detrich, I., Westerfield, M. & Zon, L., 2011. *The Zebrafish*, Academic Press.
- Haase, V.H., 2005. The VHL tumor suppressor in development and disease: functional studies in mice by conditional gene targeting. *Seminars in Cell & Developmental Biology*, 16(4-5), pp.564–574.
- Hellström, M. et al., 2007. Dll4 signalling through Notch1 regulates formation of tip cells during angiogenesis. *Nature*, 445(7129), pp.776–780.
- Herwig, L. et al., 2011. Distinct Cellular Mechanisms of Blood Vessel Fusion in the Zebrafish Embryo. *Current Biology*, 21(22), pp.1942–1948.
- Hofer, I.E., Adel, den, B. & Daemen, M.J.A.P., 2013. Biomechanical factors as triggers of vascular growth. *Cardiovascular research*, 99(2), pp.276–283.
- Hogan, B.M., Bos, F.L., et al., 2009a. ccbe1 is required for embryonic lymphangiogenesis and venous sprouting. *Nature genetics*, 41(4), pp.396–398.
- Hogan, B.M., Herpers, R., et al., 2009b. Vegfc/Flt4 signalling is suppressed by Dll4 in developing zebrafish intersegmental arteries. *Development*, 136(23), pp.4001–4009.
- Huang, L.E. et al., 1996. Activation of hypoxia-inducible transcription factor depends primarily upon redox-sensitive stabilization of its alpha subunit. *The Journal of biological chemistry*, 271(50), pp.32253–32259.
- Iso, T., 2003. Notch Signaling in Vascular Development. *Arteriosclerosis, Thrombosis, and Vascular Biology*, 23(4), pp.543–553.
- Isogai, S., 2003. Angiogenic network formation in the developing vertebrate trunk. *Development*, 130(21), pp.5281–5290.
- Isogai, S., Horiguchi, M. & Weinstein, B.M., 2001. The vascular anatomy of the developing zebrafish: an atlas of embryonic and early larval development. *Developmental biology*, 230(2), pp.278–301.

- Ivan, M. et al., 2001. HIF α targeted for VHL-mediated destruction by proline hydroxylation: implications for O₂ sensing. *Science (New York, N.Y.)*, 292(5516), pp.464–468.
- Iwai, K. et al., 1999. Identification of the von Hippel-lindau tumor-suppressor protein as part of an active E3 ubiquitin ligase complex. *Proceedings of the National Academy of Sciences of the United States of America*, 96(22), pp.12436–12441.
- Jaakkola, P. et al., 2001. Targeting of HIF- α to the von Hippel-Lindau ubiquitylation complex by O₂-regulated prolyl hydroxylation. *Science (New York, N.Y.)*, 292(5516), pp.468–472.
- Jain, R.K., 2003. Molecular regulation of vessel maturation. *Nature medicine*, 9(6), pp.685–693.
- Jakobsson, L. et al., 2010. Endothelial cells dynamically compete for the tip cell position during angiogenic sprouting. *Nature cell biology*, 12(10), pp.943–953.
- Jou, C.J., Spitzer, K.W. & Tristani-Firouzi, M., 2010. Blebbistatin effectively uncouples the excitation-contraction process in zebrafish embryonic heart. *Cellular physiology and biochemistry : international journal of experimental cellular physiology, biochemistry, and pharmacology*, 25(4-5), pp.419–424.
- Kawakami, K., 2004. Transgenesis and gene trap methods in zebrafish by using the Tol2 transposable element. *Methods in cell biology*, 77, pp.201–222.
- Knaut, H. et al., 2003. A zebrafish homologue of the chemokine receptor Cxcr4 is a germ-cell guidance receptor. *Nature*, 421(6920), pp.279–282.
- Lagendijk, A.K., Moulton, J.D. & Bakkers, J., 2012. Revealing details: whole mount microRNA in situ hybridization protocol for zebrafish embryos and adult tissues. *Biology Open*, 1(6), pp.566–569.
- Lando, D., Peet, D.J., Gorman, J.J., et al., 2002a. FIH-1 is an asparaginyl hydroxylase enzyme that regulates the transcriptional activity of hypoxia-inducible factor. *Genes & Development*, 16(12), pp.1466–1471.
- Lando, D., Peet, D.J., Whelan, D.A., et al., 2002b. Asparagine hydroxylation of the HIF transactivation domain a hypoxic switch. *Science (New York, N.Y.)*, 295(5556), pp.858–861.
- Lauter, G., Söll, I. & Hauptmann, G., 2011. Two-color fluorescent in situ hybridization in the embryonic zebrafish brain using differential detection systems. *BMC developmental biology*, 11, p.43.
- Lawson, N.D. & Weinstein, B.M., 2002. In Vivo Imaging of Embryonic Vascular Development Using Transgenic Zebrafish. *Developmental biology*, 248(2), pp.307–318.

- Lawson, N.D. et al., 2001. Notch signaling is required for arterial-venous differentiation during embryonic vascular development. *Development*, 128(19), pp.3675–3683.
- le Noble, F. et al., 2008. Neural guidance molecules, tip cells, and mechanical factors in vascular development. *Cardiovascular research*, 78(2), pp.232–241.
- Lee, J.S. et al., 2006. Klf2 is an essential regulator of vascular hemodynamic forces in vivo. *Developmental cell*, 11(6), pp.845–857.
- Lepiller, S. et al., 2009. Comparative analysis of zebrafish nos2a and nos2b genes. *Gene*, 445(1-2), pp.58–65.
- Lepiller, S. et al., 2007. Imaging of nitric oxide in a living vertebrate using a diamino-fluorescein probe. *Free radical biology & medicine*, 43(4), pp.619–627.
- Leslie, J.D. et al., 2007. Endothelial signalling by the Notch ligand Delta-like 4 restricts angiogenesis. *Development*, 134(5), pp.839–844.
- Lieschke, G.J. & Currie, P.D., 2007. Animal models of human disease: zebrafish swim into view. *Nature reviews. Genetics*, 8(5), pp.353–367.
- Lisy, K. & Peet, D.J., 2008. Turn me on: regulating HIF transcriptional activity. *Cell death and differentiation*, 15(4), pp.642–649.
- Liu, Y. & Feng, Q., 2012. NOing the heart: role of nitric oxide synthase-3 in heart development. *Differentiation; research in biological diversity*, 84(1), pp.54–61.
- Liu, Y. et al., 1995. Hypoxia regulates vascular endothelial growth factor gene expression in endothelial cells. Identification of a 5' enhancer. *Circulation Research*, 77(3), pp.638–643.
- Martinez Arias, A., Zecchini, V. & Brennan, K., 2002. CSL-independent Notch signalling: a checkpoint in cell fate decisions during development? *Current opinion in genetics & development*, 12(5), pp.524–533.
- Maxwell, P.H. et al., 1999. The tumour suppressor protein VHL targets hypoxia-inducible factors for oxygen-dependent proteolysis. *Nature*, 399(6733), pp.271–275.
- Mélet, F. et al., 1996. Generation of a novel Fli-1 protein by gene targeting leads to a defect in thymus development and a delay in Friend virus-induced erythroleukemia. *Molecular and cellular biology*, 16(6), pp.2708–2718.
- Mole, D.R. et al., 2009. Genome-wide association of hypoxia-inducible factor (HIF)-1alpha and HIF-2alpha DNA binding with expression profiling of hypoxia-inducible transcripts. *The Journal of biological chemistry*, 284(25),

pp.16767–16775.

- Mosimann, C. & Zon, L.I., 2011. Advanced zebrafish transgenesis with Tol2 and application for Cre/lox recombination experiments. *Methods in cell biology*, 104, pp.173–194.
- Mullins, M., 1995. Genetic nomenclature guide. Zebrafish. *Trends in genetics : TIG*, pp.31–32.
- Nagai, T. et al., 2002. A variant of yellow fluorescent protein with fast and efficient maturation for cell-biological applications. *Nature biotechnology*, 20(1), pp.87–90.
- Nasevicius, A. & Ekker, S.C., 2000. Effective targeted gene “knockdown” in zebrafish. *Nature genetics*, 26(2), pp.216–220.
- Nicoli, S. et al., 2010. MicroRNA-mediated integration of haemodynamics and Vegf signalling during angiogenesis. *Nature*, 464(7292), pp.1196–1200.
- North, T.E. et al., 2009. Hematopoietic Stem Cell Development Is Dependent on Blood Flow. *Cell*, 137(4), pp.736–748.
- Nüsslein-Volhard, C. & Dahm, R., 2002. *Zebrafish*, Oxford University Press, USA.
- Packham, I.M. et al., 2009. Microarray profiling reveals CXCR4a is downregulated by blood flow in vivo and mediates collateral formation in zebrafish embryos. *Physiological Genomics*, 38(3), pp.319–327.
- Palmer, R.M., Ferrige, A.G. & Moncada, S., 1987. Nitric oxide release accounts for the biological activity of endothelium-derived relaxing factor. *Nature*, 327(6122), pp.524–526.
- Pause, A. et al., 1997. The von Hippel-Lindau tumor-suppressor gene product forms a stable complex with human CUL-2, a member of the Cdc53 family of proteins. *Proceedings of the National Academy of Sciences of the United States of America*, 94(6), pp.2156–2161.
- Pelster, B. & Burggren, W.W., 1996. Disruption of hemoglobin oxygen transport does not impact oxygen-dependent physiological processes in developing embryos of zebra fish (*Danio rerio*). *Circulation Research*, 79(2), pp.358–362.
- Phng, L.-K. et al., 2009. Nrarp Coordinates Endothelial Notch and Wnt Signaling to Control Vessel Density in Angiogenesis. *Developmental cell*, 16(1), pp.70–82.
- Phng, L.K. & Gerhardt, H., 2009. Angiogenesis: A Team Effort Coordinated by Notch. *Developmental cell*, 16(2), pp.196–208.
- Potente, M., Gerhardt, H. & Carmeliet, P., 2011. Basic and Therapeutic Aspects

- of Angiogenesis. *Cell*, 146(6), pp.873–887.
- Purow, B., 2012. Notch inhibition as a promising new approach to cancer therapy. *Advances in experimental medicine and biology*, 727, pp.305–319.
- Pursglove, S.E. & Mackay, J.P., 2005. CSL: A notch above the rest. *The International Journal of Biochemistry & Cell Biology*, 37(12), pp.2472–2477.
- Reneman, R.S., Arts, T. & Hoeks, A.P.G., 2006. Wall shear stress--an important determinant of endothelial cell function and structure--in the arterial system in vivo. Discrepancies with theory. *Journal of vascular research*, 43(3), pp.251–269.
- Rey, S. & Semenza, G.L., 2010. Hypoxia-inducible factor-1-dependent mechanisms of vascularization and vascular remodelling. *Cardiovascular research*, 86(2), pp.236–242.
- Roca, C. & Adams, R.H., 2007. Regulation of vascular morphogenesis by Notch signaling. *Genes & Development*, 21(20), pp.2511–2524.
- Sander, J.D. et al., 2010. Selection-free zinc-finger-nuclease engineering by context-dependent assembly (CoDA). *Nature methods*, 8(1), pp.67–69.
- Scheer, N. & Campos-Ortega, J.A., 1999. Use of the Gal4-UAS technique for targeted gene expression in the zebrafish. *Mechanisms of development*, 80(2), pp.153–158.
- Schier, A.F., 2007. The Maternal-Zygotic Transition: Death and Birth of RNAs. *Science (New York, N. Y.)*, 316(5823), pp.406–407.
- Schwerte, T., Uberbacher, D. & Pelster, B., 2003. Non-invasive imaging of blood cell concentration and blood distribution in zebrafish *Danio rerio* incubated in hypoxic conditions in vivo. *The Journal of experimental biology*, 206(Pt 8), pp.1299–1307.
- Sehnert, A.J. et al., 2002. Cardiac troponin T is essential in sarcomere assembly and cardiac contractility. *Nature genetics*, 31(1), pp.106–110.
- Semenza, G.L. & Wang, G.L., 1992. A nuclear factor induced by hypoxia via de novo protein synthesis binds to the human erythropoietin gene enhancer at a site required for transcriptional activation. *Molecular and cellular biology*, 12(12), pp.5447–5454.
- Semenza, G.L. et al., 1994. Transcriptional regulation of genes encoding glycolytic enzymes by hypoxia-inducible factor 1. *The Journal of biological chemistry*, 269(38), pp.23757–23763.
- Senger, D.R. et al., 1983. Tumor cells secrete a vascular permeability factor that promotes accumulation of ascites fluid. *Science (New York, N. Y.)*, 219(4587), pp.983–985.

- Sessa, W.C., 2009. Molecular control of blood flow and angiogenesis: role of nitric oxide. *Journal of Thrombosis and Haemostasis*, 7, pp.35–37.
- Siekman, A.F. & Lawson, N.D., 2007a. Notch signalling and the regulation of angiogenesis. *Cell adhesion & migration*, 1(2), pp.104–106.
- Siekman, A.F. & Lawson, N.D., 2007b. Notch signalling limits angiogenic cell behaviour in developing zebrafish arteries. *Nature*, 445(7129), pp.781–784.
- Sluimer, J.C. & Daemen, M.J., 2009. Novel concepts in atherogenesis: angiogenesis and hypoxia in atherosclerosis. *The Journal of Pathology*, 218(1), pp.7–29.
- Sprague, J. et al., 2006. The Zebrafish Information Network: the zebrafish model organism database. *Nucleic acids research*, 34(Database issue), pp.D581–5.
- Stebbins, C.E., Kaelin, W.G. & Pavletich, N.P., 1999. Structure of the VHL-ElonginC-ElonginB complex: implications for VHL tumor suppressor function. *Science (New York, N.Y.)*, 284(5413), pp.455–461.
- Swift, M.R. & Weinstein, B.M., 2009. Arterial-venous specification during development. *Circulation Research*, 104(5), pp.576–588.
- Thisse, C. & Thisse, B., 2008. High-resolution in situ hybridization to whole-mount zebrafish embryos. *Nature Protocols*, 3(1), pp.59–69.
- Thompson, M.A. et al., 1998. The cloche and spadetail genes differentially affect hematopoiesis and vasculogenesis. *Developmental biology*, 197(2), pp.248–269.
- Torres-Vázquez, J. et al., 2004. Semaphorin-plexin signaling guides patterning of the developing vasculature. *Developmental cell*, 7(1), pp.117–123.
- Traver, D. et al., 2003. Transplantation and in vivo imaging of multilineage engraftment in zebrafish bloodless mutants. *Nature Immunology*, 4(12), pp.1238–1246.
- Van Rooijen, E. et al., 2010. von Hippel-Lindau tumor suppressor mutants faithfully model pathological hypoxia-driven angiogenesis and vascular retinopathies in zebrafish. *Disease Models & Mechanisms*, 3(5-6), pp.343–353.
- Van Rooijen, E. et al., 2009. Zebrafish mutants in the von Hippel-Lindau tumor suppressor display a hypoxic response and recapitulate key aspects of Chuvash polycythemia. *Blood*, 113(25), pp.6449–6460.
- van Royen, N. et al., 2009. A critical review of clinical arteriogenesis research. *Journal of the American College of Cardiology*, 55(1), pp.17–25.
- Vitorino, M. et al., 2009. Vsx2 in the zebrafish retina: restricted lineages through

- derepression. *Neural development*, 4(1), p.14.
- Wang, G.L. et al., 1995. Hypoxia-inducible factor 1 is a basic-helix-loop-helix-PAS heterodimer regulated by cellular O₂ tension. *Proceedings of the National Academy of Sciences of the United States of America*, 92(12), pp.5510–5514.
- Warren, C.M. & Iruela-Arispe, M.L., 2010. Signaling circuitry in vascular morphogenesis. *Current opinion in hematology*, 17(3), pp.213–218.
- Weidemann, A. & Johnson, R.S., 2008. Biology of HIF-1alpha. *Cell death and differentiation*, 15(4), pp.621–627. Available at: <http://www.nature.com/doi/10.1038/cdd.2008.12>.
- Wells, S., Nornes, S. & Lardelli, M., 2011. Transgenic Zebrafish Recapitulating tbx16 Gene Early Developmental Expression H. Escrava, ed. *PloS one*, 6(6), p.e21559.
- Wenger, R.H., Stiehl, D.P. & Camenisch, G., 2005. Integration of oxygen signaling at the consensus HRE. *Science's STKE : signal transduction knowledge environment*, 2005(306), p.re12.
- Wienholds, E. et al., 2003. Efficient target-selected mutagenesis in zebrafish. *Genome research*, 13(12), pp.2700–2707.
- Wilkinson, R.N. et al., 2012. Hedgehog signaling via a calcitonin receptor-like receptor can induce arterial differentiation independently of VEGF signaling in zebrafish. *Blood*, 120(2), pp.477–488.
- Yancopoulos, G.D. et al., 2000. Vascular-specific growth factors and blood vessel formation. *Nature*, 407(6801), pp.242–248.
- Yu, M. et al., 2002. Mechanism of cGMP contribution to the vasodilator response to NO in rat middle cerebral arteries. *American journal of physiology. Heart and circulatory physiology*, 282(5), pp.H1724–31.
- Zhong, T.P. et al., 2001. Gridlock signalling pathway fashions the first embryonic artery. *Nature*, 414(6860), pp.216–220.
- Zygmunt, T. et al., 2012. In parallel interconnectivity of the dorsal longitudinal anastomotic vessels requires both VEGF signaling and circulatory flow. *Journal of cell science*.
- Zygmunt, T. et al., 2011. Semaphorin-PlexinD1 Signaling Limits Angiogenic Potential via the VEGF Decoy Receptor sFlt1. *Developmental cell*, 21(2), pp.301–314.